

Production Flux of Sea-Spray Aerosol

Gerrit de Leeuw^{1,2,3}, Edgar L Andreas⁴, Magdalena D. Anguelova⁵, C. W. Fairall⁶, Ernie R. Lewis⁷, Colin O'Dowd⁸, Michael Schulz⁹, Stephen E. Schwartz⁷

1. Finnish Meteorological Institute, Climate Change Unit, Helsinki, Finland, email:

Gerrit.Leeuw@fmi.fi

2. University of Helsinki, Department of Physics, Helsinki, Finland

3. TNO Environment and Geosciences, Dept. of Air Quality and Climate, Utrecht, The Netherlands

4. NorthWest Research Associates, Inc. (Seattle Division), Lebanon, NH 03766, USA

5. Naval Research Laboratory, Washington, DC 20375, USA

6. NOAA/ESRL, Boulder, CO 80305, USA

7. Brookhaven National Laboratory, Upton, NY 11973, USA

8. School of Physics & Centre for Climate and Air Pollution Studies, Environmental Change Institute, National University of Ireland Galway, University Road, Galway, Ireland

9. Laboratoire des Sciences du Climat et de l'Environnement, Gif-sur-Yvette, France

Abstract

Knowledge of the size- and composition-dependent production flux of primary sea-spray aerosol (SSA) particles and its dependence on environmental variables is required for modeling cloud microphysical properties and aerosol radiative influences, interpreting measurements of particulate matter in coastal areas and its relation to air quality, and evaluating rates of uptake and reactions of gases in sea-spray drops. This review examines recent research pertinent to SSA production flux, which deals mainly with production of particles with r_{80} (equilibrium radius at 80% relative humidity) less than 1 μm and as small as 0.01 μm . Production of sea-spray particles and its dependence on controlling factors has been investigated in laboratory studies that have examined the dependences on water temperature, salinity, and the presence of organics, and in field measurements with micrometeorological techniques that use newly developed fast optical

29 particle sizers. Extensive measurements show that water-insoluble organic matter contributes
30 substantially to the composition of SSA particles with $r_{80} < 0.25 \mu\text{m}$ and in locations with high
31 biological activity can be the dominant constituent. Order-of-magnitude variation remains in
32 estimates of the size-dependent production flux per white area, the quantity central to
33 formulations of the production flux based on the whitecap method. This variation indicates that
34 the production flux may depend on quantities, such as the volume flux of air bubbles to the
35 surface, that are not accounted for in current models. Variation in estimates of the whitecap
36 fraction as a function of wind speed contributes additional, comparable uncertainty to production
37 flux estimates.

38

39 Index terms: 0300, 0305, 0312, 4801

40

41 **1. Introduction**

42 Sea-spray aerosol (SSA) consists of a suspension, in air, of particles that are directly
43 produced at the sea surface. These particles exist mainly in the liquid phase (i.e., as drops). The
44 radii of these particles vary from around ten nanometers to at least several millimeters, and the
45 atmospheric residence times vary from seconds to minutes for larger particles, for which
46 gravitational sedimentation is the principal removal mechanism, to days for smaller particles, for
47 which removal is primarily by precipitation.

48 SSA particles, because of their hygroscopicity and size, function readily as cloud
49 condensation nuclei (CCN) [e.g., *Andreae and Rosenfeld, 2008* and references cited therein], and
50 can thus play a major role in determining the number concentration and size distribution of drops
51 in marine clouds. In the absence of perturbations by anthropogenic aerosols, SSA exerts an even
52 stronger influence on cloud properties; thus understanding SSA is necessary to evaluate the
53 influences of anthropogenic aerosols on cloud reflectivity and persistence (so-called indirect
54 radiative forcing) and on precipitation. A major contributor to uncertainty in evaluating the
55 indirect forcing by anthropogenic aerosols is a lack of knowledge on the background natural
56 aerosol and the associated cloud properties.

57 SSA provides a major contribution to scattering of electromagnetic radiation over
58 much of the world's oceans. The annual global average magnitude of upward scattering of
59 radiation in the solar spectrum at wavelengths 0.3-4 μm by SSA particles, which results in a
60 cooling influence on Earth's climate by decreasing the amount of radiation absorbed by the
61 oceans, has been estimated in various investigations as 0.08 to 6 W m^{-2} [Lewis and Schwartz,
62 2004 (hereinafter denoted as *LS04*), p. 183]. Quantifying light scattering by SSA is thus
63 important for understanding the perturbation by anthropogenic aerosols to Earth's shortwave
64 radiation budget during the industrial period (so-called aerosol direct forcing) [Charlson *et al.*,
65 1992; IPCC, 2007]. This cooling influence is partly offset by absorption of longwave (thermal
66 infrared) radiation [Reddy *et al.*, 2005; Satheesh and Moorthy, 2005]. Production and properties
67 of SSA as CCN are of interest also in proposals to modify climate to offset global warming
68 ("geo-engineering") by alteration of the properties of marine clouds [e.g., Latham, 1990; Bower
69 *et al.*, 2006].

70 SSA often dominates the mass concentration of marine aerosol, especially at
71 locations remote from anthropogenic or other continental sources, and SSA is one of the
72 dominant aerosols globally (along with mineral dust) in terms of mass emitted into the
73 atmosphere. Estimates of global annual mass emission of sea salt (calculated as the integral over
74 the size-distributed number production flux times the volume per particle times the mass of sea
75 salt per unit volume of seawater) with current chemical transport models and global climate
76 models (CTMs and GCMs, respectively), using various parameterizations of the sea-spray source
77 function (SSSF), range over nearly two orders of magnitude, from 0.02 to 1×10^{14} kg yr^{-1}
78 (Figure 1 and Table 1) [Textor *et al.*, 2006]. Much of this variation is due to the different
79 dependences on wind speed and to the upper size limit of particles included. This wide range
80 emphasizes the necessity of specifying the particle size range and the height or residence time in
81 reporting sea-spray emission fluxes. Critical analysis of SSA production leads to the conclusions
82 that there are large uncertainties in SSA fluxes, and that SSSF parameterizations must be viewed
83 as little more than order-of-magnitude estimates [Hoppel *et al.*, 2002; *LS04*, Section 5.11].

84 In the past several years, the contribution of organic species to SSA has been
85 quantitatively examined in laboratory studies and field measurements, and measurements of SSA

86 concentrations and production have been extended to sizes smaller than were previously thought
87 to be important. In this paper we provide an overview of recent measurements and experimental
88 investigations pertinent to SSA and its production, with the purpose of examining this work and
89 placing it in the context of previous understanding. The starting point is the review of SSA
90 production by *LS04*. Since that time, marine aerosol production has been reviewed by *Massel*
91 [2007] and by *O'Dowd and de Leeuw* [2007]. *Massel* [2007] focused mainly on wave breaking
92 and provided an overview of sea-spray aerosol production based primarily on work prior to
93 2000, complemented with more recent studies by Polish investigators. *O'Dowd and de Leeuw*
94 [2007] reviewed both primary and secondary particle formation in the marine atmosphere. With
95 regard to primary SSA production, these investigators reviewed SSSF formulations presented in
96 the period 2000-2006, results from laboratory studies concerning the sizes of the sea-spray drops
97 produced, and the first findings by *O'Dowd et al.* [2004] and *Cavalli et al.* [2004] regarding
98 organic matter in sea-spray aerosol. The current review differs from those in that work published
99 since *LS04*, including laboratory and field experimental results on sea-spray production, on the
100 enrichment in organic matter, and on the measurement and parameterization of whitecap
101 coverage, is critically examined and compared with results summarized in *LS04* to identify
102 progress.

103 Throughout this paper, we follow the common convention of specifying the size of
104 an SSA particle by its equilibrium radius at a relative humidity (RH) of 80%, r_{80} . For sea-salt
105 particles originating from seawater with typical salinity (34-36), r_{80} is about one-half the radius
106 at formation. For such particles, to good accuracy $r_{80} = 2r_{\text{dry}}$, where r_{dry} is the volume-equivalent
107 dry radius. A simple approximation for the RH dependence of the equilibrium radius ratio of an
108 SSA particle in the liquid phase r/r_{80} , is

109

$$110 \quad \frac{r}{r_{80}} = 0.54 \left(1.0 + \frac{1}{1-h} \right)^{1/3}, \quad (1)$$

111

112 where h is the fractional relative humidity ($h \equiv RH/100$) [*LS04*, p. 54]. This equation applies in
113 situations for which the effect of surface tension can be neglected (i.e., particles sufficiently large
114 and RH sufficiently low); for other situations a more detailed treatment is required [*Lewis*, 2008].

115 SSA particles are considered in three distinct size ranges based on their behavior in
116 the atmosphere and considerations of the processes that affect this behavior (e.g., *LS04*, p. 11):
117 $r_{80} \lesssim 1 \mu\text{m}$ for small SSA particles, $1 \mu\text{m} \lesssim r_{80} \lesssim 25 \mu\text{m}$ for medium SSA particles, and
118 $25 \mu\text{m} \lesssim r_{80}$ for large SSA particles. This review is restricted to particles with $r_{80} \lesssim 25 \mu\text{m}$.
119 Special attention is paid to new information on composition, concentration, and production of
120 SSA particles with $r_{80} < 0.1 \mu\text{m}$.

121 Many measurements indicate that the relative concentrations of the major solutes in
122 sea-spray particles are similar to their relative concentrations in bulk seawater, although this may
123 not be the situation for some substances as a consequence of the formation process, or of
124 exchange with the atmosphere subsequent to formation. SSA particles are said to be enriched in
125 such substances, and the enrichment factor, defined as the ratio of the concentration of a
126 substance to the concentration of one of the major constituents of bulk seawater (typically
127 sodium) in the particle to the same ratio for bulk seawater, may be less than or greater than unity.

128 In biologically productive seawater, accumulation of organic substances at the sea
129 surface can result in formation of sea-spray particles that are considerably enriched in these
130 substances, especially for particles with $r_{80} < 1 \mu\text{m}$ [*Blanchard*, 1964; *Middlebrook et al.*, 1998;
131 *O'Dowd et al.*, 2004]. As far back as 1948, *Woodcock* [1948] showed that drops produced by
132 bubbles bursting in areas with high concentrations of plankton (dinoflagellates) in red tide could
133 carry irritants across the air-sea interface into the atmosphere. *Blanchard* [1963] documented
134 enrichment of organic matter in sea spray and discussed the sea-to-air transport of surface-active
135 material [*Blanchard*, 1964]. *Blanchard and Syzdeck* [1970] further confirmed that bacteria are
136 concentrated at the sea surface, leading to enrichment of bacteria in SSA particles. Later, factors
137 influencing the organic content of marine aerosols were investigated in laboratory studies by
138 *Hoffmann and Duce* [1976]. More recently, the use of instruments such as aerosol mass
139 spectrometers has demonstrated and quantified the presence of organic species in individual
140 particles. For instance, *Middlebrook et al.* [1998] reported that more than half of all marine

141 particles with dry diameters greater than $0.16\ \mu\text{m}$ at Cape Grim, Tasmania contained organics
142 during clean marine conditions, and that the organics were nearly always found internally mixed
143 with sea salt. *Novakov et al.* [1997], based on measurements in a region minimally affected by
144 continental emissions, reported that the contribution of organic substances to the aerosol mass
145 from particles with dry aerodynamic diameter less than $0.6\ \mu\text{m}$ was greater than that of sulfate,
146 nitrate, or chloride (which would be indicative of sea salt), and suggested a marine source for
147 these particles. *Putaud et al.* [2000] reported that organics contributed roughly 20% to the mass
148 of aerosol particles with r_{80} less than $\sim 1.3\ \mu\text{m}$ in the marine boundary layer, less than non-sea
149 salt sulfate, but about the same as sea salt.

150 The aerosol consisting of sea-spray particles in the atmosphere has traditionally been
151 termed “sea-salt aerosol”, but in this review it is denoted “sea-spray aerosol” in recognition that
152 the composition of the particles may differ from that of bulk seawater. One consequence of this
153 difference is that the hygroscopic and cloud droplet activation properties of sea-spray particles
154 may differ from those calculated under the assumption that the particles are composed only of
155 sea salt.

156 **2. Production of Sea-Spray Aerosol and Flux Formulation**

157 SSA particles are formed at the sea surface mainly by breaking waves via bubble
158 bursting and by tearing of wave crests. When a wave breaks, air is entrained into the water and
159 dispersed into a cloud of bubbles [*Thorpe*, 1992], which rise to the surface and burst. The
160 resulting white area of the sea surface is often denoted a “whitecap” on account of enhanced,
161 wavelength-independent scattering of visible radiation by the interfaces between water and
162 bubbles, and the fraction of the sea surface covered by white area is defined as the whitecap
163 fraction, W . When an individual bubble bursts, the bubble cap (or film) may disintegrate into so-
164 called film drops, which are ejected at a wide distribution of angles relative to the vertical. Up to
165 a thousand such film drops may be produced per bubble, the number and size distribution (and
166 whether or not film drops are produced) depending largely on bubble size [*LS04*]. These film
167 drops have radii at formation ranging from smaller than ten nanometers to several hundreds of
168 micrometers, but most are less than $1\ \mu\text{m}$ [e.g., *Blanchard*, 1963; *Day*, 1964; *Blanchard*, 1983].

169 Individual bubbles with radius less than ~ 1 mm typically do not form film drops [LS04, p. 208].
170 The majority of SSA particles in the atmosphere with $r_{80} < 1$ μm are probably film drops.

171 After the bubble cap has burst, a vertical cylindrical jet forms in the middle of the
172 cavity left by the bubble. This jet may break up into as many as ten jet drops, the number
173 depending largely on bubble size, that are ejected vertically to heights of up to ~ 20 cm above the
174 surface [e.g., Blanchard, 1963; Blanchard, 1983; Spiel, 1995]. The initial radii of these drops are
175 roughly 10% of the radius of the parent bubble and thus range from slightly less than 1 μm to
176 more than 100 μm . Individual bubbles of radius greater than 2 mm typically do not form jet
177 drops [LS04]. The majority of SSA particles in the atmosphere with r_{80} between 1 and 25 μm are
178 probably jet drops.

179 SSA particles of the sizes considered in this review are formed mainly from bursting
180 bubbles. Another production mechanism is the formation of spume drops by tearing of wave
181 crests by the wind when the wind speed near the sea surface exceeds about 10 m s^{-1} [Monahan *et*
182 *al.*, 1983]. These drops, which are transported nearly horizontally by the wind, are typically quite
183 large, with radii from several tens of micrometers to several millimeters, and consequently fall
184 back to the sea surface within seconds to minutes [Andreas, 1992]. Spume drops are not
185 considered further here.

186 The SSSF is a numerical representation of the size-dependent production flux of
187 SSA particles. The following form of this function is employed in this review:

188

$$189 \quad f(r_{80}) \equiv \frac{dF(r_{80})}{d \log_{10} r_{80}}, \quad (2)$$

190

191 where the quantity $f(r_{80})$ denotes the number of particles in a given infinitesimal range of the
192 common logarithm of r_{80} , $d \log_{10} r_{80}$, introduced into the atmosphere per unit area per unit time,
193 and $F(r_{80})$ is the total number flux of particles of size less than r_{80} (the subscript 10 denoting the
194 base of the logarithm is suppressed in the remainder of this paper). Implicit in this definition is
195 that this quantity is averaged over areas and times sufficiently large that rapid fluctuations caused
196 by individual breaking waves are smoothed out.

197 Because SSA particles may be emitted with an initial upward velocity, because the
198 sea surface is vertically disturbed by waves, and because SSA production is enhanced near wave
199 crests, the nature of the air-sea interface and of interfacial production is difficult to characterize.
200 Additionally, some SSA particles fall back to the sea surface before spending any appreciable
201 time in the atmosphere, the fraction of such particles increasing with increasing r_{80} . For all these
202 reasons, the concept of a source of SSA particles that may be said to be introduced into the
203 marine atmosphere must also, implicitly or explicitly, take into account an effective source
204 height, which may be the mean interfacial height or some specified height above it [LS04].
205 Recognition of the need to specify an effective source height leads to a useful distinction
206 between the interfacial flux, and the effective flux at that height. The interfacial flux is defined as
207 the flux of those particles leaving the sea surface, whereas the effective flux is defined as the flux
208 of those particles produced at the sea surface that attain a given height, typically taken as 10 m
209 above mean sea level (the value used throughout this review), and thus remain in the atmosphere
210 sufficiently long to participate in processes such as cloud formation and atmospheric chemistry.

211 For many applications, such as large-scale models that describe the atmosphere in
212 terms of multiple vertical layers and consider introduction of particles only into the lowest level,
213 it is only this effective flux that is important. For small SSA particles (i.e., those with
214 $r_{80} \lesssim 1 \mu\text{m}$), the effective flux can, for all practical purposes, be considered to be the same as the
215 interfacial flux. For medium SSA particles (those with $1 \mu\text{m} \lesssim r_{80} \lesssim 25 \mu\text{m}$), the effective flux
216 becomes increasingly less than the interfacial flux with increasing r_{80} . For large SSA particles,
217 which have short atmospheric residence times and typically do not attain heights more than a few
218 meters above the sea surface, the effective flux is essentially zero.

219 An expression for the SSSF required as input to models would represent the size-
220 dependent production flux expressed by Eq. 2 as a function of the controlling ambient variables
221 a, b, \dots ; i.e., $f(r_{80}; a, b, \dots)$. Identifying these variables and developing specific parameterizations
222 for Eq. 2 rest on recognizing and understanding the controlling processes. Wind speed plays a
223 dual role in influencing the effective production flux of SSA: first by being the dominant factor
224 controlling wave generation (and subsequent breaking), and second through upward turbulent
225 transport of newly formed particles. The near-surface wind speed, commonly measured and

226 expressed at a reference height of 10 m, U_{10} , is thought to be the dominant factor affecting sea-
 227 spray production. However, different formulations of the size-dependent SSSF in terms of only
 228 U_{10} vary widely for the same U_{10} . Considerable effort has been devoted to linking SSA
 229 production to more fundamentally relevant physical parameters, such as wind stress on the
 230 surface, τ (or the friction velocity, u^* , defined by $u^* \equiv (\tau/\rho_{\text{air}})^{1/2}$, where ρ_{air} is the density of air),
 231 or whitecap fraction, W , with the expectation that such approaches might lead to a tighter relation
 232 between production flux and one of these other variables than is currently the situation with wind
 233 speed. For example, at a given U_{10} , τ can vary by a factor of two [Drennan *et al.*, 2005] and W
 234 by a factor of 10 or more [LS04; Anguelova and Webster, 2006]; this variation is likely due to
 235 variability in the wave field, surface properties, and the like. However, such efforts have not
 236 resulted in substantial narrowing of the spread in the SSSF as a function of controlling variables.
 237 Other factors that are expected to affect the SSA production flux are those affecting sea state,
 238 such as fetch (the upwind distance over the water of nearly constant wind velocity) and
 239 atmospheric stability (often parameterized by the air-sea temperature difference), which also
 240 affects vertical transport; seawater temperature and salinity; and the presence, amount, and
 241 nature of surface-active substances.

242 A simplifying assumption that is sometimes made in parameterizing the SSSF is that
 243 the dependences on drop size and controlling variables can be separated into a dimensionless
 244 function $\varphi(a, b, \dots)$ that contains all of the dependences of the SSA production flux on
 245 environmental forcing parameters a, b, \dots , including wind speed, and a universal shape function
 246 $g(r_{80})$:

$$\frac{dF(r_{80}, a, b, \dots)}{d \log r_{80}} = \varphi(a, b, \dots) g(r_{80}). \quad (3)$$

249 However, this assumption has relatively little observational support, and there are several reasons
 250 why it would not be expected to hold; for instance, under higher winds more larger particles
 251 could be transported upward and thus contribute to, and change the size distribution of, the
 252 effective production flux.
 253

254 **3. Methods of Determining SSA Production Fluxes**

255 Methods that can be used to infer the size-dependent production flux of SSA
256 particles (Table 2) were discussed in detail by *LS04*. Methods relevant to this review are the
257 steady-state dry deposition method, the statistical wet deposition method, micrometeorological
258 methods, and the whitecap method. These methods are briefly reviewed, and for each the
259 following topics are discussed: the basic assumptions inherent in its application, the quantities
260 required and how they are determined, the size range to which the method can be applied and
261 what precludes its application to other sizes, and concerns with its use. Some of the commonly
262 used production flux formulations are also discussed here and presented in the Appendix. New
263 formulations are discussed in Section 5.

264 **3.1. General Considerations**

265 The steady-state dry deposition method, the statistical wet deposition method, and
266 micrometeorological methods use field measurements of concentrations and/or fluxes, as do
267 some applications of the whitecap method; thus these methods infer the effective production
268 flux. Most applications of the whitecap method use SSA size distribution measurements from
269 laboratory-generated whitecaps, which allow inference of the interfacial production flux.

270 Methods that rely on field measurements of SSA concentrations involve counting
271 and sizing SSA particles in the atmosphere. However, even such measurements, although
272 seemingly straightforward, encounter practical difficulties as a consequence of the low number
273 concentrations of SSA particles, with values for SSA particles with $r_{80} > 1 \mu\text{m}$ typically reported
274 as less than several per cubic centimeter, and for all SSA particles as at most a few tens per cubic
275 centimeter [*LS04*, Section 4]. Such low concentrations, the consequences of which become even
276 more pronounced when size-segregated measurements are made, can result in poor counting
277 statistics and require long sampling times to achieve adequate signal-to-noise ratios.

278 Another difficulty arises from the presence in the marine atmosphere of particles
279 other than SSA particles, because in some size ranges and locations SSA particles are not the
280 most numerous. Typical concentrations of all aerosol particles in clean marine conditions are
281 several hundred per cubic centimeter. Thus, techniques are required to distinguish SSA particles
282 from particles composed of other substances. This concern becomes increasingly important with

283 decreasing particle size, as SSA particles with radii less than several tenths of a micrometer may
284 constitute only a small fraction of all aerosol particles in this size range (e.g., Figure 16 of *LS04*).
285 This concern pertains especially to coastal regions or other areas where continental aerosols may
286 be present in high abundances. Additionally, enrichment of SSA particles either during formation
287 at the sea surface or due to atmospheric uptake and exchange may make it difficult to determine
288 whether or not an aerosol particle is an SSA particle based on composition or on other properties
289 such as hygroscopicity or thermal volatility.

290 Field measurements of SSA particle concentrations or fluxes are often made at
291 coastal regions because of cost, accessibility, ability to install permanent equipment, and other
292 factors. Such measurements offer the possibility of long-term data sets that encompass a wider
293 variety of conditions than may be feasible from an individual cruise. However, concerns with
294 measurements from these locations are coastal influences such as surf-produced SSA and
295 differences in flow properties and upward transport, in addition to the greater possibility of
296 influences of continental aerosol. Typically data are screened so that they are used only when air
297 flow is from ocean to land.

298 Each of the methods that use field measurements requires certain conditions for its
299 successful application. One such condition is often referred to as “steady state,” but this phrase
300 has been used to mean different things in different applications, and this ambiguity can and has
301 led to confusion. In some instances this phrase refers to conditions in which there is no mean
302 vertical flux of SSA particles, whereas in other instances it refers to conditions in which mean
303 quantities affecting the SSA flux, such as wind speed, are unchanged over times of interest (e.g.,
304 the sampling time required to obtain a statistically representative sample), although there may
305 still be a net upward flux of SSA particles. Whether the required conditions are satisfied is rarely
306 discussed in presentations of SSA flux determinations, but spurious results can occur through
307 failure to take into account other factors that affect measurements. Key among these are time-
308 dependent meteorological conditions, which confound flux measurements, and entrainment of
309 free tropospheric air into the marine boundary layer, which causes a growth in height of this
310 layer and a decrease in particle number concentration through dilution.

311 **3.2. Steady-State Dry Deposition Method**

312 The steady-state dry deposition method infers the size-dependent effective
313 production flux of SSA particles by assuming that production of SSA particles with r_{80} in the
314 size range of interest at a given time and location is balanced by removal at the same time and
315 location through dry deposition, such that the net upward flux of particles of any given r_{80} in that
316 size range is zero. The effective production flux is thus equal to the dry deposition flux, which in
317 turn is equal to the product of the size-dependent number concentration, $dN/d\log r_{80}$, and the dry
318 deposition velocity, v_{dd} , also a function of r_{80} :

$$319 \frac{dF_{\text{eff}}}{d \log r_{80}} = \frac{dN}{d \log r_{80}} \times v_{dd}(r_{80}). \quad (4)$$

321 The size-dependent SSA number concentration, which is determined by measurements at a given
322 reference height, typically near 10 m, is often parameterized only in terms of wind speed at 10 m,
323 U_{10} . The size-dependent dry deposition velocity is modeled, usually also as a function only of
324 U_{10} . Nearly all such parameterizations are based ultimately on *Slinn and Slinn* [1980], whose
325 treatment accounts for gravitational sedimentation, turbulent transport, impaction to the sea
326 surface, Brownian diffusion, and growth of particles near the sea surface due to the higher RH
327 there, although for a given size range only some of these processes are important.

329 The assumption of local balance requires steady-state conditions with respect to dry
330 deposition during the lifetimes of SSA particles in the atmosphere and thus that the
331 meteorological conditions (i.e., wind speed and other pertinent parameters) under which the
332 particles were produced are the same as those under which they are measured. It further requires
333 that dry deposition be the dominant removal mechanism of SSA particles (i.e., that little or no
334 rainfall has occurred during the lifetimes of these particles in the atmosphere), that there has been
335 negligible decrease in concentration by entrainment and mixing of free tropospheric air, and that
336 the mean size-dependent SSA concentration is independent of time. These assumptions restrict
337 the mean atmospheric residence times of SSA particles for which this method can be accurately
338 applied to a few days at most, corresponding to an approximate size range $3 \mu\text{m} < r_{80} < 25 \mu\text{m}$.

339 There are several concerns with this method in addition to those listed in Section 3.1.
340 The large range of values of SSA concentrations reported for nominally the same wind speed, an
341 order of magnitude or more [LS04], results in a correspondingly large range of values for the
342 inferred production flux. Uncertainties in modeled dry deposition velocities can likewise lead to
343 uncertainties in the inferred production flux, and systematic errors can occur if the required
344 conditions for successful application of this method are not satisfied.

345 This approach, which is appealing because it is seemingly easy to apply, has been
346 used by several investigators (ten formulations based on this method are compared by LS04).
347 One widely used formulation (Appendix) is that of *Smith et al.* [1993], who measured size-
348 dependent aerosol concentrations with optical particle counters (OPCs) for more than 700 hours
349 from a 10 m tower on an island off the west coast of Scotland. They used measurements only
350 from maritime air masses and assumed that the majority of particles measured were SSA
351 particles. Their formulation consists of two lognormal size distributions with coefficients that
352 exhibit different dependences on U_{10} ; such a formulation is, of course, inconsistent with the
353 separability assumption (Eq. 3).

354 The steady-state dry deposition method together with numerous measurements of
355 sea-salt aerosol concentration taken from the literature was used by LS04 to determine a
356 formulation (Appendix) for the effective production flux over the r_{80} range 3 to 25 μm as a
357 power law in r_{80} with exponent -2.5, with the amplitude varying directly as U_{10} to the 2.5 power.
358 This formulation is characterized by an associated uncertainty of a multiplicative factor of 4
359 above and below the central value resulting from the variability in size-dependent number
360 concentrations in a given range of wind speeds and from estimated uncertainties in the modeled
361 dry deposition velocity.

362 **3.3. Statistical Wet Deposition Method**

363 The statistical wet deposition method infers the effective SSA production flux
364 necessary to account for measured number concentrations under the assumptions that SSA
365 particles in the size range of interest are removed from the atmosphere only by wet deposition
366 (coagulation being negligible for SSA particles primarily because of their low concentrations)
367 and that precipitation, when it occurs, removes nearly all SSA particles in this size range. These

368 assumptions restrict application of this method to SSA particles with $r_{80} \lesssim 1 \mu\text{m}$ and imply that
 369 for this size range the size dependence of the number concentration of SSA particles is the same
 370 as that of their production.

371 This method is essentially a budget argument that provides a consistency check,
 372 ensuring that unrealistically high production fluxes are not calculated. On average, the total
 373 number of SSA particles in a given size range produced since the last precipitation event, per
 374 unit area of sea surface, is equal to the column burden (i.e., integral over height) of the
 375 concentration of such particles. Because SSA particles in this size range are expected to be
 376 nearly uniformly mixed over the height of the marine boundary layer H_{mbl} , and because
 377 concentrations of SSA particles are quite low above the marine boundary layer relative to
 378 concentrations within this layer, this column burden can be approximated by the product of the
 379 number concentration at an arbitrary measurement height (typically near 10 m) and H_{mbl} .
 380 Consequently, the production flux required to produce the measured concentration is equal to
 381 that column burden divided by the time between rainfall events, τ_{wet} .

382

$$383 \quad \frac{dF_{\text{eff}}}{d \log r_{80}} = \frac{dN}{d \log r_{80}} \times \frac{H_{\text{mbl}}}{\tau_{\text{wet}}}. \quad (5)$$

384

385 This method was applied by *LS04* (Appendix) with the parameters $\tau_{\text{wet}} = 3$ days,
 386 $H_{\text{mbl}} = 0.5$ km, and the value $dN/d \log r_{80} = 5 \text{ cm}^{-3}$ (based on numerous measurements reported in
 387 the literature at typical wind speeds) to yield an estimate of $dF/d \log r_{80} \approx 10^4 \text{ m}^{-2} \text{ s}^{-1}$, nearly
 388 independent of r_{80} , over the range $0.1 \mu\text{m} \lesssim r_{80} \lesssim 1 \mu\text{m}$, with an associated uncertainty of a
 389 factor of 5 above and below the central value based on uncertainties in the above quantities.

390 **3.4. Micrometeorological Methods**

391 Micrometeorological methods infer the effective SSA production flux from
 392 measurements of fluctuations or gradients of concentration in the lowest portion of the marine
 393 boundary layer (typically within several tens of meters from the sea surface). Techniques such as
 394 eddy correlation, eddy accumulation, relaxed eddy accumulation, and gradient methods are
 395 commonly used to determine net vertical turbulent fluxes of other quantities such as heat,

396 momentum, or gases. Both eddy correlation and gradient methods have been used to determine
 397 fluxes of SSA particles. These methods assume that the production of SSA particles is not in
 398 steady state with respect to removal of these particles through dry deposition, although steady-
 399 state conditions in the sense of time-invariance of mean quantities over the duration of the
 400 measurement are assumed.

401 3.4.1. Eddy Correlation Method

402 Eddy correlation (e.g., *Businger* [1986]; *Kaimal and Finnigan* [1994]) determines
 403 the net vertical flux F_χ of a quantity χ , such as the number concentration of SSA particles in a
 404 given size range, by decomposing the vertical wind speed w into a mean component, \bar{w} , and a
 405 fluctuating component, w' , as $w = \bar{w} + w'$, and similarly for χ , where the overbar denotes an
 406 average over a time sufficiently long that meaningful statistics are obtained but sufficiently short
 407 that environmental conditions do not appreciably change. Because \bar{w} is zero, the net vertical flux
 408 is $F_\chi = \overline{w' \chi'}$.

409 In contrast to the situation for heat, momentum, and gases for which the measured
 410 fluxes are due to turbulent transport alone, for SSA particles dry deposition and gravitational
 411 settling, which act as downward fluxes, must be taken into account in determining production
 412 fluxes [*LS04*, p. 81]:

$$413 \quad \frac{dF_{\text{eff}}}{d \log r_{80}} = \overline{w' \left(\frac{dN}{d \log r_{80}} \right)'} + \overline{\left(\frac{dN}{d \log r_{80}} \right)} \times [v_{\text{dd}}(r_{80}) - v_{\text{grav}}(r_{80})]. \quad (6)$$

415 Hence the effective production flux of SSA particles exceeds the net flux measured by eddy
 416 correlation (the first term on the right-hand side of Eq. 6) by the difference between the dry
 417 deposition flux, which is calculated from the mean SSA particle number concentration and the
 418 dry deposition velocity, and the gravitational flux. As gravitational settling does not contribute to
 419 the measured eddy correlation flux, the dry deposition velocity, which includes gravitational
 420 settling, must itself be diminished by the gravitational settling velocity. Either of the terms on the
 421 right-hand side of Eq. 6 can be confounded by the presence of other types of aerosol particles.
 422

423 3.4.2. Gradient Method

424 Another micrometeorological method is the gradient method, by which the effective
425 production flux of particles sufficiently small that the effect of gravity is negligible compared to
426 upward turbulent diffusion (i.e., r_{80} smaller than a few micrometers) can be determined from
427 measurements of the dependence of the concentration on height. This approach was proposed by
428 *Petelski* [2003] as an extension of Monin-Obukhov similarity theory, which is commonly used to
429 relate fluxes of quantities such as momentum and heat to the vertical gradients of wind speed and
430 temperature, respectively. *Petelski* and colleagues have argued that in steady state conditions
431 (which in this sense refers to mean quantities being independent of time) and neutral atmospheric
432 stability, the height dependence of the number concentration can be written as [*Petelski and*
433 *Piskozub*, 2006, 2007; also *Andreas*, 2007]

$$434 \frac{dN}{d \log r_{80}}(z) = \left(\frac{-1}{\kappa u^*} \right) \left(\frac{dF}{d \log r_{80}} \right) \ln \left(\frac{z}{z_{\text{ref}}} \right) + \frac{dN}{d \log r_{80}}(z_{\text{ref}}), \quad (7)$$

436 where u^* is the friction velocity, κ is the von Karman constant (approximately 0.40), and z_{ref} is
437 an arbitrary reference height. Thus, the production flux of SSA particles of a given size could, in
438 principle, be determined from the difference in number concentrations at two heights or from the
439 slope of the number concentration plotted against the logarithm of the height. Because of the
440 small change in the number concentration over heights at which measurements are typically
441 made, accurate determination of this difference, or slope, imposes high accuracy and precision
442 requirements on the concentration measurements. For particles with $r_{80} < 1 \mu\text{m}$ concentration
443 differences are extremely difficult to measure; for larger particles the concentrations are so small
444 that accurate measurements require very long sampling times. Determination of SSA production
445 fluxes by this approach is discussed in Section 4.2.2.

447 3.4.3. Discussion of Micrometeorological Methods

448 Successful application of micrometeorological methods requires that the downward
449 flux of SSA particles due to dry deposition, if not negligible, be taken into account. However,
450 because there is typically no discrimination with regard to particle composition, dry deposition of

451 other aerosol particles can lead to spurious results if not accurately taken into account. This
452 effect also reduces the signal-to-noise ratio because uncertainties of modeled dry deposition
453 fluxes of small particles may be greater than the measured upward fluxes themselves. Use of
454 micrometeorological methods implicitly assumes that the ocean surface is a uniform source of
455 particles, but fluctuations caused by the discrete nature of breaking waves would interfere with
456 measurements, or at least require long times for averaging. Implementation of these methods also
457 involves several practical difficulties. Gradients and fluctuations in RH must be accurately taken
458 into account, and measurements from a ship at sea, for example, must take into account
459 perturbation of the turbulent characteristics of the flow by the ship or sampling devices and the
460 motion of the ship.

461 There are several concerns with micrometeorological methods. Because of the relatively
462 low concentrations of SSA particles in the atmosphere accurate results require long sampling
463 times, which may be beyond practical limits or extend through meteorological conditions that are
464 changing. The consequences of these low concentrations are more pronounced for
465 micrometeorological methods than for other methods because micrometeorological methods
466 determine the SSA production flux from small differences of much larger quantities;
467 uncertainties can, thus, result in much greater fractional uncertainty for the estimated flux.

468 The SSA production flux determined by eddy correlation measurements is based on
469 turbulent deviations of the concentrations from the mean values for a sampling rate on the order
470 of a few tenths of a second. These concentration fluctuations inherently have large uncertainties
471 which are enhanced when concentrations are small. In effect, this approach also determines the
472 production flux as a difference of two much larger values, as the dominant contribution to this
473 flux is provided by the sum of the positive values of $w'(dN/d\log r_{80})'$ minus the sum of the
474 negative values of this quantity. The concern of long sampling times required for accurate results
475 is sometimes addressed by determining total number fluxes at the cost of size resolution. These
476 long sampling times, which become more pronounced with increasing particle size due to the
477 associated decreasing concentrations, provide a practical limit on the size to which these methods
478 can be applied to values of r_{80} less than several micrometers.

479 Eddy correlation has been used to infer SSA fluxes in only a few studies. *Nilsson*
480 *and Rannik* [2001] and *Nilsson et al.* [2001] made 175 hours of measurements of all particles
481 with dry mobility diameter (roughly equal to r_{80}) greater than $0.01 \mu\text{m}$ from shipboard in the
482 Arctic at wind speeds (at 35 m above sea level) from 4 to 13 m s^{-1} . Measured number
483 concentrations of particles of these sizes were reported as $100\text{-}200 \text{ cm}^{-3}$. Using modeled dry
484 deposition fluxes, the investigators converted the measured net total (as opposed to size-
485 dependent) flux to a total effective production flux, which they fitted to an exponential
486 dependence on wind speed (Appendix). There are concerns as to the confidence that can be
487 placed in their formulation because of the large magnitude of the modeled dry deposition flux
488 (which sometimes exceeded the net upward flux), the lack of any significant correlation between
489 wind speed and sea-salt mass for dry mobility particle diameter $d_p < 0.16 \mu\text{m}$, discrepancies in
490 the relations between wind speed and concentrations of total aerosol number and those of sea-salt
491 mass for larger and for smaller particles, and ambiguity about what types of particles contributed
492 to the upward fluxes. Recognizing these concerns, *Nilsson et al.* [2001] stated that “a more
493 careful examination of all data is needed before we can make any conclusion about the source
494 and characteristics of the upward aerosol number flux.” An additional concern with the
495 expression presented by *Nilsson et al.* [2001] is that it yields an unrealistically high production
496 flux; for $U_{10} = 10 \text{ m s}^{-1}$, this expression would result in a rate of increase in the number
497 concentration of aerosol particles (assumed uniformly distributed over a marine boundary layer
498 height of 0.5 km) of approximately 320 cm^{-3} per day. Such a rate would be inconsistent with
499 measured concentrations and a typical residence time against precipitation of ~ 3 days [*LS04*, p.
500 72].

501 **3.5. Whitecap Method**

502 The whitecap method infers the SSA production flux from measurements of size-
503 dependent SSA production from laboratory simulations or from the surf zone, as a proxy for
504 oceanic whitecaps, by scaling the production flux per white area, $dF_{\text{wc}}/d\log r_{80}$, to the ocean using
505 the oceanic whitecap fraction, W . The oceanic production flux is thus given by

506

$$507 \quad \frac{dF}{d \log r_{80}} = W \times \frac{dF_{wc}}{d \log r_{80}}. \quad (8)$$

508
 509 The fundamental assumption of this method is that the number of SSA particles of any given size
 510 produced per unit time and area is the same for any white area, either in the laboratory, the surf
 511 zone, or over the ocean, independent of the means by which this white area was produced,
 512 provided the whiteness exceeds some threshold.

513 **3.5.1. Determination of the Oceanic Whitecap Fraction**

514 The oceanic whitecap fraction has been determined from photographs or video
 515 recordings of the sea surface from ships, towers, or aircraft, with aircraft measurements typically
 516 yielding values of W that are up to an order of magnitude greater than those from shipboard
 517 photographs [LS04]. In the past, video determinations of W have typically resulted in values
 518 roughly an order of magnitude less than those determined by photographs, although
 519 technological improvements in video and use of digital video may have changed this situation
 520 (an intercomparison of whitecap determination from film, video, and digital images would
 521 provide much needed information on this subject). However, for both photos and videos,
 522 regardless of the medium (i.e., film, analog magnetic tape, or digital), the decision on what is
 523 "white" must be made arbitrarily, introducing unavoidable subjectivity in determining W and,
 524 thus, in the production flux. Moreover, nothing in the choice of this threshold ensures that the
 525 resulting values of W are the pertinent ones for determining SSA production and, in fact, what is
 526 "suitable" cannot be determined from image analysis.

527 Observations from space-based sensors offer the prospect of routinely determining W on
 528 regional and global scales and of determining parameterizations by use of local (*in situ*) or
 529 remote-sensing measurements of controlling variables such as wind speed and air and sea
 530 temperatures. Such observations would permit characterizing the whitecap fraction, its temporal
 531 and spatial variability, and its dependence on controlling variables, with the expectation of
 532 leading eventually to improved models of W and, with this, of the SSSF via Eq. 8.

533 The whitecap fraction can be detected with satellite-based instruments because of the
 534 distinct remote sensing signature of whitecaps in several regions of the electromagnetic spectrum

535 [Koepke, 1986]. In the visible region the whitecap fraction can be quantified photographically on
536 the basis of enhanced reflectivity of solar radiation by whitecaps [Whitlock *et al.*, 1982; Frouin *et*
537 *al.*, 1996; Kokhanovsky, 2004]. In the infrared (IR), both reflectivity and emissivity contribute to
538 the signal from the whitecaps [Jessup *et al.*, 1997; Marmorino and Smith, 2005]. In the
539 microwave region, for which measurements yield the surface brightness temperature T_B ,
540 whitecaps are highly emissive compared to adjacent non-white areas [Nordberg *et al.*, 1971;
541 Rose *et al.*, 2002; Aziz *et al.*, 2005; Padmanabhan *et al.*, 2006].

542 Different regions of the electromagnetic spectrum exhibit different advantages and
543 challenges for remote sensing of whitecap fraction. Measurements in the visible have the
544 advantage of the direct relation of the signal to the white area commonly characterized in
545 laboratory experiments, but correction for extinction and for scattering of light out of and into the
546 optical path through the atmosphere (atmospheric correction) is especially demanding in the
547 visible and IR regions. The advantages of using microwave frequencies, specifically the ability
548 to determine whitecap fraction at night, penetration of microwave radiation through clouds, and
549 minimal difficulty in atmospheric correction, make this approach very attractive. However,
550 difficulties arise in modeling the sea surface emissivity, especially in distinguishing signals
551 emanating from foamy regions (i.e., whitecaps) from those emanating from areas where the sea
552 surface has been roughened by the wind. As noted above, there is no demonstration that the
553 whitecap fraction determined by remote sensing in any region of the electromagnetic spectrum is
554 the most pertinent to SSA production.

555 The oceanic whitecap fraction W has typically been parameterized as a function of
556 only U_{10} . Numerous expressions for $W(U_{10})$ have been proposed, many of which are power laws
557 with an exponent near 3. The expression of Monahan and O'Muircheartaigh [1980, hereinafter
558 *MO'M80*],

559
560
$$W(U_{10}) = 3.84 \times 10^{-6} U_{10}^{3.41}, \quad (9)$$

561
562 where U_{10} is in m s^{-1} , is frequently used, despite nearly 30 years of subsequent measurements.
563 These later measurements have demonstrated many uncertainties regarding the dependence of W

564 on U_{10} ; as noted in Section 2, W can vary by over an order of magnitude for the same U_{10} [LS04;
565 *Anguelova and Webster, 2006*]. W must thus depend also on other atmospheric and/or oceanic
566 properties in addition to U_{10} ; attempts to include additional variables in the parameterization of
567 W are examined in Section 4.1.1.

568 **3.5.2. Determination of the SSA particle Flux per White Area**

569 Determinations of the SSA production flux per white area have employed several
570 types of laboratory “whitecaps,” both continuous (such as those formed by a falling stream of
571 water or by forcing air through a frit below the water surface) and discrete (such as those formed
572 by simulating a wave-breaking event by colliding two parcels of water). For experiments using
573 the former approach, bubbles and resulting SSA are generated by one of two basic mechanisms:
574 the first being air forced through diffusers, sintered glass filters, or other porous material, and the
575 second being plunging water jets or weirs, each mechanism producing a continuous whitecap
576 from which the resultant SSA is entrained into an air stream and the number concentration
577 measured. Measurements of size-dependent number concentrations $dN/d\log r_{80}$ can be used to
578 determine the size-dependent SSA production flux per white area $dF_{wc}/d\log r_{80}$ using the flow
579 rate Q of air entraining the resultant SSA and the area of the surface covered by bubbles A
580 according to

$$581 \frac{dF_{wc}}{d \log r_{80}} = \frac{Q}{A} \frac{dN}{d \log r_{80}}. \quad (10)$$

583 Such an approach requires determination of the “white” area, the criterion for which, as in field
584 measurements, is necessarily somewhat arbitrary.

585 Estimation of the SSA production flux from measurements involving discrete
586 whitecaps additionally requires knowledge of lifetimes of oceanic whitecaps; these have been
587 determined from photographs or videos of laboratory whitecaps. The SSA production flux per
588 white area has also been estimated from measurements in the surf zone. Specifically, the integral
589 over height of the number concentration of the aerosol resulting from the surf zone is used
590 together with the wind speed and the fraction of the white area in the surf zone to estimate the
591 production flux per white area. For both the surf-zone and laboratory approaches, the

592 contribution from background aerosols must be subtracted out, although in many situations this
593 is negligible compared to the much larger signal resulting from active production by the
594 surrogate whitecap.

595 Interpretation of the type of flux determined by the whitecap method requires some
596 care. The production flux per white area determined from laboratory whitecaps is an interfacial
597 flux, whereas that determined from measurements of aerosol production in the surf zone more
598 closely approximates an effective flux. Additionally, because laboratory experiments are
599 currently incapable of simulating upward entrainment of SSA particles, they are restricted to
600 determining the interfacial production flux. However, such laboratory experiments determine the
601 flux of only bubble-produced drops and not spume drops, and thus yield only a fraction of the
602 interfacial production flux. Because nearly all applications of the whitecap method have been
603 restricted to particles with $r_{80} \lesssim 10 \mu\text{m}$, over which range the interfacial and effective production
604 fluxes are nearly the same, no further distinction is made regarding the type of flux determined
605 by investigations involving the whitecap method, and it is assumed that such fluxes can be
606 compared with those inferred by other methods discussed here.

607 Laboratory investigations allow for controlled experiments on the effects of
608 parameters such as salinity, water temperature, and surface-active substances on the magnitude
609 and size distribution of the production flux. However, interpretation of laboratory experiments
610 requires assumptions regarding the applicability of laboratory conditions to conditions
611 representative of breaking waves in the open ocean. Laboratory breaking waves and whitecaps
612 have different characteristics from those over the ocean, and vastly different sizes. Few
613 laboratory experiments have employed more than a single method for producing whitecaps or
614 determined whether scaling holds over a range of sizes of these whitecaps; such work might
615 enhance confidence in extrapolating results from laboratory whitecaps to SSA production by
616 oceanic whitecaps.

617 A concern with investigations involving bubbles produced by frits is the accuracy
618 with which the size-dependent SSA production flux (including its salinity and temperature
619 dependences) characteristic of breaking waves in the open ocean is modeled by the laboratory
620 study because the bubble formation process at the frit is an entirely different physical process

621 than that by which bubbles are produced in the ocean. Additionally, because bubbles produced
622 by frits are typically smaller than those thought capable of producing film drops, and the
623 particles produced are smaller than those reported for jet drops, the question arises as to the
624 extent to which production fluxes determined from these measurements might be artifacts of the
625 experimental approach.

626 Similarly, a concern with the surf zone approach is the representativeness of surf-
627 zone white area as a model for breaking waves and SSA production in the open ocean. In
628 contrast to the open ocean, wave breaking in the surf zone is strongly influenced by drag against
629 the shallow sea floor, whose depth is comparable to that to which air bubbles are entrained by
630 breaking waves. Interaction with the sea floor almost certainly modifies the wave-breaking
631 process and bubble production. The width of the surf zone, the turbulent dispersion velocity, and
632 the height of the plume of the aerosol produced by the surf zone are influenced by wind speed,
633 and these quantities are also affected by local conditions and topography. These influences
634 further call into question the assumption of constant flux per white area needed to extrapolate
635 results from the surf zone to SSA production in the open ocean.

636 **3.5.3. SSA production flux formulations**

637 The whitecap method of estimating the SSA production flux has seen and continues
638 to see widespread use; ten formulations based on this method are compared by *LS04*. One widely
639 used formulation (Appendix) is that of *Monahan et al.* [1986], who combined results from
640 measurements of SSA production from a discrete laboratory whitecap of initial area 0.35 m^2 , the
641 lifetime of other laboratory whitecaps calculated assuming exponential decay, and Eq. 9 for W ;
642 the stated range of validity was $r_{80} = 0.8\text{-}8 \text{ }\mu\text{m}$. Other formulations from the same group differed
643 from this one by as much as an order of magnitude over this size range. A modification of this
644 formulation (Appendix), which extended the r_{80} range of applicability to 0.07 to $20 \text{ }\mu\text{m}$, was
645 proposed by *Gong* [2003], who tuned the formulation so that size-dependent SSA number
646 concentrations calculated with a 1-D column model matched those reported by *O'Dowd et al.*
647 [1997] from measurements on a single cruise in the North Atlantic. The limits attributed to this
648 formulation might also be questioned; *Gong* stated (incorrectly) that the *Monahan et al.* [1986]
649 formulation applied for r_{80} up to $20 \text{ }\mu\text{m}$ (instead of $8 \text{ }\mu\text{m}$), and that their new formulation yields

650 “reasonable” size distributions for r_{80} as low as $0.07 \mu\text{m}$, despite the fact that the measurements
651 of *O’Dowd et al.* [1997] were limited to $r_{80} > 0.1 \mu\text{m}$.

652 Another formulation of the SSA production flux formulation based on the whitecap
653 method was presented by *Mårtensson et al.* [2003], who measured the flux of particles produced
654 from a white area of $3 \times 10^{-4} \text{m}^2$ formed by forcing air through a frit with pore size (presumably
655 diameter) $20\text{--}40 \mu\text{m}$ that was located 4cm below the water surface. Based on such measurements
656 at four different temperatures and three different salinities (but only a single frit size and flow
657 rate), *Mårtensson et al.* presented a formulation for the size- and temperature-dependent
658 production flux per white area at salinity 33 (near that of seawater) for dry mobility particle
659 diameter d_p (approximately equal to r_{80}) between $0.02 \mu\text{m}$ and $2.8 \mu\text{m}$. They combined this result
660 with the *MO’M80* formula given above for W (Eq. 9) to arrive at a formulation for the oceanic
661 SSA production flux (Appendix). The temperature dependence of this formulation accounts only
662 for the temperature dependence of SSA production per white area determined in the laboratory
663 and does not account for any possible temperature dependence of the whitecap fraction, although
664 there are indications that such a dependence exists [LS04]. For $U_{10} = 10 \text{m s}^{-1}$, this formulation
665 yields a rate of increase in the SSA number concentration (assumed uniformly distributed over a
666 marine boundary layer height of 0.5km) of near 170cm^{-3} per day at 25°C , and near 270cm^{-3} per
667 day at 5°C , resulting in atmospheric number concentrations much greater than those typically
668 measured.

669 The surf zone approach was used by *de Leeuw et al.* [2000], who reported
670 concentration measurements at piers at two locations on the coast of California and presented a
671 formulation for the SSA production flux per white area (Appendix) over the r_{80} range ~ 0.4 to
672 $\sim 5 \mu\text{m}$ on the assumption that the entire surf zone acted like a whitecap (i.e., the whitecap
673 fraction in the surf zone was unity); note that as originally presented, this formulation was
674 missing a factor of 10^6 [LS04, p.222]. The integral of the number concentration over the height
675 of the plume was based on concentration measurements at two heights (7 and 15m in La Jolla; 5
676 and 12m in Moss Landing) under the assumption of an exponential decrease with height.
677 According to this formulation, the production flux per white area depends exponentially on wind
678 speed, with nearly an order of magnitude difference between the flux at the lowest wind speeds

679 ($U_{10} = 0-2 \text{ m s}^{-1}$) and the highest (9 m s^{-1}). This dependence likely reflects transport phenomena
680 and possibly higher swell resulting in more vigorous wave breaking with increasing wind speed,
681 but such a dependence calls into question the extent to which this approach simulates production
682 in the open ocean and additionally violates the assumption of constant production flux per white
683 area.

684 **3.6. Summary**

685 Intrinsic to any formulation for the SSA production flux, either effective or
686 interfacial, is an associated uncertainty. In view of the large spread of determinations of
687 production flux for a given set of environmental conditions, *LS04* characterized this uncertainty
688 as a multiplicative quantity, denoted by \times , equivalent to an additive uncertainty of \pm associated
689 with the logarithm of the production flux, and thus in a plot of the logarithm of the production
690 flux versus r_{80} , such a measure of uncertainty corresponds to equal distances above and below
691 the best estimate production flux. They intended this quantity to provide an estimate of the range
692 about the central value within which the actual production flux might be expected to lie such that
693 it would be difficult to restrict the range to much less than this factor. Presenting the uncertainty
694 associated with a given formulation provides a criterion for whether or not two different
695 formulations can be said to “agree” and allows a means for determining the precision to which a
696 formulation should be presented. Additionally, such an uncertainty provides context for deciding
697 whether features in the size distribution might be considered to be characteristic of actual
698 production fluxes rather than statistical fluctuations. This uncertainty is essential also as input to
699 subsequent use of a formulation, for example, in assessing the relative enhancement of CCN
700 number concentration pertinent to the enhancement of cloud albedo by anthropogenic aerosols.

701 Some 40 SSA production flux formulations were presented and compared by *LS04*.
702 Based on their analysis of these formulations and numerous other data sets, *Lewis and Schwartz*
703 proposed a formulation (Appendix) for the effective SSA production flux for particles with
704 $0.1 \mu\text{m} < r_{80} < 25 \mu\text{m}$ as a lognormal size distribution of the form $dF/d\log r_{80}$ with a single mode,
705 and a 2.5 power wind speed dependence for $5 \text{ m s}^{-1} < U_{10} < 20 \text{ m s}^{-1}$. Associated with this
706 formulation is a multiplicative uncertainty of a factor of 5 about the central value. Because of the
707 large number of data sets upon which this formulation was based, *LS04* expressed the view that a

708 substantial reduction of this uncertainty would require more than close agreement of a few new
709 formulations.

710 Although it had been conclusively demonstrated that sea-spray particles with
711 $r_{80} < 0.1 \mu\text{m}$ are formed by the bursting of individual bubbles [e.g., *Blanchard*, 1963; *Day*, 1964;
712 *Resch and Afeti*, 1992] and from bubble bursting associated with swarms of bubbles [*Cipriano*
713 *and Blanchard*, 1981; *Cipriano et al.*, 1983; *Cipriano et al.*, 1987; *Mårtensson et al.*, 2003],
714 extensive measurements from a large number of investigators led *LS04* to conclude that sea-salt
715 particles with $r_{80} < 0.1 \mu\text{m}$ constitute only a small fraction of the number of aerosol particles
716 present in that size range in the marine atmosphere, and only a small fraction of the number of
717 sea-spray particles produced. However, recent observations (Section 4) suggest that SSA
718 particles with $r_{80} < 0.1 \mu\text{m}$ may occur in appreciable concentrations in the marine atmosphere. If
719 these observations are correct, then one possibility is that the particles detected are *sea-spray*
720 particles, that is, particles formed at the sea surface by bursting bubbles consisting mostly of
721 organics or other substances but containing little *sea salt*. A possible explanation for the previous
722 results is that differences in composition would result in differences in hygroscopic and other
723 properties, causing the particles not to have been recognized as SSA particles. This issue remains
724 qualitatively and quantitatively unresolved, and the production and fate of SSA particles in this
725 size range are currently major topics in this field.

726 **4. Recent Experimental and Observational Findings**

727 Experimental and data-processing techniques have been further developed in the last
728 several years, and results from laboratory and field experiments have provided new insights
729 pertinent to the SSA production flux. These results relate, in particular, to the whitecap method,
730 micrometeorological methods, and the chemical composition of SSA. The following sections
731 discuss each of these aspects.

732 **4.1. Whitecap Method**

733 **4.1.1. Photographic Measurements of Whitecap Fraction**

734 Five new data sets of whitecap fraction have been reported, four in coastal regions under
735 fetch-limited conditions [*Lafon et al.*, 2004, 2007; *Sugihara et al.*, 2007; *Callaghan et al.*,

736 2008a], and one in open-ocean (unlimited fetch) conditions [*Callaghan et al.*, 2008b]. Details of
737 these data sets (Table 3) show the ranges of various meteorological and oceanographic variables
738 (in addition to wind speed) that were recorded to investigate possible dependencies on these
739 other quantities, and the means by which the images were collected and processed.

740 Recent developments in image processing of sea-state photographs have aimed at
741 decreasing the uncertainty in measured whitecap fraction in two ways, both of which have been
742 facilitated by developments in digital technology. One is removing the subjectivity in
743 determining the intensity threshold that distinguishes whitecaps from the surrounding water. The
744 other is averaging a large number of ‘instantaneous’ W values measured during an observation
745 period to obtain a single W data point.

746 To determine more objectively the intensity thresholds separating whitecaps from the
747 surrounding water, the change in instantaneous W values when the threshold was varied was
748 examined by *Sugihara et al.* [2007; their Figure 5]. An optimum threshold was identified for
749 which a change in threshold of $\pm 6\%$ resulted in a relative change in W of 10-20%; this same
750 threshold was selected and applied to all processed images. An automated whitecap extraction
751 technique was devised by *Callaghan and White* [2009] that involved two major elements: an
752 ‘image structure,’ defined as the fraction of pixels with intensities greater than a given threshold,
753 which decreased as the threshold was increased from a predetermined minimum intensity to the
754 maximum intensity of the image; and analysis of the first, second, and third derivatives of this
755 image structure with respect to the threshold intensity. The image structure was used to identify
756 whether an image contains a whitecap, and the derivative analysis was used to determine the
757 intensity threshold for an image containing a whitecap. This procedure yielded a unique
758 threshold applicable to an individual image [*Callaghan et al.*, 2008a].

759 The changes in the value of W that resulted from increasing the number of individual
760 determinations of W obtained in series of measurements during 30-minute periods to yield an
761 average was also investigated by *Callaghan and White* [2009]. The relative difference of each
762 such value of W from the data-set mean was as great as $\pm 25\%$ when 10 to 30 values were
763 averaged, gradually decreasing to about $\pm 10\%$ when 100 values were averaged and to less than
764 $\pm 3\%$ when about 500 values were averaged. Such decrease in the relative difference would be

765 consistent with expectation for averages of independent measurements. Although use of a greater
766 number of images reduced the difference from the mean calculated from 700 images, there did
767 not appear to be any bias associated with using fewer images (as would also be consistent with
768 expectation for averages of independent measurements). Similar findings were reported by
769 *Callaghan et al.* [2008a]. Additionally, it was found that the value of W for many of the images
770 would not be substantially different if sampled only a second or two apart. *Callaghan et al.*
771 [2008a] noted that the optimal sampling frequency (beyond which little improvement is seen)
772 was once every 3-4 s, approximately the lifetime of an individual whitecap. Several of these data
773 sets would appear to contain valuable information concerning statistics on the lifetimes and sizes
774 of individual whitecaps and on the temporal autocorrelation of W which have not yet been fully
775 exploited.

776 The new whitecap fraction data are plotted in Figure 2 as a function of wind speed, U_{10} ,
777 together with previous measurements that are summarized in Table 20 of *LS04* and in Table 2 of
778 *Anguelova and Webster* [2006]. The $W(U_{10})$ relationship from *MO'M80* (Eq. 9) is also shown.
779 As determinations of W by analog video are thought not to be as accurate as those by film
780 photography [*LS04*], the 'previous' measurements in Figure 2 include only photographic
781 determinations of W (Table 20 in *LS04*). Three of these new data sets were obtained using digital
782 photography or digital video (Table 3); digital video has better resolution and lower noise than
783 analog video, although it is not yet as good as film photography in spatial resolution and
784 dynamic range [*Brady and Legge, 2009; Kroeker, 2009*].

785 The newly measured values of W appear to exhibit less scatter than, but are consistently
786 less than, the bulk of those of the previous data sets. Geometric means of the ratios of the new
787 values of W to those calculated according to the *MO'M80* relationship ranged from 0.24 to 0.64
788 for the new data sets (Table 3). Furthermore, the wind speed dependence of W for these new data
789 sets seems to differ from that of the older data sets: at low wind speeds ($U_{10} < 7 \text{ m s}^{-1}$), the new
790 measurements indicate that $W(U_{10})$ increases faster than *MO'M80*, resulting in a strong increase
791 of W (from $\sim 10^{-5}$ to $\sim 5 \times 10^{-4}$) over a narrow range of wind speeds (5-7 m s^{-1}). In contrast, and in
792 agreement with the previous results, $W(U_{10})$ increases slowly for $U_{10} > 16 \text{ m s}^{-1}$, and the few data
793 for $U_{10} > 20 \text{ m s}^{-1}$ seem to plateau at a constant value, albeit that the new data are consistently

794 lower than the *MO'M80* curve throughout the entire range of wind speeds. As the new data sets
795 were based on both film photography (two sets) and digital imagery (three sets), and were
796 characterized by both limited fetch (four sets) and open ocean (one set), there seems to be no
797 obvious reason for the consistently lower values.

798 Most of the new whitecap data [*Lafon et al.*, 2004, 2007; *Sugihara et al.*, 2007;
799 *Callaghan et al.*, 2008a] have also been examined for their dependence on friction velocity u^* ,
800 but there seems to be little or no decrease of the scatter in plots of W versus u^* , compared to that
801 in plots of W versus U_{10} , a similar conclusion to that reached from the analysis of previous data
802 by *LS04*. It has been suggested that u^* could be more accurately determined if the expression of
803 roughness length explicitly included wave field characteristics (or combinations of them) such as
804 wave age (a measure of and proxy variable for fetch), significant wave height, wave steepness, or
805 energy dissipation in the breaking waves [e.g., *Drennan et al.*, 2005]. By the same token, models
806 of W that directly involve wave field characteristics might better account for variability in
807 whitecap fraction [cf. *Massel*, 2007, Chapter 7]. For example, using the so-called breaking-wave
808 parameter, or windsea Reynolds number, $R_b = u^{*2}/(\nu_a f_p)$ [*Zhao and Toba*, 2001], where ν_a is the
809 kinematic viscosity of air and f_p the frequency peak of the wave spectrum, to represent the sea-
810 state-dependent whitecap fraction has yielded improved prediction of the transfer velocity of
811 CO_2 [*Wolf*, 2005; *Soloviev et al.*, 2007]. Consequently it has been suggested that
812 parameterizations of W in terms of wave age [*Lafon et al.*, 2004, 2007; *Guan et al.*, 2007;
813 *Sugihara et al.*, 2007; *Callaghan et al.* 2008a] might lead to similar improvement in predicting
814 the SSA particle flux in Eq. 8 through improved estimates of W .

815 The analysis of whitecap observations by *Callaghan et al.* [2008b] supports this premise.
816 *Callaghan et al.* sorted data into periods with decreasing and increasing wind as surrogates for
817 developed (old) seas (defined as a sea state produced by winds blowing steadily for fetch of
818 hundreds of kilometers and duration of several days) and undeveloped (young) seas,
819 respectively, and reported that for U_{10} below 9 m s^{-1} there seemed to be no difference in the
820 relation between W and U_{10} between the two data sets, whereas for U_{10} greater than 9 m s^{-1} W
821 values from periods of decreasing wind were 30-70% higher than those from periods of
822 increasing wind. Although such measurements demonstrate the contribution of sea state to the

823 variability of W at a given U_{10} , the reported dependence accounts for only a small fraction of this
824 order-of-magnitude variability.

825 **4.1.2. Satellite-Based Measurements of Whitecap Fraction**

826 Measurements made with satellite-borne microwave sensors infer W from surface
827 brightness temperature T_B determined from the emitted radiance, which increases with increasing
828 whitecap fraction, as opposed to detecting individual whitecaps. Although the dependence of W
829 on T_B might be calculated from a simple empirical relationship [Wang *et al.*, 1995], a physically
830 sound approach for obtaining W requires an algorithm containing multiple steps. The feasibility
831 of acquiring whitecap fraction globally from space using T_B and variables necessary for the
832 atmospheric correction (columnar water vapor and cloud liquid water path) from the Special
833 Sensor Microwave/Imager (SSM/I) was demonstrated by Anguelova and Webster [2006].
834 Because the algorithm uses satellite observations with a wide cross-track swath, W is determined
835 twice a day (once in daytime, once at night) at almost every oceanic location on Earth. Each
836 satellite-based determination of W is a value spatially averaged over the sensor footprint
837 (approximately $50 \times 50 \text{ km}^2$) at a specific local time for a given location.

838 There are two main contributions to the uncertainty of satellite-based estimates of W . One
839 is the error associated with the accuracy of models used in the algorithm that represent the
840 various relationships needed for determining W , e.g., the emissivities of the rough sea surface
841 and of whitecaps at microwave frequencies. This error might be characterized by comparing
842 satellite- and surface- or aircraft-based observations collocated in time and space. The second
843 source of uncertainty is the measurement error, which results from random and systematic errors
844 in the data used in the determination of W . Random error is quantified as the variance, σ_W^2 , of
845 the calculated W . This method does not identify or quantify systematic errors. In their feasibility
846 study Anguelova and Webster [2006, Section 3.4] evaluated the measurement error and assigned
847 a standard deviation σ_W to each W estimate; lack of concurrent *in situ* measurements prevented
848 evaluation of the modeling error. Analysis of whitecap fraction determined by the satellite-based
849 method for all days in 1998 showed that the relative standard deviation, σ_W/W , was less than
850 30% for about half of the determinations, whereas less than one-third of the individual

851 photographic measurements available at the time had this accuracy [Anguelova and Webster,
852 2006].

853 The satellite-based results for W from the algorithm of Anguelova and Webster [2006],
854 binned (as arithmetic means) by wind speed in intervals of 1 m s^{-1} , are compared in Figure 3 to
855 bin (arithmetic) averages of W determined from photographic measurements and to the $W(U_{10})$
856 parameterization of *MO'M80*. These determinations of W yield a nearly constant value of
857 approximately 0.03, independent of wind speed over the range $8 \text{ m s}^{-1} < U_{10} < 17 \text{ m s}^{-1}$, with
858 somewhat lower W as wind speed decreases for $U_{10} < 8 \text{ m s}^{-1}$, in contrast to the much stronger
859 wind-speed dependence exhibited by the photographic data and by the *MO'M80*
860 parameterization.

861 The differences between the satellite results and *in situ* photographic measurements are
862 likely due to three factors. First, the signal from a whitecap may be different in different regions
863 of the spectrum because of difference in the observed physical process, e.g., skin depth of the
864 foam in the microwave region vs. penetration depth of scattered visible radiation. Second, the
865 satellite retrieval algorithm may be incomplete; for instance, simplified emissivity models were
866 employed for foamy and rough surfaces by Anguelova and Webster [2006; Section 5]. Finally,
867 the influence of various geophysical factors captured by the satellite estimates of W , which are
868 not currently extracted nor reliably quantified, may be important. Improvement of the satellite-
869 based estimates of W requires understanding and characterizing all these factors.

870 In view of concerns over the accuracy of the space-based microwave determination of W ,
871 Anguelova and Webster [2006] suggested several possible modifications of their initial
872 algorithm, including different models for foamy and rough surfaces and independent data sets for
873 atmospheric correction. Microwave observations from the new satellite radiometric sensor
874 WindSat [Gaiser et al., 2004; Bettenhausen et al., 2006; Freilich and Vanhoff, 2006] in addition
875 to those of SSM/I provide a possibility to use independent data sets. To better represent the
876 emissivity of whitecaps in different lifetime stages, Anguelova and Webster suggested using a
877 depth profile of the void fraction within the thickness of the whitecaps instead of a constant value
878 and assuming a distribution of whitecap thicknesses over the ocean. Details of these suggestions
879 are given by Anguelova [2008] and Reul and Chapron [2003], respectively.

880 **4.1.3. Laboratory Experiments on SSA production**

881 Recent experimental studies of SSA production from laboratory-generated bubble plumes
882 by *Sellegrì et al.* [2006], *Tyree et al.* [2007], *Keene et al.* [2007], *Facchini et al.* [2008], and
883 *Fuentes et al.* [2010] have provided new data on effects of salinity, water temperature, means of
884 bubble production, and surfactants on resulting SSA particle size distributions and on the
885 resultant size-dependent organic enrichment and hygroscopic properties of these particles. Key
886 features of these experiments, and of prior similar experiments of *Mårtensson et al.* [2003], are
887 summarized in Table 4.

888 The range of conditions in these experiments could in principle provide a test of the key
889 premise of the whitecap method (Section 3.5), specifically the assumption that the size-
890 dependent production flux per white area is independent of the means by which that white area is
891 formed. However, several of the investigations reported only normalized concentrations and/or
892 did not report the white area characterizing their experiment. Nonetheless, under the assumption
893 of negligible particle loss, such normalized concentrations would exhibit the same size
894 dependence as production fluxes, permitting comparison of the results of the several studies.
895 Those experiments which provided sufficient data to allow determination of both a magnitude
896 and size distribution of a production flux are discussed further in Section 5.1.

897 There are several concerns with laboratory experiments simulating SSA production. One
898 is the extent to which laboratory whitecaps can accurately simulate breaking waves over the
899 ocean, as discussed in Section 3.5. All of the laboratory whitecaps discussed in this section,
900 whether formed by diffusers or water jets, were continuous, as opposed to open ocean whitecaps,
901 which are discrete. Large bubbles (those thought to be responsible for the production of most of
902 the small drops—i.e., those with r_{80} less than several tenths of a micrometer, which are thought
903 to be film drops) rise quickly to the surface, and after several seconds the only bubbles that
904 remain in the ocean are smaller ones, which are thought to be too small to produce film drops.
905 Thus the vast majority of the film drops would be produced during only a small fraction of the
906 lifetime of a whitecap in the ocean, in contrast to the laboratory whitecaps. Another concern with
907 laboratory experiments is the possible influences of the sides of the container on the resultant
908 whitecap. In some experiments [e.g., *Keene et al.*, 2007; *Tyree et al.*, 2007] the white area was

909 constrained by the size of the tank such that the white area was nearly the same for a range of
910 bubble volume flux (i.e., the rate of air volume in bubbles reaching the surface divided by the
911 white area, which *Tyree et al.* called the superficial bubbling velocity). Other experiments used
912 only one bubble volume flux, or varied this quantity only little. However, whether the values
913 chosen are in the range of those in oceanic whitecaps, and the possible consequences of those
914 values not being in the oceanic range, are not known.

915 Another concern with laboratory experiments as models for oceanic behavior of bubbles
916 is the short bubble rise times and distances compared to those for bubbles produced by breaking
917 ocean waves, which reach depths of up to several meters, depending on wave height, as shown
918 by acoustic observations of bubble plumes near the ocean surface (e.g., *Thorpe [1992]*). Rise
919 distances in laboratory studies are often much shorter. For example *Sellegrri et al. [2006]* and
920 *Fuentes et al., [2010]* used bubble rise distances of only a few centimeters. *Tyree et al. [2007]*
921 used rise distances of ~ 0.35 m, which they claimed approximated the circulation depth of
922 oceanic bubbles. *Keene et al. [2007]* used bubble rise distances greater than 1 m, over which
923 distance they assumed that the equilibrium size distribution would be attained before bubbles
924 reached the surface and burst.

925 A possible basis for a dependence of drop production on bubble rise time or distance is
926 the time required for organic substances to equilibrate on the air-water interface of the bubbles.
927 This equilibration time was examined by *Fuentes et al. [2010]*, who provided a theoretical
928 analysis demonstrating that equilibrium with respect to adsorption of organics would be reached
929 within 0.05 ms, much less time than rise times of bubbles even for the short distances of some of
930 the laboratory studies. On the basis of this analysis *Fuentes et al.* concluded that the depth of
931 bubble generation would play little role in the effect of organics on production and properties of
932 SSA. However this result would seem to be in contradiction with findings reported in a series of
933 laboratory studies by *Blanchard* and colleagues which indicated that the equilibrium attachment
934 of organics to the air-water interface of bubbles is attained much more slowly. *Blanchard and*
935 *Syzdek [1972, 1975]* reported that ejection heights of jet drops exhibited a dependence on bubble
936 rise distance over the range 6 to 23 cm and on bubble age for up to 10-20 s. *Detwiler and*
937 *Blanchard [1978]* reported that both bubble rise speeds and top jet drop ejection heights

938 decreased with increasing bubble age (time spent in the water), with rise speeds decreasing by
939 nearly a factor of two over the first ten or so seconds, effects that they attributed to attachment of
940 organic material to the bubble interface. In several studies Blanchard and colleagues examined
941 the dependence of enrichment of bacterial concentration in drops relative to the bulk
942 concentration on bubble age or rise distance. *Blanchard and Syzdek* [1970] reported that bacterial
943 enrichment in the top jet drop increased by approximately a factor of five when the bubble rise
944 distance increased from 1 to 30 cm. *Blanchard and Syzdek* [1972] and *Blanchard et al.* [1981]
945 reported that bacterial enrichment in jet drops increased with increasing bubble age for ages of
946 20 s or more. All of these results, which were attributed to organic attachment to the bubbles,
947 would appear to indicate that this process does not rapidly attain equilibrium.

948 Several of the size-dependent production flux measurements obtained in the newly
949 reported studies, normalized to the maximum values in the representation $dF/d\log r_{80}$, are shown
950 in Figure 4. A common feature is a rather broad maximum of the production flux in this
951 representation at r_{80} near 0.05-0.1 μm rather independent of the means of production and of the
952 bubble size distribution, although the spectral shapes differ markedly among the different
953 examples. The large differences in the size distributions of the normalized concentration (and
954 thus of the production flux), which may be as great as two orders of magnitude at $r_{80} = 0.01 \mu\text{m}$,
955 rather strongly refute the assumption that the production flux per white area is independent of the
956 means by which the white area is produced. The results presented in Figure 4 were obtained for
957 different conditions, such as artificial vs. natural sea water, water temperature, salinity, effects of
958 surfactants, and bubble generation method, the effects of which were assessed in different
959 studies. The results of these studies are presented here and possible causes for differences are
960 examined.

961 The effect of salinity on the production flux size distribution was examined by
962 *Mårtensson et al.* [2003] (salinities 0, 9.2, and 33) and by *Tyree et al.* [2007] (salinities 1, 10, 20,
963 33, and 70). Both studies reported an increase in particle number production with increasing
964 salinity. *Mårtensson et al.* (their Figure 5) reported that size distributions for r_{80} between ~ 0.05
965 and 0.1 μm were nearly the same for salinities 9.2 and 33, and that for larger SSA particles the
966 number fluxes for salinity 33 were increasingly greater than for salinity 9.2 as r_{80} increased, up to

967 nearly an order of magnitude for r_{80} larger than approximately 1 μm . *Mårtensson et al.* argued
968 that the size distributions near $r_{80} = 0.05 \mu\text{m}$ shifted to slightly lower sizes at lower salinity,
969 consistent with the hypothesis that formation radii were independent of salinity, although this
970 shift did not occur for larger particles. In contrast to these results, *Tyree et al.* observed little
971 change in the shape of their size distributions, with only a small increase ($\sim 15\%$) in the value of
972 r_{80} of particles with increasing salinity from 10 to 70 (their Figure 4). *Tyree et al.* did, however,
973 report an increase in total particle number production by a factor of 2.5 with salinity increasing
974 from 10 to 70. As discussed by *LS04*, there is a transition in the coalescence behavior of bubbles
975 that occurs near salinity 10, which results in very different bubble size distributions and thus
976 perhaps SSA particle size distributions between lower and higher salinities to which it may be
977 possible to attribute some of these results.

978 The effect of water temperature on the resultant size distribution was investigated by
979 *Mårtensson et al.* [2003] (-2, 5, 15, and 25°C) and by *Sellegrì et al.* [2006] (4 and 23°C).
980 *Mårtensson et al.* found nearly identical size distributions for -2 and 5°C, and little change
981 between these and the size distribution at 15°C, although at both 15 and 25°C there was a
982 decrease in the magnitude of the production flux by a factor of 2-3 for $r_{80} < 0.1 \mu\text{m}$ and an
983 increase by a factor of 5-10 for $r_{80} > 1 \mu\text{m}$. *Sellegrì et al.* reported an increase in the production
984 flux of particles with $r_{80} < 0.7 \mu\text{m}$ at 4°C relative to that at 23°C, and a decrease at greater r_{80} ,
985 although much of this difference could alternatively be attributed to a decrease in the values of
986 r_{80} by $\sim 30\%$ at the lower temperature.

987 The effects of different bubble generation methods on the resultant aerosol size
988 distribution and properties were examined by *Sellegrì et al.* [2006], *Tyree et al.* [2007], and
989 *Fuentes et al.* [2010]. *Sellegrì et al.* noted different size distributions (their Figure 2) for different
990 methods, a weir and diffusers with three pore sizes, with $dN/d\log r_{80}$ exhibiting a maximum near
991 $r_{80} = 0.1 \mu\text{m}$ for each method, but with the size distribution produced by the weir having a
992 narrower distribution near this maximum and an additional contribution from particles with r_{80}
993 near 0.35 μm . *Tyree et al.* reported that the production flux per white area obtained using a
994 diffuser with a pore size (presumably diameter) 140 μm was up to a factor of 4 greater than when
995 using one with pore size 80 μm at the same bubbling rate. *Fuentes et al.* [2010] reported large

996 differences in the magnitude and shape of the size distribution of number concentration (their
997 Figure 6) and hence of inferred SSA production flux, produced by plunging water jets and by
998 diffusers with different pore sizes, with the size distribution (in the form $dN/d\log r_{80}$) produced by
999 the water jets being bimodal with maxima at r_{80} near 0.05 and 0.15 μm , that from an aquarium
1000 diffuser having a single broad maximum near $r_{80} = 0.06 \mu\text{m}$, and that from the sintered glass
1001 filter (pore size, presumably diameter, 30 μm) having a narrow maximum near $r_{80} = 0.06 \mu\text{m}$,
1002 with a much smaller secondary maximum near $r_{80} = 0.25 \mu\text{m}$. These size distributions are also
1003 shown in Figure 4.

1004 The dependence of production flux on bubble volume flux was investigated by *Tyree et*
1005 *al.* [2007] and *Keene et al.* [2007]. *Tyree et al.* reported that a higher bubble volume flux could
1006 yield more than an order of magnitude increase in the total number production flux per white
1007 area. *Keene et al.* also reported an increase in the magnitude of this quantity with increased
1008 bubble volume flux, although shapes of size distributions were similar. These dependences,
1009 together with results of *Mårtensson et al.* [2003], are shown in Figure 5. In view of the strong
1010 dependences shown in the figure, bubble volume flux would seem to be an important property of
1011 whitecaps influencing the SSA production flux per white area. Certainly it would seem that a
1012 whitecap property such as this would be much more useful than an arbitrary threshold of "white"
1013 in relating SSA production flux to white area and ultimately in developing more accurate
1014 parameterizations for SSA production flux.

1015 The effects of surfactants on SSA production were investigated by *Sellegrì et al.* [2006],
1016 who added sodium dodecyl sulfate (SDS) to artificial seawater, *Tyree et al.* [2007], who
1017 investigated natural seawater containing different organic compositions and artificial seawater to
1018 which 0.1 and 10 mg L^{-1} oleic acid was added, and *Fuentes et al.* [2010], who added exudate of
1019 the diatom *Thalassiosira rotula* to natural filtered seawater at a concentration 512 μM ,
1020 representative of dissolved organic carbon (DOC) concentration in seawater in areas of high
1021 biological activity.

1022 Particle size distributions produced using artificial seawater were reported by *Sellegrì et*
1023 *al.* [2006] as being similar to those using natural seawater, although they were shifted toward
1024 smaller values of r_{80} for SDS concentrations greater than 3 mg L^{-1} . The investigators stated that

1025 these results should be considered exploratory because their comparison to long-term, seasonally
1026 varying data of particle size distributions obtained at the Mace Head atmospheric research station
1027 (located on the west coast of Ireland) showed that SDS does not accurately simulate the effects
1028 of the surfactants present in the natural environment.

1029 The natural seawater samples of *Tyree et al.* [2007] exhibited differing organic
1030 composition because they had been collected in winter (DOC concentration 2.3 mg C L^{-1} ;
1031 chlorophyll concentration 0.1 mg m^{-3}) and summer (DOC concentration 3.1 mg C L^{-1} ;
1032 chlorophyll concentration 1.8 mg m^{-3}). The size distributions of the SSA particles produced in
1033 their experiments were nearly the same, regardless of the type of water (artificial, filtered, or
1034 unfiltered seawater), with little dependence on the amount of surfactant added. The winter
1035 samples of natural seawater produced 20-40% more SSA particles than the summer samples.
1036 Comparison of the size distributions of the SSA particles produced with the summer and winter
1037 samples showed that the natural organic matter exerted little effect on the numbers or radii of the
1038 produced SSA particles. Bubbling artificial seawater artificially enriched with oleic acid
1039 produced approximately twice as many drops as natural seawater. The investigators concluded
1040 that the nature of organic matter affects foam droplet production and that oleic acid is a poor
1041 surrogate for natural organic matter for studies of foam production. These findings, as well as
1042 those of *Sellegrì et al.* [2006], would seem to raise questions over the accuracy of laboratory
1043 experiments as models for oceanic SSA production.

1044 Hygroscopic growth and CCN activity for artificial seawater were examined by *Fuentes*
1045 *et al.* [2010], who reported that these properties were not affected by the bubble generation
1046 technique; however for the organically enriched natural seawater hygroscopic growth was
1047 suppressed, with the degree of suppression depending on the aerosol generation technique. The
1048 main differences in hygroscopic growth resulting from different generation techniques were
1049 observed for $\text{RH} > 75\%$, with the plunging-water jet presenting the greatest suppression of
1050 growth. The influence of organics on the CCN activity exhibited little size dependence, with only
1051 a slight increase in the critical supersaturation compared to seawater samples to which no
1052 organics were added.

1053 Chamber studies aimed at determining the size-dependent mass fraction of organic
1054 material in SSA particles produced from natural seawater were conducted by *Keene et al.* [2007]
1055 and *Facchini et al.* [2008]. *Keene et al.* used highly oligotrophic seawater (concentrations of
1056 organic substances such as formate, acetate, oxalate, and methylsulfonate were below detection
1057 limits) pumped from the ocean into a laboratory near the coast of Bermuda, and produced SSA
1058 by bubbling the water through diffusers. *Facchini et al.* used highly productive seawater
1059 (average chlorophyll-a concentration 1.4 mg m^{-3}) pumped into a sealed tank on a ship in the
1060 North Atlantic west of Ireland during an algae bloom, and produced SSA using a water jet.

1061 Enrichment of calcium with respect to surface water concentrations (median enrichment
1062 factor 1.2), which may have been caused by fragments of biogenic CaCO_3 or from complexes
1063 with organic matter, was reported by *Keene et al.* [2007]. These investigators also reported that
1064 all size-resolved and bulk aerosol samples were highly enriched in organics, with the enrichment
1065 decreasing from greater than 10^5 for r_{80} near $0.06 \mu\text{m}$ (the lowest size range) to slightly greater
1066 than 10^2 for r_{80} near $4 \mu\text{m}$, and again increasing slightly to near 10^3 for r_{80} near $14 \mu\text{m}$; the
1067 median enrichment factor for all samples was near 400. The organic mass fraction exhibited
1068 similar behavior, decreasing from near 80% for r_{80} near $0.06 \mu\text{m}$ to 40-50% for r_{80} between 0.06
1069 and $0.6 \mu\text{m}$ and to less than a few percent for r_{80} between 0.6 and $4 \mu\text{m}$, then again increasing to
1070 near 40% for r_{80} near $14 \mu\text{m}$. In all size ranges except the smallest, the dominant contribution to
1071 aerosol mass was provided by sea salt.

1072 A strong dependence of the organic (water-soluble and water-insoluble organic matter)
1073 mass fraction on particle size (Figure 6), with the enrichment factor (relative to the bulk
1074 seawater) increasing with decreasing particle size, was also reported by *Facchini et al.* [2008].
1075 SSA particles with ambient radii greater than $0.5 \mu\text{m}$ contained more than 90% of the inorganic
1076 sea-salt mass; particles with ambient radii less than $0.25 \mu\text{m}$ consisted mainly of organic matter,
1077 most of which was water-insoluble. This water-insoluble organic matter (WIOM) exhibited
1078 substantial enrichment (relative to the bulk solution) with mass fraction increasing from 3 to 77%
1079 as radius (at 50-70% RH) decreased from 4 to $0.06 \mu\text{m}$, with only a very minor fraction ($\sim 3\%$) of
1080 water-soluble organic matter (WSOM); the remaining mass was sea salt. The WIOM was
1081 attributed to colloids and aggregates exuded by phytoplankton on the basis of functional nuclear

1082 magnetic resonance spectroscopy. Such an increasing fraction of organic matter with decreasing
1083 drop radius is consistent with the volume fraction of adsorbed surfactant organic matter as a
1084 function of SSA particle size as evaluated with a thermodynamic model [*Oppo et al.*, 1999].
1085 Despite the small mass fraction of organic matter in larger particles (radius 2 to 4 μm at 50-70%
1086 RH), the total mass of organic matter in these particles was approximately half the total organic
1087 mass in aerosol particles with radius (at these RH values) less than 4 μm . *Facchini et al.* also
1088 reported that the WIOM-to-sea-salt mass ratio was similar to that observed in aerosol samples at
1089 Mace Head.

1090 **4.1.4. Surf Zone Measurements**

1091 The production of SSA in a surf zone was determined by *Clarke et al.* [2006] from
1092 measurements on a 20-m tower, 20-30 m from the water's edge on a beach in Hawaii, during
1093 onshore winds (typical wind speed 7 m s^{-1}). Aerosol properties were characterized using a
1094 differential mobility analyzer (DMA), an optical particle counter (OPC), and an aerodynamic
1095 particle sizer (APS), which together covered the size range of $0.01 \mu\text{m} < r_{80} < 8 \mu\text{m}$. The DMA
1096 and OPC included options for sampling aerosol at ambient temperature or at 300-360°C to permit
1097 determination of size distributions of volatile and residual refractory aerosol (the latter being
1098 typically sea salt, non-volatile organics, dust, or soot). These instruments were complemented
1099 with two condensation particle counters (CPCs), one operated at ambient temperature, the other
1100 at 360°C; a tandem DMA (TDMA) and a humidified TDMA (HTDMA) to examine the thermal
1101 and humidification response of selected sizes; and a three-wavelength nephelometer to determine
1102 particle light scattering. Inlets for all these instruments were placed at heights of 5, 10, and 20 m,
1103 and sampling was cycled at regular intervals.

1104 Comparison of measurements at these three heights showed that the highest level was not
1105 influenced by surf production and could thus be used for determining the upwind background
1106 concentration. SSA production in the surf zone was evaluated from the SSA concentrations
1107 measured at 5 m, after correction for background concentrations using the 20-m data. The
1108 production flux per white area was determined as described in Section 3.5 using a mean whitecap
1109 fraction in the surf zone of 40%, based on visual examinations of images. Substantial production
1110 of particles with dry radius less than 0.05 μm was found.

1111 Heated and ambient sample volumes were used by *Clarke et al.* [2006] to discriminate
1112 between refractory aerosol particles, assumed to be mainly sea salt, and other components. To
1113 further ascertain whether the detected particles were sea salt, the investigators made several tests.
1114 First, they noted the strong correlation between the concentrations of the refractory particles,
1115 most of which had dry radii less than $0.05 \mu\text{m}$, and light scattering, which would be dominated
1116 by particles with dry radius greater than $0.25 \mu\text{m}$. Chemical analysis using a flame photometric
1117 aerosol sodium detector confirmed that particles with $r_{80} > 0.09 \mu\text{m}$ were composed mainly of
1118 sea salt. SSA particles with r_{80} of $0.05 \mu\text{m}$ (previously heated to 300°C) exhibited a humidity
1119 growth factor near 1.8 from low RH to RH 76%, as expected for sea-salt particles, from which
1120 *Clarke et al.* concluded that these particles were composed mainly or entirely (80% up to
1121 possibly 100%) of sea salt. They further concluded that most of the particles with $r_{80} \geq 0.03 \mu\text{m}$
1122 produced from breaking waves were primarily sea salt. Based on their measurements, *Clarke et*
1123 *al.* presented an SSSF that extended to r_{80} as small as $0.01 \mu\text{m}$. This formulation, presented in the
1124 Appendix and discussed in Section 5.1, is shown in Figure 4 as a normalized size distribution .

1125 **4.1.5. Summary**

1126 The whitecap method requires the capability of measuring or modeling the whitecap
1127 fraction W under a given set of conditions to known accuracy and demonstration that the
1128 whitecap fraction so determined yields, within a given uncertainty, the same size-distributed flux
1129 per white area as obtained in laboratory experiments or field studies. So far, these goals have not
1130 been achieved. Demonstrating that field measurements of W are reproducible and transferable
1131 would seem, at minimum, to require simultaneous measurements by multiple groups using
1132 different platforms (e.g., shipborne, aircraft, satellite, fixed offshore platforms) and techniques at
1133 a variety of locations differing in controlling properties such as fetch and surfactant content.
1134 Simultaneous field measurements of production flux per white area would then allow
1135 comparison with flux per white area determined in laboratory experiments. Finally, algorithms
1136 for calculating W would have to be compared to measurements under a wide variety of
1137 conditions and locations by different investigators using different techniques. Only when all
1138 these requirements are fulfilled would it seem that the SSSF and the associated uncertainty can
1139 be considered accurately parameterized and confidently represented in models. However, the

1140 laboratory experiments have demonstrated that the size-dependent flux per white area depends
1141 on the means by which the white area was created, raising intrinsic questions concerning the
1142 applicability and accuracy of the whitecap method, especially with regard to the assumption of a
1143 universal production flux per white area.

1144 **4.2. Micrometeorological Methods**

1145 **4.2.1. Eddy Correlation Measurements**

1146 Eddy correlation measurements were made by *Geever et al.* [2005] at a 22 m tower at
1147 Mace Head, Ireland over a 4 week period in June and July, 1992 during which U_{22} was between
1148 7 and 18 m s^{-1} . Data were restricted to periods when the winds were from the ocean to the land
1149 and during high tide, when the distance from the base of the tower to the water was
1150 approximately 80 m. Total concentrations of particles with ambient radii from 0.005-0.5 μm (RH
1151 not reported) were measured by a CPC, and total concentrations of particles with dry radii from
1152 0.05-0.5 μm were measured by an OPC; these measurements together with 3-D wind speed
1153 measurements were used to determine particle fluxes (Appendix). The wind speed dependences
1154 of the fluxes in the two size ranges were essentially the same. A potential concern with these
1155 measurements is coastal influence and effects of surf-produced aerosol on particle fluxes.
1156 Footprint analysis by *O'Dowd, de Leeuw* and colleagues [*Geever et al.*, 2005] showed that the
1157 region contributing to the measured fluxes was almost entirely over water both at high tide and at
1158 low tide, at which the distance from the base of the tower to the water was 180 m. However, at
1159 low tide at wind speeds less than 10 m s^{-1} measured fluxes showed little correlation with wind
1160 speed and were greater than at high tide, indicating influence of the exposed intertidal zone and
1161 thereby raising concern over the applicability of such measurements even at high tide to
1162 determining SSA production fluxes representative of the open ocean. Drag coefficients measured
1163 during high tide conditions yielded a slightly stronger dependence on wind speed than mid North
1164 Atlantic values, but were comparable to values from the North Sea when water depth was greater
1165 than 30 m, from which *Geever et al.* concluded that fluxes measured during high tide conditions
1166 were characteristic of open ocean values.

1167 Fast sizing and counting of aerosol particles, required for the application of the eddy
1168 correlation technique to determination of size-dependent production flux, has become feasible

1169 with the development of the Compact Light Aerosol Spectrometer Probe (CLASP) [Hill *et al.*,
1170 2008], which measures the size distribution of particles with radii of 0.1-7 μm at a frequency of
1171 10 Hz. CLASP is a compact and lightweight OPC which can be mounted close to the wind
1172 sensor with minimal flow distortion and a short inlet tube. The combination of high sample rate,
1173 high flow rate ($50 \text{ cm}^3 \text{ s}^{-1}$), and compact design makes CLASP highly suitable for determining
1174 aerosol production flux. The accuracy of the size determination, which is by means of light
1175 scattering, depends on particle shape and index of refraction.

1176 Eddy correlation measurements using a CLASP and a traditional OPC (Passive Cavity
1177 Aerosol Spectrometer Probe – PCASP-X) to determine SSA fluxes were conducted at the 560 m
1178 pier at the Field Research Facility (FRF) in Duck (NC, USA) in autumn 2004 and 2005 [*de*
1179 *Leeuw et al.*, 2007; *Norris et al.*, 2008]. The sonic anemometer and the aerosol inlets were
1180 mounted at the seaward end of the pier at a height of 16 m above mean sea level. *De Leeuw et al.*
1181 [2007] reported measurements of fluxes in three partly overlapping ranges of r_{80} as inferred from
1182 the reported dry radii measured with the PCASP equipped with an inlet heated at 300°C :
1183 0.11 - 0.15 μm , 0.15 - 0.19 μm , and 0.11 - 0.375 μm , and as an integrated flux over the r_{80} range
1184 from 0.11 – 9.0 μm , when the wind was from the ocean at U_{10} between 3 and 16 m s^{-1} ; flux
1185 results for wind speeds lower than 7 m s^{-1} were considered unreliable. Based on the analysis of a
1186 small subset of the data, the gross particle number fluxes increased with increasing wind speed.
1187 These fluxes were fitted to a power law U^b , with values of b between 2.9 and 3.4, although the
1188 integrated flux could be better fitted (in terms of minimizing the variance) by a linear function of
1189 U_{10} than by a cubic. *Norris et al.* [2008] measured SSA particle fluxes in six size ranges of
1190 ambient radius from 0.145-1.6 μm during twenty 20-min periods in October, 2005 during which
1191 the wind was from the ocean with U_{10} from 4-12 m s^{-1} . Fluxes were converted to r_{80} values for
1192 U_{10} of 5, 10 and 12 m s^{-1} , and were fitted as linear functions of wind speed for each of the six
1193 size ranges; these fluxes are discussed in Section 5 and, normalized to the maximum value at
1194 each wind speed, presented in Figure 4, from which they can be seen to exhibit different size
1195 dependences from the majority of the production fluxes from the laboratory experiments.
1196 Reported fluxes were not corrected for dry deposition (cf. Eq. 6); this correction was estimated
1197 as 2 to 30% depending on the dry deposition formulation employed, well less than the estimated

1198 overall uncertainty, suggesting that these measurements may yield an accurate determination of
1199 the production flux. Although whitecap fraction was not reported in this study, simultaneous
1200 measurement of this quantity in conjunction with such eddy correlation measurements would
1201 permit another means of determining the flux per white area, an essential element of the
1202 whitecap method. CLASP has also been used to determine SSA production flux on a cruise in
1203 the North Atlantic in the spring of 2007 [Brooks *et al.*, 2009].

1204 **4.2.2. Gradient Method**

1205 The gradient method (Section 3.4.2) was applied by *Petelski and Piskozub* [2006] to
1206 determine the SSA production flux from 61 measurements of vertical profiles of the aerosol
1207 concentration obtained during four cruises in Arctic Seas (Norwegian Sea, Greenland Sea, and
1208 Barents Sea) in 2000-2003 [*Petelski*, 2003; *Petelski and Piskozub*, 2006]. The wind speed range
1209 was $5 \text{ m s}^{-1} < U_{10} < 12 \text{ m s}^{-1}$, and stability conditions were close to neutral. Concentrations of
1210 particles with ambient radii from 0.25 to 15 μm , at RH varying between 65 and 95%, were
1211 measured with an OPC [*Petelski*, 2005]; a single instrument was used for consecutive
1212 measurements at 5 levels between 5 and 20 m above sea level, with at least four 2-minute
1213 measurements at each level.

1214 There are several concerns with this work. For many of the size ranges, the
1215 concentrations showed no obvious decrease with height [*Petelski and Piskozub*, 2006, Figures 3
1216 and 4] with scatter around the logarithmic profile fit much larger than the stated relative
1217 uncertainties in the concentrations of 1% for particles with radius 1 μm to 20% for radius 10 μm .
1218 *Petelski and Piskozub* [2006] considered only those size bins for which the concentrations could
1219 be fitted to logarithmic profiles in height with a given accuracy, although only 60% of all
1220 measured profiles matched this criterion; such a procedure might be expected to bias the results.
1221 A wind speed dependence of U_{10}^3 was drawn on a graph of the calculated flux of surface area,
1222 although this dependence does not seem to be supported by statistical analysis (a linear least-
1223 squares fit of the logarithm of the flux versus the logarithm of the wind speed results in an
1224 exponent of 1.75 ± 0.45 if all the data are included, or 1.07 ± 0.71 if two data for $U_{10} < 3 \text{ m s}^{-1}$ are
1225 excluded).

1226 **4.3. Chemical Composition of Sea-Spray Aerosol**

1227 The size-dependent chemical composition of SSA, especially the distribution of organic
1228 material, is important in determining the RH-dependent growth of SSA particles and their ability
1229 to serve as CCN. Although prior work going back to the 1940s has shown the presence of
1230 organic material in SSA particles (Section 1), only recently have studies attempted to quantify
1231 the organic mass fraction as a function of particle size and elucidate the production mechanisms.
1232 Here recent field measurements that complement studies that have shown substantial organic
1233 fraction of laboratory-generated SSA are examined.

1234 In a series of field measurements at Mace Head, Ireland, conducted in clean marine air
1235 with minimal anthropogenic or terrestrial influences (wind from ocean to land; number
1236 concentration of particles with radii at 40-70% RH greater than $0.007 \mu\text{m}$ less than 700 cm^{-3} and
1237 black carbon mass concentration less than 50 ng m^{-3}), *O'Dowd* and colleagues [*O'Dowd et al.*,
1238 2004; *Cavalli et al.*, 2004; *Yoon et al.*, 2007] found substantially greater concentrations of
1239 organic matter in SSA during periods of high biological activity than during periods of low
1240 biological activity, which occurred during winter and during which the composition was
1241 predominantly sea salt. The enrichment of organic matter was much greater for SSA particles
1242 with ambient radius (at approximately 70% RH) in the range $0.03\text{-}0.5 \mu\text{m}$ than in the range 1-
1243 $4 \mu\text{m}$ (Figure 7). During periods of low biological activity particles with ambient radii greater
1244 than $0.25 \mu\text{m}$ were composed almost entirely of sea salt, with only 2-3% of the mass consisting
1245 of organic material, and a substantial fraction of that was WSOM. For smaller particles (ambient
1246 radius $0.06\text{-}0.25 \mu\text{m}$), sea salt accounted for about 70% of the mass, with the principal remaining
1247 components being nss-sulfate and organic carbon, each contributing about 15%. Of the organic
1248 aerosol mass, roughly 60% was WIOM. During high biological activity periods also, larger
1249 particles (ambient radius $0.5\text{-}4 \mu\text{m}$) were composed almost entirely of sea salt, although the
1250 organic mass fraction increased marginally to about 5%. However, in contrast to the low
1251 biological activity periods, organic material contributed 60% to the mass of particles with
1252 ambient radius in the range $0.125\text{-}0.25 \mu\text{m}$, with the organic fraction increasing to 85% for
1253 particles with ambient radius $0.03\text{-}0.06 \mu\text{m}$. Also striking was that the WIOM constituted

1254 approximately two-thirds of the total organic aerosol mass. Approximately half of the total
1255 WIOM mass resided in particles with ambient radius less than 0.5 μm .

1256 The hypothesis that WIOM was primary in origin was examined by *O'Dowd* and
1257 colleagues [*Ceburnis et al.*, 2008] by means of the vertical gradients of concentrations of aerosol
1258 constituents. Measurements were made of chemically speciated mass concentration for particles
1259 with ambient radii less than 0.5 μm at heights of 3, 10, and 30 m above the shore at Mace Head.
1260 Footprint analysis determined that the peak contribution to the flux was approximately 1.5-3 km
1261 off shore and that the vast majority of the contribution was from less than 10 km. These
1262 measurements showed that concentrations of sea salt and WIOM decreased with increasing
1263 height between 3 and 10 m (Figure 8), indicative of a surface source, whereas concentrations of
1264 WSOM and nss-sulfate increased with increasing height over the same range, indicative of an
1265 atmospheric source. A concern with this study is that at times the measurements at the lower two
1266 heights were influenced by surface properties differently from the measurements at the highest
1267 level as discussed in Section 4.2.1; it is thus likely that in such situations the flow at these heights
1268 was perturbed by the land and hence that observed gradients were not representative of mixing
1269 processes in the unperturbed atmosphere and cannot be used to derive quantitative flux
1270 information on transport and removal processes. Nevertheless, the gradients suggest important
1271 qualitative information on production processes, namely a surface, or primary, source for WIOM
1272 but a surface sink for WSOM, pointing to secondary aerosol formation processes. A further
1273 caveat to quantitative interpretation is that an undetermined fraction of WSOM may have
1274 originally been produced as primary WIOM, and through chemical aging may have become
1275 more oxidized and hence water-soluble. The similarity of WIOM-to-sea-salt mass ratios in
1276 ambient aerosols measured simultaneously over productive waters in the Northeast Atlantic and
1277 at Mace Head by *Facchini et al.* [2008], noted above, provides additional evidence for a primary
1278 source of the WIOM in marine aerosol.

1279 A series of field studies by *Bigg, Leck*, and colleagues suggests that aerosol particles with
1280 dry radius smaller than 0.1 μm produced by bubble bursting over the ocean consist almost
1281 entirely of organic matter [*Bigg and Leck*, 2008]. In these studies, the particles were sampled by
1282 an impactor operating at vacuum, and their chemical properties were examined with transmission

1283 electron microscopy [Bigg and Leck, 2001]. Initially, Leck and Bigg [1999] and Bigg and Leck
1284 [2001] reported occurrences of a relatively large concentration (up to 300 cm^{-3}) of solid, water-
1285 insoluble aerosol particles with dry radii less than about $0.025 \mu\text{m}$ in the Arctic marine boundary
1286 layer. These particles were accompanied by larger particles ($r_{\text{dry}} > 0.05 \mu\text{m}$), obviously of marine
1287 origin, such as bacteria and fragments of diatoms that showed very similar characteristics to
1288 colloidal particles present in bulk seawater.

1289 Strong temperature inversions during the measurements by Bigg and Leck excluded the
1290 possibility of a tropospheric source, and the presence of these particles in stable air masses over
1291 the ice that had not been in contact with open water for at least four days suggested a surface
1292 source for the observed particles. To identify such a source, Bigg et al. [2004] sampled the
1293 microlayer of open water between ice floes in the Arctic and reported the presence of suspended
1294 particulate organic matter with dry radii of $0.005\text{-}0.025 \mu\text{m}$. Comparing the properties of the
1295 particles from the Bigg et al. microlayer samples to those of aerosol particles previously
1296 observed in the overlaying atmosphere in the Arctic Ocean, Leck and Bigg [2005a, b] concluded
1297 that the particles originated from the ocean surface microlayer and were ejected into the
1298 atmosphere via bubble bursting.

1299 Subsequent studies in tropical regions have shown the presence of particles with r_{80} of a
1300 few hundredths of micrometers having chemical composition similar to that observed in particles
1301 in the Arctic, including exopolymer gels, marine micro-organisms, fragments of marine biota,
1302 and bacteria; sea salt was markedly absent from such particles [Leck and Bigg, 2005b; Leck and
1303 Bigg, 2008]. This, according to these investigators, suggests a common pattern over the ocean.
1304 The implications of these findings and the discrepancy [Leck and Bigg, 2008] between these
1305 results and those of others are discussed in Section 6.2.

1306 **5. Parameterizations of the Sea-Spray Production Flux**

1307 In view of the importance of the SSA as background, non-anthropogenic, aerosol over much
1308 of the planet, much effort has been directed to representing this aerosol in chemical transport
1309 models and climate models to examine its effects and those of anthropogenic aerosol on clouds,
1310 atmospheric radiation, atmospheric chemistry, and air quality. Such models generally simulate
1311 the life cycle of aerosols and therefore represent emissions, new particle formation, chemical and

1312 physical transformations, interactions with clouds, and removal by wet and dry deposition. An
1313 essential component of such life-cycle models is representation of the size- and composition-
1314 dependent emission of aerosol particles as a function of time and location, specifically including
1315 primary production of SSA particles as a function of meteorological and other controlling
1316 variables. Since the publication of *LS04*, several new estimates of such fluxes have been
1317 presented or may be calculated from reported laboratory studies discussed in Section 4.1.3.
1318 These newer formulations are discussed below and presented in Figure 9 for r_{80} (or r_{amb} or d_p)
1319 between 0.005 and 25 μm . To provide context, several previous flux estimates are also included
1320 in Figure 9. Both the recent and older formulations discussed in this section are listed in the
1321 Appendix together with the applicable size and wind-speed ranges.

1322 Nearly all formulations of the SSA production flux presented before 2004 were discussed,
1323 evaluated, and compared by *LS04*. Based on their analysis of these formulations and numerous
1324 other data sets these investigators presented the parameterization for the production flux of sea-
1325 salt aerosol particles for $0.1 \mu\text{m} < r_{80} < 25 \mu\text{m}$ which is presented in Figure 9 for $U_{10} = 8 \text{ m s}^{-1}$
1326 together with its associated uncertainty, to allow comparison of formulations based on newly
1327 available measurements. Several other parameterizations of the SSA production flux discussed in
1328 Section 3.1 are also presented in Figure 9 at $U_{10} = 8 \text{ m s}^{-1}$: those of *Smith et al.* [1993] and *LS04*
1329 (together with associated uncertainty) based on the steady-state dry deposition method; *LS04*
1330 (together with associated uncertainty) based on the statistical wet deposition method; *Nilsson et*
1331 *al.* [2001] based on eddy correlation; and *Monahan et al.* [1986], extrapolation of this
1332 formulation by *Gong* [2003], and formulations of *Mårtensson et al.* [2003] and by *de Leeuw et*
1333 *al.* [2000], all based on the whitecap method. The parameterizations of *Mårtensson et al.* and of
1334 *de Leeuw et al.* used the *MO'M80* formulation for W as a function of U_{10} (Eq. 9). The flux
1335 reported by *Nilsson et al.* [2001], a particle number production flux without size resolution, is
1336 plotted as if the flux is independent of d_p (approximately equal to r_{80}) over the indicated size
1337 range, such that the measured number flux is obtained as an integral over this range.

1338 **5.1. Whitecap Method**

1339 Laboratory experiments and field measurements that have been or might be used to infer
1340 the SSA production flux per white area and its dependence on water temperature, salinity, and

1341 surfactant concentration were described in Section 4.1.3. The investigations by *Tyree et al.*
1342 [2007] and *Keene et al.* [2007], provided sufficient information to permit determination of the
1343 production flux per white area. As noted in Section 4.1.3, the magnitudes of these production
1344 fluxes also differed greatly depending on experimental conditions such as the bubble volume
1345 flux, resulting in large differences even among SSA production flux estimates from a given
1346 study. These estimates, used together with the dependence of W on wind speed according to
1347 *MO'M80*, yield size-dependent SSA production fluxes.

1348 The size dependence of the production flux per white area in the representation $dF_{wc}/d\log r_{80}$
1349 was approximated by *Tyree et al.* [2007] as a single lognormal, with the geometric mean r_{80}
1350 between approximately 0.085 μm and 0.115 μm , and the geometric standard deviation between
1351 approximately 1.6 and 1.8, depending on conditions, specifically bubble volume flux and pore
1352 size of the diffuser used to produce the bubbles (their Table 1). The magnitude of the
1353 concentration of the particles thus produced increased nearly linearly with bubble volume flux
1354 (their Figure 5), implying that the production flux per white area (taken as the surface area of
1355 water in the apparatus) increased nearly quadratically with bubble volume flux according to
1356 Eq. 10 (Figure 5), varying by nearly a factor of 60 for the different bubble volume fluxes for
1357 salinity 33. Examples of size-dependent production fluxes for artificial seawater of salinity 33 at
1358 two different bubble volume fluxes are shown in Figure 9 for $U_{10} = 8 \text{ m s}^{-1}$, based on the
1359 *MO'M80* parameterization for W .

1360 The SSA production flux per white area determined from the laboratory studies of *Keene et*
1361 *al.* [2007] exhibits a nearly linear dependence on bubble volume flux (their Figures 3 and 4), in
1362 contrast to the quadratic dependence found by *Tyree et al.* (Figure 5). An estimate of the SSA
1363 production flux at $U_{10} = 8 \text{ m s}^{-1}$ based on the production flux per white area for a single bubble
1364 volume flux from *Keene et al.*, together with the *MO'M80* formulation for W , is shown in
1365 Figure 9.

1366 Measurements of SSA production resulting from a surf zone were used by *Clarke et al.*
1367 [2006] (Section 4.1.4) to derive a new formulation for the size-dependent SSA production flux
1368 per white area for dry particle diameter (approximately equal to r_{80}) range 0.01-8 μm . This
1369 formulation, together with the *MO'M80* formulation for W , provides a formulation for the SSA

1370 production flux; this is shown in Figure 9 for $U_{10} = 8 \text{ m s}^{-1}$. According to this formulation, the
1371 daily rate of increase of the number concentration of aerosol particles (assumed uniformly
1372 distributed over a marine boundary layer height of 0.5 km) for $U_{10} = 10 \text{ m s}^{-1}$ would be nearly
1373 150 cm^{-3} . As discussed in Section 4, *Clarke et al.* concluded that the majority of particles were
1374 sea-salt particles.

1375 With respect to application of the whitecap method, in addition to uncertainty arising
1376 from the SSA production flux per white area, any uncertainty in whitecap fraction W also
1377 transfers directly to production flux. From examination of Figure 2, this uncertainty at
1378 $U_{10} = 8 \text{ m s}^{-1}$ appears to be roughly a factor of ≈ 5 . Also if the lower values of W shown in that
1379 figure relative to previous measurements are sustained by further observations, a high bias in W
1380 from values calculated by the *MO'M80* parameterization by roughly a factor of 3 at this wind
1381 speed, previous estimates of production fluxes using that expression for W would appear to
1382 likewise be biased high by such a factor.

1383 **5.2. Eddy Correlation**

1384 Eddy-correlation measurements by *Geever et al.* [2005] at Mace Head (Section 4.2.1) in
1385 each of two size ranges, $r_{\text{amb}} = 0.005\text{-}0.5 \text{ }\mu\text{m}$, and $d_p = 0.1\text{-}1 \text{ }\mu\text{m}$, corrected for dry deposition to
1386 yield production fluxes, were expressed as exponential functions of wind speed at 22 m above
1387 the sea surface, U_{22} . The resulting fluxes are plotted in Figure 9, for $U_{22} = 8 \text{ m s}^{-1}$, as if the fluxes
1388 in the representation $dF/d\log r_{\text{amb}}$ (or $dF/d\log d_p$) are independent of r_{amb} (or d_p) over the
1389 respective size ranges, such that the measured number fluxes are equal to the integrals over these
1390 size ranges. According to these expressions, the daily increases in the number concentration of
1391 aerosol particles (assumed uniformly distributed over a marine boundary layer height of 0.5 km)
1392 for $U_{10} = 10 \text{ m s}^{-1}$ would be 320 and 135 cm^{-3} for the two size ranges.

1393 Noting that an exponential wind-speed dependence can introduce an artificial bias in sea-
1394 spray production at low wind speeds, *O'Dowd et al.* [2008] refitted the data in the larger size
1395 range as a power law for their regional climate model (Section 5.7). This fit agreed with that
1396 presented by *Geever et al.* to within $\sim 20\%$ for U_{22} greater than 6 m s^{-1} , below which there were
1397 only two measurements; in view of the limited range of the measurements it would seem that

1398 either functional form (or perhaps others) would yield equally good fits to the observations and
1399 thus it is not possible to identify a preferred wind-speed dependence.

1400 Eddy-correlation measurements of *Norris et al.* [2008] at Duck, NC were parameterized
1401 in terms of an exponential dependence on either U_{10} or u^* in six ranges of ambient radius. There
1402 was no clear reduction in the scatter of the flux estimates based on u^* compared to that based on
1403 U_{10} . As these measurements were not corrected for dry deposition, they yield net fluxes rather
1404 than production fluxes, although as noted in Section 4.2.1, the corrections are likely small. The
1405 fluxes according to this formulation are shown in Figure 9 for $U_{10} = 8 \text{ m s}^{-1}$. According to this
1406 formulation, the daily rate of increase of the number concentration of aerosol particles (assumed
1407 uniformly distributed over a marine boundary layer height of 0.5 km) for $U_{10} = 10 \text{ m s}^{-1}$ would
1408 be near 50 cm^{-3} .

1409 **5.3. Gradient Method**

1410 The size-dependent production flux formulation presented by *Petelski and Piskozub*
1411 [2006] based on the gradient method using measurements of the vertical distribution of aerosol
1412 concentration was modified by *Andreas* [2007; see also *Petelski and Piskozub*, 2007] to include a
1413 factor of κ , the von Karman constant. According to this formulation the size dependence of the
1414 production flux depends on wind speed. This production flux, including the factor of κ , is
1415 presented in Figure 9 for $U_{10} = 8 \text{ m s}^{-1}$. As noted in Section 4.2.2, there are serious concerns with
1416 these measurements that limit the confidence that can be placed in this parameterization.

1417 **5.4. Steady-State Dry Deposition Method**

1418 The steady-state dry deposition method was applied by *Petelski and Piskozub* [2006] to
1419 determine SSA production fluxes for ambient radii 0.25-7.5 μm based on concentrations of
1420 aerosol particles measured during cruises to the Arctic [*Petelski*, 2005]. The dry deposition
1421 velocity required to obtain the production flux from measured concentrations was parameterized
1422 using a formulation of *Carruthers and Choularton* [1986], which includes only gravitational
1423 settling and turbulent diffusion (and not impaction, molecular diffusion, or growth of particles
1424 due to increased RH near the sea surface); this formulation yields dry deposition velocities that
1425 are considerably greater than those from most other formulations for r_{80} less than several

1426 micrometers. Measured concentrations were converted by *Petelski* [2005] to r_{80} values and fitted
 1427 to the product of an exponential function of wind speed (despite a poor correlation) and a factor
 1428 that gives the dependence on r_{80} , with a multiplicative uncertainty given as a factor of 7.
 1429 Concentrations were plotted in *Petelski* [2005] for radii up to 7.5 μm , although the resulting
 1430 production fluxes were plotted for radii up to only 5 μm in *Petelski and Piskozub* [2006]; as
 1431 noted in Section 3.2, the dry deposition method can be accurately applied only for r_{80} greater
 1432 than approximately 3 μm . Additionally, as the concentrations measured by *Petelski* [2005] were
 1433 not specific as to composition and included all marine aerosol particles, it was implicitly
 1434 assumed that all particles counted were sea-salt particles, with resultant overestimation of the
 1435 production flux by the proportion of particles that were not SSA particles. The SSA production
 1436 flux according to the formulation of *Petelski and Piskozub* [2006] is presented in Figure 9
 1437 (without the multiplicative uncertainty) for $U_{10} = 8 \text{ m s}^{-1}$, evaluated according to the expression
 1438 in the Appendix, which employs values of the drag coefficient and gravitational settling velocity
 1439 not specified by these investigators.

1440 **5.5. Other formulations**

1441 Several investigators have used combinations of different SSSF formulations in models.
 1442 This is evident in the models listed in Table 1. One such recent approach is that of *Caffrey et al.*
 1443 [2006], which was based on the *Monahan et al.* [1986] formulation for r_{80} from 0.3-5 μm
 1444 (although the *Monahan et al.* expression had been given by the original investigators for
 1445 $r_{80} = 0.8\text{-}8 \mu\text{m}$), together with that of *Smith et al.* [1993] for r_{80} from 5-30 μm , as corrected by
 1446 *Hoppel et al.* [2002], to account for what those investigators had considered spume drops
 1447 (although it has not been established that those particles in this range were spume drops). *Caffrey*
 1448 *et al.* accounted for the findings of *Mårtensson et al.* [2003] and *Clarke et al.* [2006] of a large
 1449 production flux of particles with $0.02 \mu\text{m} < r_{80} < 0.2 \mu\text{m}$ by multiplying the *Monahan et al.*
 1450 [1986] production flux (extended to $r_{80} = 0.02 \mu\text{m}$) by a factor (their Eq. 2):

$$1451 \quad C(r_{80}) = 0.794^{(r_{80}^{-0.855})} \left(1 + \frac{0.4}{r_{80}} \right), \quad (11)$$

1453

1454 where r_{80} is in micrometers (here the expression is given in terms of r_{80} rather than r_{dry} as given
1455 by *Caffrey et al.*, with r_{80} taken as $2r_{\text{dry}}$). Production, transport, wet and dry deposition, and clear-
1456 air and in-cloud reactions of sea-salt aerosol were represented in a 33-bin
1457 ($0.02 \mu\text{m} < r_{80} < 50 \mu\text{m}$) sectional model. For the conditions examined SSA contributed 20-30%
1458 of the CCN concentration for the activation threshold taken as $r_{80} = 0.066 \mu\text{m}$.

1459 Yet another production flux formulation based on that of *Monahan et al.* [1986] was
1460 presented by *Zakey et al.* [2008], who extended the *Monahan* production flux (which had been
1461 given only for $r_{80} \geq 0.8 \mu\text{m}$) to $r_{80} = 0.015 \mu\text{m}$, multiplied by a factor to better reproduce high
1462 concentrations of SSA particles reported by *O'Dowd et al.* [1997]. Specifically, for
1463 $0.015 \mu\text{m} < r_{80} < 0.2 \mu\text{m}$ this factor is given by

1464

$$1465 \quad C(r_{80}) = \exp \left\{ -6.43 \left[\log \left(\frac{r_{80}}{0.2 \mu\text{m}} \right) \right]^2 \right\} \quad (12)$$

1466

1467 (as above, this expression is presented here in terms of r_{80} rather than r_{dry} , with r_{80} taken as $2r_{\text{dry}}$).
1468 This production flux formulation was employed in a regional climate model to determine the
1469 climate influences of sea-salt aerosol. As the model represented SSA by only two size bins and
1470 as the r_{80} range of the lower size bin was 0.1 to 2 μm , it would seem that the consequences of the
1471 modification to the production flux would be minimal, especially so as the reported emissions
1472 and concentrations were presented on a mass basis.

1473 Although formulations such as those of *Caffrey et al.* [2006] and *Zakey et al.* [2008]
1474 permit calculation of SSA production fluxes to r_{80} as low as $0.02 \mu\text{m}$ or below in large scale
1475 models, it would seem that little confidence can be placed in such formulations or in the resultant
1476 calculations, especially in the extended size ranges, owing to the large extrapolations and the
1477 paucity of data upon which they were based. As seen in Figure 9 there remains substantial
1478 uncertainty in SSA production flux estimates in this size range.

1479 **5.6. Organic Production Formulation**

1480 A key finding of recent work is the identification of a large contribution of biogenic
1481 WIOM to SSA (Section 4.3). *O'Dowd* and colleagues have presented several formulations of the

1482 production flux of this substance and its representation in global models [O'Dowd *et al.*, 2008;
 1483 Langmann *et al.*, 2008a,b; Vignati *et al.*, 2010] based on the concentration of chlorophyll-a in the
 1484 ocean surface layer as determined by satellite observations as a proxy for the mass fraction of
 1485 WIOM in sea spray, Φ_{om} . These observations, together with seasonal variation of Φ_{om}
 1486 determined from measurements of aerosol chemical composition, have been combined with an
 1487 SSA production flux formulation to yield the oceanic production flux of WIOM associated with
 1488 sea-spray production and to examine WIOM emissions in several model studies.

1489 The relation between Φ_{om} and chlorophyll-a concentrations was investigated by O'Dowd
 1490 *et al.* [2008] using aerosol composition measurements from the 3-year dataset of Yoon *et al.*
 1491 [2007] from Mace Head, Ireland, in which only clean marine air masses were sampled. It was
 1492 assumed, based on experimental work discussed in Section 4.3, that the aerosol mass for r_{80} less
 1493 than approximately $1 \mu\text{m}$ was composed mainly of sea salt and WIOM, with a minor
 1494 contribution from WSOM, arbitrarily taken as 5% of the WIOM mass concentration.
 1495 Chlorophyll-a concentration, Chl , was taken as the spatial average over a grid of
 1496 $1000 \text{ km} \times 1000 \text{ km}$ upwind of Mace Head. A linear fit of Φ_{om} to Chl for 37 data points was
 1497 presented by O'Dowd *et al.* [2008] and a revised fit, taking into account small corrections to the
 1498 chemical analysis, was presented by Langmann *et al.* [2008b, as corrected by Vignati *et al.*,
 1499 2010]. More recently a fit to a subset (24) of these data was presented by Vignati *et al.* [2010] as

$$1500$$

$$1501 \quad \Phi_{om} = 0.435 \left(\frac{Chl}{\text{mg m}^{-3}} \right) + 0.14, \quad Chl < 1.43 \text{ mg m}^{-3}, \quad (13)$$

1502

1503 (the range of validity was incorrectly stated as $Chl < 1.43 \mu\text{g m}^{-3}$ in their Eq. 3). The several fits
 1504 are shown in Figure 10. Only about 30% of the variance of Φ_{om} is accounted for by any of the
 1505 fits.

1506 To obtain a formulation for the size-dependent production flux of WIOM in SSA,
 1507 O'Dowd *et al.* [2008] assumed that the size dependence of the SSA production flux was given by
 1508 a lognormal distribution with the geometric mean value of r_{80} given as a function of time of year
 1509 so as to capture changes in Φ_{om} (although a more physically based quantity such as water

1510 temperature or chlorophyll-a concentration would be more appropriate). The magnitude of the
1511 SSA production flux was given by the formulation of *Geever et al.* [2005] for particles with dry
1512 diameter $d_p = 0.1\text{-}1\ \mu\text{m}$, which was refitted to a power law as $F\ (\text{m}^{-2}\ \text{s}^{-1}) = 1.854 \times 10^3 U_{22}^{2.706}$.
1513 The WIOM mass fraction Φ_{om} was constrained to a maximum value of 0.9. This procedure
1514 yielded a parameterization of the production flux of SSA number and chemical composition for
1515 particles with approximate r_{80} range $0.1\text{-}1\ \mu\text{m}$ and was combined with monthly average wind
1516 speed fields (from SeaWinds on the QuickScat satellite) and chlorophyll-a concentrations (from
1517 MODIS Aqua and Terra satellites) to produce estimates of the global annual production of
1518 WIOM as $2.3\ \text{Tg C yr}^{-1}$ for 2003 and $2.8\ \text{Tg C yr}^{-1}$ for 2006 [*Langmann et al.*, 2008b].

1519 A similar approach was used by *Vignati et al.* [2010] to determine the production flux of
1520 WIOM associated with sea spray in the accumulation mode (approximate r_{80} range $0.1\text{-}1\ \mu\text{m}$),
1521 for which the size dependence of the production flux was assumed to be a lognormal with
1522 geometric mean radius at 80% RH equal to $0.09\ \mu\text{m}$ and the magnitude of the production flux
1523 was that of *Gong et al.* [2003]. The maximum value of Φ_{om} was constrained to 0.76. This
1524 formulation was used in a global chemical transport model to determine the production of
1525 WIOM and sea salt in this mode for a one-year period in 2002-2003 (Figure 11). Global annual
1526 emissions of WIOM and sea salt in this mode were 8.2 and 24 Tg, respectively. It should be
1527 noted that there is likely a significant but, to date, unquantified flux of WIOM in particles with
1528 $r_{80} > 1\ \mu\text{m}$ [*Facchini et al.*, 2008]. The production rate for WIOM estimated by *Vignati et al.*
1529 [2010] was nearly three times that reported by *Langmann et al.* [2008b]; no reasons for the
1530 difference were presented. A possible explanation is that the model of *Langmann et al.*, in
1531 contrast to *Vignati et al.*, used a single fixed particle size ($r_{80}=0.09\ \mu\text{m}$) and did not account for
1532 possible variation of particle size with *Chl*.

1533 Although a calculation such as this can hardly be taken as a definitive estimate in view of
1534 the uncertainties associated with the production flux formulation, the estimate of the organic
1535 fraction of the primary SSA emission flux, and the poor correlation between satellite
1536 determinations of chlorophyll-a concentrations and organic mass fraction, this methodology
1537 suggests an approach for modeling these emissions on a global scale as input to chemical
1538 transport models and climate models.

1539 **6. Discussion**

1540 As discussed in Section 1 there is continuing and indeed heightened interest in
1541 characterization of the number concentration, composition, and other properties of SSA and in
1542 the processes that govern its production. Unfortunately, the present state of understanding of
1543 production, concentrations, and removal rates of SSA particles is so low that it is not possible to
1544 constrain the mass emission flux even to an order of magnitude, as reflected in the differing
1545 emission rates shown in Figure 1, and the situation for particle number production is even more
1546 uncertain.

1547 This review has examined recent findings regarding the size-dependent production
1548 of SSA, and parameterizations of this production flux since the critical review of *Lewis and*
1549 *Schwartz* [2004]. New work has added a substantial body of findings to those which were
1550 presented in that review. An important new finding is the recognition that sea spray contains
1551 other substances in addition to sea salt and that the major, and in some instances, dominant
1552 contribution to SSA in some size ranges is from organics, especially at smaller sizes. Along with
1553 this finding is the recognition that SSA production extends to much lower size than was
1554 previously recognized, with both laboratory experiments and field measurements showing
1555 substantial production of SSA at values of r_{80} below $0.1 \mu\text{m}$, and down to as low as $0.01 \mu\text{m}$, as
1556 many of these smaller particles are composed primarily of organic substances. However, despite
1557 the new work there seems to be little convergence on understanding of important elements of the
1558 SSA production process, as characterized by quantities needed to determine SSA production
1559 fluxes, such as the flux per white area and the whitecap fraction. This discussion examines the
1560 several approaches taken in recent work to measurement of the quantities pertinent to
1561 determination of SSA production flux, its dependence on controlling variables, and to the
1562 numerical representation of this production flux.

1563 **6.1. Laboratory Investigations of SSA Production**

1564 Key among the findings of recent work is the demonstration in laboratory
1565 experiments that the SSA production flux per white area can depend strongly, by up to two
1566 orders of magnitude, on the volume flux of air in bubbles passing through the white area
1567 (Figure 5). However, experiments to date have explored only a very limited subset of the

1568 physical and chemical variables controlling SSA production flux per white area. With respect to
1569 physical conditions, the studies of *Tyree et al.* [2007] and *Keene et al.* [2007] relied on artificial
1570 constraints on the size of the bubble swarm reaching the surface, specifically confinement of the
1571 resulting white area by the walls of the vessel in which these bubbles were produced. Whether
1572 such a constraint is a good mimic of the barrier to lateral diffusion of bubbles in an unconfined
1573 situation such as the open ocean following entrainment of air during wave breaking is not
1574 known. One fruitful line of future investigation would be systematic examination of the SSA
1575 production flux as the flow rate of air is varied through an array of multiple diffusers (frits) in a
1576 vessel sufficiently large that the spread of the bubble swarm would not be limited by the vessel
1577 walls. Likewise it would seem essential to examine other possible reasons for differences
1578 between the production flux per white area in the studies of *Mårtensson et al.* [2003], *Tyree et al.*
1579 [2007], *Keene et al.* [2007], and *Fuentes et al.* [2010], such as dependence of production flux per
1580 white area on the depth of the diffuser producing the bubbles, which differed in these
1581 experiments by more than an order of magnitude, from a few centimeters to more than a meter.
1582 Another fruitful line of investigation might be systematic examination of the effects of
1583 temperature on bubble formation, bubble dynamics, and bubble bursting as components of the
1584 SSA production process. Experiments such as these would permit measurement of the bubble
1585 spectrum and volume flux that might be compared to such fluxes following wave breaking in the
1586 open ocean.

1587 Oceanic bubble spectra obtained to date are averages over long periods and thus
1588 include breaking waves and background spectra which do not contain the large bubbles
1589 generated just after wave breaking which are responsible for the generation of film drops. These
1590 very large bubbles are probably not generated in any of the laboratory experiments discussed
1591 above. Considerations such as these also invite determination of the bubble spectrum and volume
1592 flux resulting from wave breaking as a function of location and time relative to wave breaking in
1593 laboratory studies and in the open ocean, and relating bubble volume flux and SSA production in
1594 such studies to "whiteness" determined by optical measurements. As well, a systematic
1595 examination of the dependence of SSA production flux on bubble volume flux (and perhaps
1596 other variables) beyond the measurements reported to date would be useful, especially given the

1597 substantial differences reported by different investigations shown in Figure 5. Such studies
1598 would be valuably informed by laboratory investigations examining the dependence of SSA
1599 production on means of bubble production such as that of *Fuentes et al.* [2010]. It might be noted
1600 that for none of these methods is it established that the bubble spectrum and resultant SSA
1601 production are representative of open ocean conditions. In this regard the conclusion reached by
1602 some of the investigators that a weir is more appropriate than bubbles produced by diffusers for
1603 generating SSA has little justification.

1604 A further open question amenable to laboratory investigation is the mechanism
1605 responsible for the temperature dependence of SSA production that has been observed in
1606 laboratory experiments [*Mårtensson et al.*, 2003; *Sellegri et al.*, 2006], as temperature might
1607 affect bubble generation at the frit employed to generate the bubbles and the dynamics of bubble
1608 rise in addition to the production of particles associated with bubble bursting, through the
1609 temperature dependence of viscosity, surface tension, or other controlling properties. Systematic
1610 examination of these dependences might lead to improved understanding and parameterization of
1611 the overall dependence of SSA production on temperature.

1612 **6.2. Composition of SSA**

1613 A very important line of investigation in recent studies has been the dependence of
1614 SSA composition as a function of particle size in laboratory experiments and field
1615 measurements, and the role of seawater composition on particle composition. These studies have
1616 shown, especially for particles with $r_{80} < 0.25 \mu\text{m}$, that organic material can comprise a
1617 substantial fraction of SSA particles that approaches unity, especially under conditions of high
1618 biological activity [*O'Dowd et al.*, 2004; *Facchini et al.*, 2008]. It seems increasingly likely that
1619 production of particles highly enriched in organic material derives from fragmentation of the
1620 film cap from which much of the seawater has drained prior to bursting, leaving behind a film
1621 that is highly enriched in surfactant material. Laboratory studies with flowing seawater (on ships
1622 or at coastal laboratories) would be well suited to systematic examination of such influences,
1623 especially as studies with organic compounds introduced into laboratory-prepared artificial
1624 seawater as proxies for actual oceanic organic material have not proved very successful in
1625 reproducing the effects observed in actual seawater. These studies also raise questions regarding

1626 the attribution of high production fluxes of SSA particles to inorganic sea salt in instances where
1627 the composition has not been determined by chemically specific methods. It appears [e.g., *Bigg*
1628 *and Leck, 2008*] that the water-insoluble organic matter associated with very small particles may
1629 be persistent at temperatures as high as 300°C which have been used in many studies to
1630 distinguish what has been taken as refractory material, such as inorganic sea salt, from
1631 substances such as sulfates and secondary organic matter which are volatilized at such
1632 temperatures. Thus the use of volatility alone is not sufficient to determine the composition of
1633 particles that originate from the ocean surface and suggest the need for specific chemical
1634 determination in future such studies.

1635 A major development in the past several years has been sustained measurements of
1636 the size-distributed composition of marine aerosol at a coastal site downwind of open ocean. By
1637 restricting the measurements to the oceanic sector it has been possible to obtain a much larger
1638 data set than would be available from cruises of limited duration. Although there is much
1639 precedent for such measurements at island and coastal sites [*Prospero, 2002*] that has established
1640 the role of long-range transport of mineral dust and continental anthropogenic aerosol to the
1641 marine environment, the new measurements show the value of much better size resolution in the
1642 range $r_{80} < 1 \mu\text{m}$ together with determination of the size-dependent organic component of the
1643 aerosol. Importantly these measurements have shown that the organic material is present
1644 predominantly in particles of $r_{80} \lesssim 0.5 \mu\text{m}$. Examination of vertical profiles of composition
1645 (Figure 8) provides convincing evidence that the organic material, specifically WIOM, has an
1646 origin at the sea surface, i.e., is a component of SSA.

1647 Extended measurements of size-distributed composition of marine aerosols over
1648 several years [*O'Dowd et al., 2004; Facchini et al., 2008*] have permitted examination of the
1649 hypothesis that WIOM is of biological origin, specifically from surfactant materials in the
1650 surface layer that arise from biological activity, perhaps exudates or chemical decomposition
1651 products of organisms. The data from these measurements have been employed in a first
1652 systematic attempt to relate organic material in marine aerosol to biological activity in seawater
1653 by examination of correlation with *Chl* obtained from satellite measurements of ocean color
1654 [*O'Reilly et al., 1998*]. Although aerosol organic fraction exhibited some correlation with *Chl*

1655 ($r^2 = 0.3$), there is much variation in this fraction that is not accounted for in the oceanic
1656 chlorophyll data product (Figure 10). As this variation is much greater than the scatter between
1657 *in situ* measurements of *Chl* and the satellite data product [O'Reilly *et al.*, 1998], it would seem
1658 that *Chl* is not wholly adequate as a proxy for the biological activity responsible for the organic
1659 material comprising the aerosol. Nonetheless the relationship between aerosol organic matter and
1660 satellite-determined oceanic chlorophyll concentration provides convincing evidence of the role
1661 of biological activity in producing this organic matter.

1662 The correlation of organic matter in SSA with satellite-derived *Chl* found by
1663 O'Dowd and colleagues has been incorporated into a parameterization of the organic component
1664 of a SSA production flux to calculate the global distribution of WIOM production [Vignati *et al.*,
1665 2010]. However this correlation is based only on measurements at a single nonrepresentative
1666 site, being a region of high biological productivity; this situation suggests the need for additional
1667 similar studies at other locations. For these reasons, at the present stage of understanding
1668 calculations such as those of Vignati *et al.* should perhaps be viewed more as proof of concept
1669 than as definitive estimates of the globally distributed production of primary marine organic
1670 aerosol. Certainly the insights gained thus far by the extended measurement campaigns by
1671 O'Dowd and colleagues at the Mace Head Ireland site suggest the utility of conducting such
1672 measurements at other sites characterized by different temperature, different biological
1673 productivity, and the like to build a more comprehensive global picture of the composition of
1674 marine aerosol generally and of the concentration and properties of sea-spray aerosol.

1675 Although the identification and quantification of organic material in very small SSA
1676 particles represents a substantial advance, an important piece of the picture that is still missing is
1677 the mixing state (internal vs. external) of sea salt and organic matter in particles in the r_{80} range
1678 from approximately 0.05-0.2 μm . This mixing state would be expected to influence the ability of
1679 these particles to serve as CCN and consequently their turnover times against removal through
1680 wet deposition. The suggestion of recent research that many, perhaps most, of the SSA particles
1681 with $r_{80} \lesssim 0.1 \mu\text{m}$ consist of WIOM thus has important implications for the budget of these
1682 primary aerosol particles. The need for information on particle mixing state suggests the utility
1683 of alternative means of characterizing the composition and properties of SSA particles. Aerosol

1684 mass spectrometry and single-particle aerosol mass spectrometry provide real-time information
1685 on aerosol composition that has greatly informed understanding of aerosol properties and
1686 processes in terrestrial environments but that has thus far seen limited application in the marine
1687 environment and specifically for characterization of SSA particles. It seems likely as well that
1688 much important information on the properties of SSA particles would be gained from developing
1689 and applying techniques that can determine the composition of particles with $r_{80} < 0.1 \mu\text{m}$ which
1690 are difficult to study by mass spectrometry, such as transmission electron microscopy, which can
1691 examine the composition and structure of individual particles, or more exotic techniques such as
1692 x-ray absorption fine structure, which can determine composition and oxidation state of material
1693 present in ensembles of particles.

1694 The variability in the amount and nature of organic material and the resulting surfactants
1695 in seawater would appear to be major sources of variability in the SSA production flux. Based on
1696 a combination of laboratory experiments with observations on the open ocean and at the coastal
1697 site at Mace Head, *Facchini et al.* [2008] showed that the composition of particles generated in
1698 laboratory experiments with bursting bubbles was similar to that observed in aerosols in the open
1699 ocean. Furthermore the seasonality of sea-spray emissions and chemical composition follows the
1700 chlorophyll cycle obtained using satellite measurements [*Sellegrì et al.*, 2006]. When biological
1701 activity is low in the ocean, with resultant low concentrations of organic matter in the ocean
1702 surface layer, sea-spray is comprised predominantly of inorganic sea salt. In contrast, when
1703 biological activity is high and organic matter is present at the ocean surface, this organic matter
1704 is enriched in sea-spray particles with $r_{80} < 0.25 \mu\text{m}$. These considerations suggest that
1705 improving knowledge in this area will require combinations of laboratory and field experiments
1706 and that this effort will require multi-disciplinary cooperation among oceanographers, marine
1707 biologists, meteorologists, physicists, and chemists to understand the effects of biological
1708 species, such as phytoplankton and algae, on the formation, physical properties, and composition
1709 of SSA.

1710 Although *O'Dowd* and co-workers report the fraction of the mass of SSA particles
1711 that is composed of organics varying, depending on the season and the size of the particles, from
1712 2-3% to 60-80% (Section 4.3), *Bigg and Leck* [2008] argue that bubble-mediated particles with

1713 $r_{80} < 0.1 \mu\text{m}$ are purely organic (Section 4.3). In contrast, the experiments by *Clarke et al.* [2006]
1714 argued that particles with $r_{80} > 0.03 \mu\text{m}$ produced from breaking waves in the surf zone were
1715 composed almost entirely of sea salt. The contrasting findings raise the question whether
1716 *O'Dowd et al.* [2004] and *Leck and Bigg* [2008] observed the same type of particles. For
1717 example, the size distributions of concentration reported by *Bigg et al.* [2004] appeared as two
1718 separate modes, whereas *O'Dowd et al.* [2004] observed a continuous size distribution of organic
1719 aerosol.

1720 **6.3. Whitecap Fraction**

1721 A further important line of recent investigation is examination of the dependence of
1722 the whitecap fraction on controlling factors. Recent studies using digital photographic techniques
1723 have indicated systematically lower whitecap fraction at a given wind speed (by as much as a
1724 factor of 4 or so) than has characterized the bulk of previous determinations of this quantity as
1725 summarized in *LS04*. The reasons for this difference are not known, although one possibility is
1726 differences in technique, for example differences in dynamic range of digital photography versus
1727 that of film; a similar situation resulted in the whitecap fraction as determined by analog video
1728 being an order of magnitude lower than that determined by film photography. It is clear that the
1729 reasons for these differences need to be better understood than at present.

1730 Studies examined in Section 4.1.1 reported advances in image processing,
1731 specifically in defining thresholds that distinguish white area from non-white areas. However
1732 although such approaches to defining thresholds remove the subjectivity from determining white
1733 area in individual images, this subjectivity is transferred to the choice of the threshold for the
1734 batch processing. More intrinsically, it is not established which if any threshold yields a white
1735 area that corresponds to that for which the flux per white area has been determined in laboratory
1736 studies. It seems likely that there may be variation in the "whiteness" that characterizes the
1737 bubble swarm that follows a breaking wave as the bubble volume flux diminishes with time
1738 following a wave breaking event; a whitecap property such as this would be much more useful
1739 than an arbitrary threshold of "white" in relating SSA production flux to white area and
1740 ultimately in developing more accurate parameterizations for SSA production flux.

1741 A major strength of the digital photography technique is the ability to quantitatively
1742 examine the temporal variation of white area both by following the course of white area and
1743 whiteness subsequent to the breaking of individual waves, and by statistical techniques such as
1744 examination of the temporal autocorrelation of whiteness, that may yield information on the
1745 statistical independence of successive photographs and on the duration of white area following
1746 wave breaking as a function of wind speed, thus leading to improved estimates of whitecap
1747 behavior and of SSA production flux.

1748 Another recent advance is the availability of satellite determination of whitecap
1749 fraction through microwave radiometry. Initial developments show that this approach offers the
1750 potential for further understanding and parameterizing this quantity and for determining W
1751 globally on spatial scales of 50 km with daily or better temporal resolution, which could in turn
1752 diminish the uncertainty of SSA production as obtained with the whitecap method. However, at
1753 present there are discrepancies of an order of magnitude or more between whitecap fraction
1754 determined by satellite-borne microwave radiometers and those determined by photographic
1755 measurements at visible wavelengths, especially the high values of W found at low wind speed
1756 by the microwave measurements (Figure 3); possible reasons for these discrepancies are
1757 examined in Section 4.1.2. Based on these comparisons satellite measurements are not
1758 sufficiently accurate at present to provide reliable estimates of whitecap fraction. It would seem
1759 essential to use airborne radiometers in conjunction with simultaneous airborne photographic
1760 measurements to facilitate further developments of this approach.

1761 **6.4. SSA Production Flux Parameterization**

1762 Many parameterizations of the SSA source function continue to be based on the
1763 whitecap method, according to which the SSA production flux is evaluated as the product of the
1764 production flux per white area, assumed to be a constant in both the magnitude of the flux and
1765 the size dependence, independent of the nature or properties of the white area, and the whitecap
1766 fraction, a function of meteorological and ocean conditions, but in practice parameterized mainly
1767 in terms of wind speed (Eq. 9). It should be stressed that the separability of the production flux
1768 into the product of two such independent quantities remains an unproved assumption. Indeed this
1769 separability is subject to increasing question, especially on the basis of recent laboratory studies

1770 and field measurements summarized in Figure 4, which shows strong differences in the size
1771 dependence of the SSA production flux under different conditions. These differences, if not
1772 measurement artifacts, are orders of magnitude in some size ranges. Likewise the measurements
1773 of the production flux per white area of *Tyree et al.* [2007] and *Fuentes et al.* [2010] indicate that
1774 the magnitude of this quantity can depend strongly on the nature of the white area. Finally the
1775 composition, especially of particles with $r_{80} < 0.25 \mu\text{m}$, depends strongly on the organic
1776 composition of the seawater, as determined by *in situ* measurement or as inferred from proxy
1777 measurements. In sum these measurements raise important questions over the accuracy of the
1778 whitecap method in its current formulation (Eqs. 3, 8 and 9) especially as this method has
1779 provided parameterizations for the SSA production flux which are widely used by the aerosol
1780 modeling community. It would thus seem essential to re-examine the premises of the whitecap
1781 method in laboratory experiments and field measurements to determine how this method can be
1782 reformulated.

1783 Alternatively the SSA production flux determined by field measurements for
1784 particular meteorological conditions and ocean state can be compared to that evaluated by the
1785 whitecap method for the wind speed of the measurement and/or to that evaluated for whitecap
1786 fraction. In this respect the measurements of *Clarke et al.* [2006] of SSA production in the surf
1787 zone and of *de Leeuw et al.* [2007] and *Norris et al.* [2008] of SSA production at a coastal site
1788 during onshore winds provide determinations of SSA production under specific meteorological
1789 and oceanic conditions. Such measurements, in principle, could be extended to a variety of
1790 conditions. It would be important as well to increase the size resolution of such measurements in
1791 view of the large variation in particle properties such as CCN activity within the range of size
1792 bins of existing instrumentation. The surf-zone method would seem limited in its application to
1793 rather specific situations and might suffer from site-specific conditions that make the results not
1794 representative of the open ocean (e.g., the influence of bottom drag on the wave breaking
1795 process). Eddy correlation with fast, size-resolved measurements of the net particle flux, which
1796 may be employed on long piers, off-shore platforms, or ships in the deep ocean, might provide a
1797 repertoire of measurements that would permit evaluation of the whitecap method and/or become

1798 the basis for a more differentiated picture of the SSA production flux and its dependence on
1799 controlling variables.

1800 Recent estimates of the SSA production flux (Figure 9) appear to be greater than
1801 previous estimates, especially toward smaller particle sizes. Although these new estimates
1802 coincide with that of *LS04* for the largest particles ($r_{80} \gtrsim 3 \mu\text{m}$), towards smaller sizes they are
1803 increasingly higher, by up to 1 to 2 orders of magnitude at $r_{80} = 0.1 \mu\text{m}$, near which size these
1804 fluxes, in the representation $dF/d\log r_{80}$, exhibit their maximum values. Possible reasons for and
1805 consequences of this behavior are discussed in Section 6.5.

1806 **6.5. Consistency between SSA production and observed particle** 1807 **concentrations**

1808 As the number concentration of aerosol particles in clean marine air, often as low as
1809 200 cm^{-3} (Section 3), is controlled by transport, production, and removal, consideration of rates
1810 of removal processes together with reported number concentrations leads to a check on the
1811 consistency of estimates of SSA production flux by various formulations.

1812 Removal processes are wet deposition, dry deposition, and coagulation onto larger
1813 particles and cloud drops, of which wet deposition is dominant in most circumstances.
1814 Coagulation in the marine atmosphere is almost certainly not important for two reasons: first, the
1815 low concentration of aerosol particles that could scavenge such smaller particles, and second, the
1816 low diffusion coefficients of these small particles, that for particles with $r_{80} > 0.01 \mu\text{m}$ being
1817 prohibitively low for this to be an important process. Coagulation on cloud drops is slow for
1818 similar reasons and is diminished further by the time that particles spend in clouds at the top of
1819 the marine boundary layer. For particles of the sizes under consideration, dry deposition, through
1820 gravitational sedimentation, impaction on and diffusion to the sea surface, although highly
1821 uncertain, is expected to be so slow that characteristic removal times would be at least several
1822 days to a week. Removal through activation during non-precipitating periods might still occur,
1823 but cloud drop concentrations are too low for this to be a major removal mechanism, and
1824 additionally a large fraction of the marine aerosol particles of the size range under consideration
1825 are too small to activate in the low-updraft conditions of the marine environment. The major
1826 removal mechanism is thus almost certainly wet deposition, through both activation to form

1827 cloud drops that precipitate and scavenging by falling hydrometeors, which typically occurs on a
1828 time scale of several days. Thus, unless other currently unknown or unappreciated loss processes
1829 are found, it must be concluded that characteristic turnover times of SSA particles with
1830 $r_{80} < 0.1 \mu\text{m}$ are several days.

1831 A turnover time of 3 days [LS04, p. 72], together with the assumption of a typical
1832 marine boundary layer height of 0.5 km and the observation that the marine boundary layer is
1833 largely decoupled from the free troposphere (implying little transport out of the marine boundary
1834 layer), allows estimation of the number concentration of SSA particles that would be expected to
1835 be present in the marine boundary layer for a given SSA production flux. For this flux taken as
1836 $1 \times 10^6 \text{ m}^{-2} \text{ s}^{-1}$ as is indicated by several of the production flux formulations shown in Figure 9, the
1837 rate of increase in concentration would be nearly $200 \text{ cm}^{-3} \text{ day}^{-1}$, resulting in a steady-state
1838 number concentration of sea-spray particles alone of about 500 cm^{-3} . Such a concentration would
1839 be comparable to or exceed typical measured number concentrations of all marine aerosol
1840 particles in clean conditions, several hundred per cubic centimeter (Section 3.1), raising concerns
1841 over formulations yielding such large production fluxes. This concern is heightened by the fact
1842 that aerosol particles in the clean marine boundary layer may derive from sources other than
1843 production at the sea surface and the resultant possibility that SSA particles often constitute only
1844 a fraction, perhaps only a small fraction, of measured total particle number concentrations.
1845 Apportionment of the particles that derive from primary production at the sea surface is difficult
1846 and this difficulty hinders extension of the statistical wet deposition method beyond sea-salt
1847 aerosol (as by LS04) to sea-spray aerosol.

1848 **7. Conclusions**

1849 A major finding of recent work is the recognition of the large contribution of organic
1850 substances to SSA particles, especially in locations of high biological activity, which becomes
1851 increasingly important with decreasing particle size, and which may be dominant for
1852 $r_{80} < 0.25 \mu\text{m}$, leading to the distinction noted in Section 1 between sea-salt particles (the focus
1853 of the review by LS04) and sea-spray particles. Possible consequences of this difference in
1854 composition are differences in properties such as cloud-drop activation and resultant error in
1855 models that do not account for these differences.

1856 Determinations of the SSA production flux have been made at sizes smaller than
1857 those previously examined, with some formulations extending to particle size as low as
1858 $r_{80} = 0.01 \mu\text{m}$; no estimate for the production flux of sea-salt aerosol particles with $r_{80} < 0.1 \mu\text{m}$
1859 had been presented by *LS04*. However, as noted above, uncertainties remain in the composition
1860 of such particles and in what is responsible for the variable amount of organic material in these
1861 particles. Additionally, the magnitude and the size distribution of the production flux of particles
1862 with $r_{80} < 0.3 \mu\text{m}$ are both highly variable (Figures 4 and 9), and laboratory experiments have
1863 demonstrated that the means by which the white area is produced results in large differences in
1864 both of these quantities that cannot be accounted for by factors such as temperature.
1865 Consequently, it must be concluded that the assumption, central to applications of the whitecap
1866 method, that the SSA production flux per white area is independent of the means by which that
1867 white area is produced is not valid, and thus that determinations of the SSA production flux
1868 based on the whitecap method are potentially subject to large error. A possible fruitful direction
1869 for research would be to investigate the dependence of the SSA production flux on the means of
1870 production of white area, as discussed in Section 6.1.

1871 The best estimate for the production flux of SSA particles with $r_{80} > 1 \mu\text{m}$ remains as
1872 that given by *LS04* based on multiple methods, with uncertainty a multiplicative factor of $\times 4$ to
1873 5 (Figure 9; dashed black line and gray shaded region). For decreasing r_{80} from 1 to $\sim 0.3 \mu\text{m}$
1874 recent flux determinations are increasingly greater than the best estimate of *LS04*, and for smaller
1875 sizes they are greater still. However, a concern with such large SSA production flux formulations
1876 is that they imply number concentrations for SSA particles in the marine boundary layer that are
1877 unrealistically high, as discussed in Section 6.5. The realization that some or much of the aerosol
1878 may consist of organic matter rather than sea salt may resolve some of this discrepancy, but by
1879 no means all of it.

1880 Recent advances in determination of the whitecap fraction W , also central to
1881 evaluation of the SSA production flux by the whitecap method, by both photographic methods
1882 and satellite retrievals may eliminate some of the subjectivity in measurement of this quantity,
1883 but direct relation to SSA production is lacking. Recent determinations of W by digital
1884 photographic measurements are systematically lower, by up to a factor of 4, than those

1885 previously determined by film photography for reasons that are not yet understood. Satellite
1886 retrieval of W by brightness temperature at microwave frequencies is a promising possibility, but
1887 this approach is currently unable to capture the dependence of this quantity on wind speed that is
1888 exhibited in photographic measurements at visible wavelengths.

1889 Based on long-term measurement of aerosol chemical composition and its relation to
1890 biological activity at a coastal site (Mace Head, Ireland), it is clear that similar data sets from
1891 other sites could permit assessment of the generality of conclusions drawn from those
1892 measurements and more broadly on the factors that control the properties of marine aerosols.
1893 Additionally, measurements of composition and structure of individual marine aerosol particles
1894 with $r_{80} < 0.1 \mu\text{m}$ at multiple sites and over multiple seasons would provide a wealth of data that
1895 could help elucidate sources and production mechanisms. Laboratory experiments of SSA
1896 production under varying conditions and determination of the composition of these laboratory-
1897 generated particles may provide some insight into controlling mechanisms, but it would seem
1898 that direct measurement of SSA fluxes, e.g., by eddy-correlation measurements, would yield a
1899 quicker route to determination of the SSA production flux and in any event would be essential to
1900 evaluate models of the production flux.

1901 Despite the many gains in understanding in recent years, the uncertainty in the SSA
1902 production flux remains sufficiently great that present knowledge of this quantity cannot usefully
1903 constrain the representation of emissions of SSA in chemical transport models or climate models
1904 that include aerosols. As a consequence it is not yet possible to improve the modeling of these
1905 emissions much beyond the state of affairs represented in Figure 1, which shows nearly two
1906 orders of magnitude spread in current estimates of global annual SSA emissions. It is clear as
1907 well that this situation cannot be resolved by demonstration of the ability to generate reasonable
1908 concentration fields with one or another source function, given the demonstrated ability of such
1909 greatly varying emissions to yield concentration fields that compare reasonably with
1910 observations [Textor *et al.*, 2006]. Rather it would seem essential that the SSA production flux be
1911 constrained directly by field observations, or preferably be overconstrained by consistency of
1912 determinations by multiple approaches.

1913 In addition to representing mass concentrations of SSA in chemical transport models
1914 and climate models it is essential that such models also include some representation of SSA
1915 number concentration, both magnitude and size distribution, given the importance of these
1916 aerosol properties: magnitude affecting cloud properties, and both magnitude and size
1917 distribution affecting the optical depth (commonly used as a measure of skill of such models)
1918 and atmospheric radiation transfer. Finally, as it is becoming clear that the organic fraction of
1919 SSA depends on particle size and likely on the composition of seawater as influenced by
1920 biological activity, it would seem important that this component of SSA be represented in
1921 models, especially as composition may exert a strong influence on the cloud nucleating
1922 properties of these aerosols, affecting the microphysical properties of marine clouds and the
1923 sensitivity of cloud properties to perturbation by anthropogenic aerosols.

1924 **Appendix: SSA production flux formulations**

1925 Units of total and size-dependent fluxes (F_{eff} , $\frac{dF_{\text{eff}}}{d \log r_{80}}$, $\frac{dF_{\text{int}}}{d \log r_{80}}$, $\frac{dF_{\text{int}}}{d \log d_p}$, $\frac{dF_{\text{eff}}}{d \log r_{\text{amb}}}$, and

1926 $\frac{dF_{\text{net}}}{d \log r_{\text{amb}}}$) are $\text{m}^{-2} \text{s}^{-1}$; U_{10} and U_{22} are m s^{-1} ; and d_p (dry mobility diameter; $d_p \approx r_{80}$ for most

1927 sizes), r_{amb} (ambient radius), and r_{80} are μm .

1928

1929

1930 **Formulations based on the steady-state dry deposition method:**

1931 **Smith et al. [1993]:**

1932
$$\frac{dF_{\text{eff}}}{d \log r_{80}} = 1400 \times \exp(0.16 U_{10}) \exp\left\{-3.1 \left[\ln\left(\frac{r_{80}}{r_1}\right)\right]^2\right\} + 0.76 \times \exp(2.2 U_{10}^{1/2}) \exp\left\{-3.3 \left[\ln\left(\frac{r_{80}}{r_2}\right)\right]^2\right\}$$

1933

1934 $r_1 = 2.5 \mu\text{m}$; $r_2 = 11 \mu\text{m}$

1935 $r_{80} = 1\text{-}25 \mu\text{m}$ (although as noted above, it cannot be accurately applied to particles with

1936 $r_{80} < \sim 3 \mu\text{m}$)

1937 $U_{10} < 34 \text{ m s}^{-1}$

1938

1939

1940 **Lewis & Schwartz [2004]:**

1941
$$\frac{dF_{\text{eff}}}{d \log r_{80}} = \left(800 \frac{U_{10}^{2.5}}{r_{80}^{2.5}}\right) \times 4$$

1942 $r_{80} = 3\text{-}25 \mu\text{m}$

1943 $U_{10} = 5\text{-}20 \text{ m s}^{-1}$

1944

1945

1946 **Petelski & Piskozub [2006]:**

1947
$$\frac{dF_{\text{eff}}}{d \log r_{80}} = \frac{70 \exp(0.21 U_{10}) r_{80}^3 \exp(-0.58 r_{80})}{1 - \exp\left(\frac{-0.11 r_{80}^2}{U_{10}}\right)} \times 7$$

1948 $r_{80} = 0.25-7.5 \mu\text{m}$ (although as noted above, it cannot be accurately applied to particles with

1949 $r_{80} < \sim 3 \mu\text{m}$)

1950 $U_{10} < 17 \text{ m s}^{-1}$

1951 This expression was obtained from that presented by these investigators with drag coefficient

1952 taken as 0.0013 and gravitational terminal velocity (Stokes' Law) as given by Eq. 2.6-8 of *LS04*.

1953

1954

1955 **Formulations based on the statistical wet deposition method:**

1956 **Lewis & Schwartz [2004]:**

1957
$$\frac{dF_{\text{eff}}}{d \log r_{80}} = 10^4 \times 5$$

1958 $r_{80} = 0.1-1 \mu\text{m}$

1959 $U_{10} = 5-20 \text{ m s}^{-1}$

1960

1961

1962 **Formulations based on the whitecap method:**

1963 (Formulations for $dF_{\text{wc}}/d \log r_{80}$ were converted to $dF_{\text{int}}/d \log r_{80}$ using $W(U_{10})$ from *Monahan and*

1964 *O'Muircheartaigh* [1980]).

1965 **Monahan et al. [1986], laboratory:**

1966
$$\frac{dF_{\text{int}}}{d \log r_{80}} = 3.2 U_{10}^{3.41} r_{80}^{-2} \left(1 + 0.057 r_{80}^{1.05}\right) \times \exp \left\{ 2.74 \times \exp \left[-2.4 (0.38 - \log r_{80})^2 \right] \right\}$$

1967 $r_{80} = 0.8-8 \mu\text{m}$

1968

1969

1970 **Gong [2003]; modified from Monahan et al. [1986]:**

1971
$$\frac{dF_{\text{int}}}{d \log r_{80}} = 3.2 U_{10}^{3.41} r_{80} \times \left(1 + 0.057 r_{80}^{3.45}\right) \times \exp \left\{ \begin{array}{l} 3.68 \times \exp \left[-5.33 (0.433 - \log r_{80})^2 \right] \\ -4.7 \ln r_{80} \left[1 + \Theta r_{80} \right]^{-0.017 r_{80}^{-1.44}} \end{array} \right\}$$

1972 $\Theta = 30$

1973 $r_{80} = 0.07-20 \mu\text{m}$

1974

1975

1976 **Mårtensson et al. [2003], laboratory:**

1977
$$\frac{dF_{\text{int}}}{d \log d_p} = U_{10}^{3.41} (a_4 d_p^4 + a_3 d_p^3 + a_2 d_p^2 + a_1 d_p + a_0)$$

1978 $d_p = 0.02\text{-}2.8 \mu\text{m}$

1979 salinity 33

1980 The coefficients a_i are linear functions of temperature that take on different values in each of
1981 three different size ranges (the expression does not yield values that match at the junctions of the
1982 intervals).

1983 These coefficients yield values that are within 0.25% of those of *Mårtensson* (rounding off the
1984 coefficients may yield results that differ by more); for T in °C:

	d_p range/ μm		
	0.02-0.145	0.145-0.419	0.419-2.8
a_0	$-(1.00013+0.11063T)\times 10^2$	$(1.6786-0.02589T)\times 10^3$	$(6.0442+0.8375T)\times 10^1$
a_1	$(3.8735-0.011532T)\times 10^4$	$-(2.1336-0.04543T)\times 10^4$	$-(1.2545+0.15994T)\times 10^2$
a_2	$-(3.9944+0.11009T)\times 10^5$	$(1.1611-0.03129T)\times 10^5$	$(9.9094+1.2027T)\times 10^1$
a_3	$(1.6611+2.2779T)\times 10^5$	$-(2.8549-0.092314T)\times 10^5$	$-(3.3435+0.37789T)\times 10^1$
a_4	$(5.8236-0.98918T)\times 10^6$	$(2.5742-0.09416T)\times 10^5$	$(4.0196+0.41664T)$

1985

1986

1987 **de Leeuw et al. [2000], surf zone:**

1988
$$\frac{dF_{\text{int}}}{d \log r_{80}} = 4.0 \times \exp(0.23 U_{10}) \times U_{10}^{3.41} \times r_{80}^{-0.65}$$

1989 $r_{80} = 0.4\text{-}5 \mu\text{m}$

1990 $U_{10} = 0\text{-}9 \text{ m s}^{-1}$

1991

1992

1993 **Clarke et al. [2006], surf zone:**

1994
$$\frac{dF_{\text{int}}}{d \log d_p} = U_{10}^{3.41} (a_5 d_p^5 + a_4 d_p^4 + a_3 d_p^3 + a_2 d_p^2 + a_1 d_p + a_0)$$

1995 $d_p = 0.01\text{-}8 \mu\text{m}$

1996 The coefficients a_i are linear functions of temperature that take on different values in each of
 1997 three different size ranges. These coefficients yield values that are within 1% of those of *Clarke*
 1998 *et al.*

1999

	$d_p/\mu\text{m}$ range		
	0.01-0.132	0.132-1.2	1.2-8
a_0	-1.920×10^2	1.480×10^2	1.727×10^1
a_1	3.103×10^4	4.485×10^2	3.222×10^1
a_2	-7.603×10^5	-2.524×10^3	-2.071×10^1
a_3	8.402×10^6	3.852×10^3	4.677
a_4	-4.393×10^7	-2.4603×10^3	-4.658×10^{-1}
a_5	8.794×10^7	5.733×10^2	1.733×10^{-2}

2000

2001

2002 **Formulations based on micrometeorological methods:**

2003 **Nilsson & Rannik [2001], Nilsson et al. [2001]; eddy correlation:**

2004 $F_{\text{eff}} = 1.9 \times 10^4 \exp(0.46 U_{10})$

2005 $d_p > 0.01 \mu\text{m}$

2006 $U_{10} = 4\text{-}13 \text{ m s}^{-1}$

2007

2008

2009 **Geever et al. [2005]; eddy correlation:**

2010 $F_{\text{eff}} = 1.9 \times 10^5 \exp(0.23 U_{22})$

2011 $r_{\text{amb}} = 0.005\text{-}0.5 \mu\text{m}$

2012 $U_{22} = 7\text{-}18 \text{ m s}^{-1}$

2013

2014 $F_{\text{eff}} = 6.5 \times 10^4 \exp(0.25 U_{22})$

2015 $d_p = 0.1\text{-}1 \mu\text{m}$

2016 $U_{22} = 4\text{-}17 \text{ m s}^{-1}$

2017

2018

2019 **Petelski & Piskozub [2006] modified by Andreas [2007], gradient method:**

2020
$$\frac{dF_{\text{eff}}}{d \log r_{\text{amb}}} = 1.2 \times 10^3 \exp\left[0.52 U_{10} - (0.05 U_{10} + 0.64) r_{\text{amb}}\right] \times r_{\text{amb}}$$

2021 $r_{\text{amb}} = 0.25\text{-}7 \mu\text{m}$

2022 $U_{10} = 5\text{-}12 \text{ m s}^{-1}$

2023

2024

2025 **Norris et al. [2008]; eddy correlation:**

2026

$r_{\text{amb}}/\mu\text{m}$ range	$\frac{dF_{\text{net}}}{d \log r_{\text{amb}}}$
0.145-0.155	$2.7 \times 10^3 \exp(0.55 U_{10})$
0.155-0.165	$9.3 \times 10^2 \exp(0.90 U_{10})$
0.165-0.21	$1.7 \times 10^2 \exp(0.71 U_{10})$
0.21-0.27	$2.2 \times 10^2 \exp(0.64 U_{10})$
0.27-0.9	$4.3 \times 10^2 \exp(0.46 U_{10})$
0.9-1.6	$7.2 \times 10^2 \exp(0.32 U_{10})$

2027 $U_{10} = 4\text{-}12 \text{ m s}^{-1}$

2028 These are net fluxes (i.e., they have not been corrected for dry deposition).

2029

2030

2031 **Lewis & Schwartz [2004]; based on several methods:**

2032
$$\frac{dF_{\text{eff}}}{d \log r_{80}} = 50 U_{10}^{2.5} \exp\left\{-\left(\frac{1}{2}\right) \left[\frac{\ln\left(\frac{r_{80}}{r_1}\right)}{\ln(4)}\right]^2\right\} \times 5$$

2033 $r_1 = 0.3 \mu\text{m}$

2034 $r_{80} = 0.1\text{-}25 \mu\text{m}$

2035 $U_{10} = 5\text{-}20 \text{ m s}^{-1}$

2036

2037 **Acknowledgements.**

2038 The work of G. de Leeuw and C. O'Dowd was supported by the EU (European Union) FP6
2039 projects MAP (Marine Aerosol Production, project number GOCE-018332), EUCAARI
2040 (European Integrated project on Aerosol Cloud Climate and Air Quality Interactions) project
2041 number 036833-2 and MACC (Monitoring Atmospheric Composition and Climate: FP7
2042 Collaborative Project). Work by C. O'Dowd was further supported by Irish EPA and the HEA
2043 PRTL14 programme and the EU FP6 project GEMS (Global and regional Earth-system
2044 (Atmosphere) Monitoring using Satellite and *in situ* data; contract number SIP4-CT-2004-
2045 516099). The U.S. Office of Naval Research supported E. Andreas's work on this project with
2046 award N000140810411. Work by E. R. Lewis and S. E. Schwartz was supported by the U.S.
2047 Department of Energy's Atmospheric System Research Program (Office of Science, OBER,
2048 contract No. DE-AC02-98CH10886). Work by M.D. Angelova was supported by the U.S.
2049 Office of Naval Research, NRL program element 61153N. Work by C. W. Fairall supported by
2050 NOAA's (National Oceanic and Atmospheric Administration) Office of Climate Observations
2051 and NOAA's Health of the Atmosphere Program. We thank three anonymous reviewers for
2052 helpful comments and suggestions.
2053

2054 **References**

- 2055 Andreae, M. O., and D. Rosenfeld (2008), Aerosol-cloud-precipitation interactions. Part 1. The
2056 nature and sources of cloud-active aerosols, *Earth-Science Rev.*, *89*, 13–41.
- 2057 Andreas, E. L (1992), Sea spray and the turbulent air–sea heat fluxes, *J. Geophys. Res.*, *97*,
2058 11,429–11,441.
- 2059 Andreas, E. L (2007), Comments on “Vertical coarse aerosol fluxes in the atmospheric surface
2060 layer over the North Polar Waters of the Atlantic” by Tomasz Petelski and Jacek Piskozub, *J.*
2061 *Geophys. Res.*, *112*, C11010, doi: 10.1029/2007JC004184.
- 2062 Anguelova, M. D. (2008), Complex dielectric constant of sea foam at microwave frequencies, *J.*
2063 *Geophys. Res.*, *113*, C08001, doi: 10.1029/2007JC004212.
- 2064 Anguelova, M. D., and F. Webster (2006), Whitecap coverage from satellite measurements: A
2065 first step toward modeling the variability of oceanic whitecaps, *J. Geophys. Res.*, *111*,
2066 C03017, doi:10.1029/2005JC003158.
- 2067 Aziz, M. A., S. C. Reising, W. E. Asher, L. A. Rose, P. W. Gaiser, and K. A. Horgan (2005),
2068 Effects of air-sea interaction parameters on ocean surface microwave emission at 10 and 37
2069 GHz, *IEEE Trans. Geosci. Remote Sensing*, *43*, 1763–1774.
- 2070 Bettenhausen, M. H., C. K. Smith, R. M. Bevilacqua, Nai-Yu Wang, P. W. Gaiser, and S. Cox,
2071 (2006), A nonlinear optimization algorithm for WindSat wind vector retrievals, *IEEE Trans.*
2072 *Geosci. Remote Sensing*, *44*, 597–610.
- 2073 Bigg, E. K., and C. Leck (2001), Properties of the aerosol over the central Arctic Ocean, *J.*
2074 *Geophys. Res.*, *106*(D23), 32,101–32,109.
- 2075 Bigg E. K., and C. Leck (2008), The composition of fragments of bubbles bursting at the ocean
2076 surface, *J. Geophys. Res.*, *113*, D11209, doi:10.1029/2007JD009078.
- 2077 Bigg, E. K., C. Leck, and L. Tranvik (2004), Particulates of the surface microlayer of open water
2078 in the central Arctic Ocean in summer, *Marine Chem.*, *91*, 131–141, doi:
2079 10.1016/j.marchem.2004.06.005.
- 2080 Blanchard, D. C. (1963), The electrification of the atmosphere by particles from bubbles in the
2081 sea, *Prog Oceanogr.*, *1*, pp. 71–202, Pergamon Press, New York.

2082 Blanchard, D. C. (1964), Sea to air transport of surface active material, *Science*, *146*, 396–397,
2083 doi: 10.1126/science.146.3642.396.

2084 Blanchard, D. C. (1983), The production, distribution, and bacterial enrichment of the sea-salt
2085 aerosol, in *Air-Sea Exchange of Gases and Particles*, edited by P. S. Liss and W. G. N. Slinn,
2086 pp. 407-454, D. Reidel, Dordrecht.

2087 Blanchard, D. C., and L. D. Syzdeck (1970), Mechanism for the water-to-air transfer and
2088 concentration of bacteria, *Science*, *170*, 626–628.

2089 Blanchard, D. C., and L. D. Syzdek (1972), Concentration of bacteria in jet drops from bursting
2090 bubbles, *J. Geophys. Res.*, *77*, 5087-5099.

2091 Blanchard, D. C., and L. D. Syzdek (1975), Electrostatic collection of jet and film drops,
2092 *Limnology and Oceanography*, *20*, 762-774.

2093 Blanchard, D. C., L.D. Syzdek and M.E. Weber (1981), Bubble scavenging of bacteria in
2094 freshwater quickly produces bacterial enrichment in airborne jet drops, *Limnology and*
2095 *Oceanography*, *26*, 961-964.

2096 Bower, K., T. Choulaton, J. Latham, J. Sahraei, & S. Salter (2006), Computational assessment
2097 of a proposed technique for global warming mitigation via albedo-enhancement of marine
2098 stratocumulus clouds, *Atmos. Res.*, *82*, 328-33.

2099 Brady, M., and G.E. Legge (2009), Camera calibration for natural image studies and vision
2100 research, *J. Opt. Soc. Am. A*, **26**(1), 30-42.

2101 Brooks, I. M., M. J. Yelland, R. C. Upstill-Goddard, P. D. Nightingale, S. Archer, E. D'Asaro, R.
2102 Beale, C. Beatty, B. Blomquist, A. A. Bloom, B. J. Brooks, J. Cluderay, D. Coles, J. Dacey,
2103 M. DeGrandpre, J. Dixon, W. M. Drennan, J. Gabriele, L. Goldson, N. Hardman-Mountford,
2104 M. K. Hill, M. Horn, P.-C. Hsueh, B. Huebert, G. de Leeuw, T. G. Leighton, M. Liddicoat, J.
2105 J. N. Lingard, C. McNeil, J. B. McQuaid, B. I. Moat, G. Moore, C. Neill, S. J. Norris, S.
2106 O'Doherty, R. W. Pascal, J. Prytherch, M. Rebozo, E. Sahlee, M. Salter, U. Schuster, I.
2107 Skjelvan, H. Slagter, M. H. Smith, P. D. Smith, M. Srokosz, J. A. Stephens, P. K. Taylor, M.
2108 Telszewski, R. Walsh, B. Ward, D. K. Woolf, D. Young, and H. Zemmeling (2009), Physical
2109 exchanges at the air-sea interface: UK-SOLAS field measurements, *Bull. Amer. Meteorol.*
2110 *Soc.*, *90*, 629–644, doi: 10.1175/2008BAMS2578.1.

2111 Businger, J. A. (1986), Evaluation of the accuracy with which dry deposition can be measured
2112 with current micrometeorological techniques, *J. Climate Appl. Meteorol.*, 25, 1100–1124.

2113 Caffrey, P. F., W. A. Hoppel, and J. J. Shi, (2006), A one-dimensional sectional aerosol model
2114 integrated with mesoscale meteorological data to study marine boundary layer aerosol
2115 dynamics, *J. Geophys. Res.*, 111, D24201, doi: 10.1029/2006JD007237.

2116 Callaghan, A. H., G. B. Deane, and M. D. Stokes (2008a), Observed physical and environmental
2117 causes of scatter in whitecap coverage values in a fetch-limited coastal zone, *J. Geophys. Res.*,
2118 113, C05022, doi: 10.1029/2007JC004453.

2119 Callaghan, A. H., G. de Leeuw, L. Cohen, and C. D. O’Dowd (2008b), Relationship of oceanic
2120 whitecap coverage to wind speed and wind history, *Geophys. Res. Lett.*, 35, L23609, doi:
2121 10.1029/2008GL036165.

2122 Callaghan, A. H., and M. White (2009), Automated processing of sea surface images for the
2123 determination of whitecap coverage, *J. Atmos. Oceanic Technol.*, 26, 383–394, doi:
2124 10.1175/2008JTECHO634.1.

2125 Carruthers, D. J., and T. W. Choullarton (1986), The microstructure of hill cap clouds. *Quarterly*
2126 *Journal of the Royal Meteorological Society*, 112, 113-129.

2127 Cavalli, F., M. C. Facchini, S. Decesari, M. Mircea, L. Emblico, S. Fuzzi, D. Ceburnis, Y. J.
2128 Yoon, C. D. O’Dowd, J.-P. Putaud, and A. Dell’Acqua (2004), Advances in characterization
2129 of size-resolved organic matter in marine aerosol over the North Atlantic, *J. Geophys. Res.*,
2130 109, D24215, doi: 10.1029/2004JD005137.

2131 Ceburnis, D., C. D. O’Dowd, S. G. Jennings, M. C. Facchini, L. Emblico, S. Decesari, S. Fuzzi,
2132 and J. Sakalys (2008), Marine aerosol chemistry gradients: Elucidating primary and secondary
2133 processes and fluxes, *Geophys. Res. Letts.*, 35, L07804, doi: 10.1029/2008GL033462.

2134 Charlson, R. J., S. E. Schwartz, J. M. Hales, R. D. Cess, J. A. Coakley, Jr., J. E. Hansen, and D.
2135 J. Hoffman (1992), Climate forcing by anthropogenic aerosols, *Science*, 255, 423–430, doi:
2136 10.1126/science.255.5043.423.

2137 Chin, M., P. Ginoux, S. Kinne, O. Torres, B. N. Holben, B. N. Duncan, R. V. Martin, J. A.
2138 Logan, A. Higurashi, and T. Nakajima (2002), Tropospheric aerosol optical thickness from
2139 the GOCART model and comparisons with satellite and Sun photometer measurements, *J.*
2140 *Atmos. Sci.*, *59*, 461–483.

2141 Cipriano, R. J., and D. C. Blanchard (1981), Bubble and aerosol spectra produced by a laboratory
2142 ‘breaking wave,’ *J. Geophys. Res.*, *86*, 8085–8092.

2143 Cipriano, R. J., D. C. Blanchard, A. W. Hogan, and G. G. Lala (1983), On the production of
2144 Aitken nuclei from breaking waves and their role in the atmosphere, *J. Atmos. Sci.*, *40*, 469–
2145 479.

2146 Cipriano, R. J., E. C. Monahan, P. J. Bowyer, and D. K. Woolf (1987), Marine condensation
2147 nucleus generation inferred from whitecap simulation tank results, *J. Geophys. Res.*, *92*,
2148 6569–6576.

2149 Clarke, A. D., S. R. Owens, and J. Zhou (2006), An ultrafine sea-salt flux from breaking waves:
2150 Implications for cloud condensation nuclei in the remote marine atmosphere, *J. Geophys.*
2151 *Res.*, *111*, D06202, doi: 10.1029/2005JD006565.

2152 Day, J. A. (1964), Production of droplets and salt nuclei by the bursting of air-bubble films, *Q. J.*
2153 *R. Meteorol. Soc.*, *90*, 72–78.

2154 de Leeuw, G., F. P. Neele, M. Hill, M. H. Smith, and E. Vignati (2000), Sea spray aerosol
2155 production by waves breaking in the surf zone, *J. Geophys. Res.*, *105*(D2), 29,397–29,409.

2156 de Leeuw, G., M. M. Moerman, C. J. Zappa, W. R. McGillis, S. J. Norris, and M. H. Smith
2157 (2007), Eddy correlation measurements of sea spray aerosol fluxes, in *Transport at the Air-*
2158 *Sea Interface*, edited by C. S. Garbe, R. A. Handler, and B. Jähne, pp. 297–311, Springer-
2159 Verlag, Heidelberg.

2160 Dentener, F., S. Kinne, T. Bond, O. Boucher, J. Cofala., S. Generoso, P. Ginoux, S. Gong, J. J.
2161 Hoelzemann, A. Ito, L. Marelli, J. Penner, J.-P. Putaud., C. Textor, M. Schulz, G. R. van der
2162 Werf, and J. Wilson (2006), Emissions of primary aerosol and precursor gases for the years
2163 2000 and 1750 prescribed data-sets for AeroCom, *Atmos. Chem. Phys.*, *6*, 4321-4344.

2164 Detwiler, A., and D. C. Blanchard (1978), Aging and bursting bubbles in trace-contaminated
2165 water, *Chemical Engineering Science*, *33*, 9-13, 1978.

2166 Drennan, W. M., P. K. Taylor, and M. J. Yelland (2005), Parameterizing the sea surface
2167 roughness, *J. Phys. Oceanogr.*, *35*, 835–848.

2168 Easter, R. C., S. J. Ghan, Y. Zhang, R. D. Saylor, E. G. Chapman, N. S. Laulainen, H. Abdul-
2169 Razzak, L. R. Leung, X. Bian, and R. A. Zaveri (2004), MIRAGE: Model description and
2170 evaluation of aerosols and trace gases, *J. Geophys. Res.*, *109*, D20210, doi:
2171 10.1029/2004JD004571.

2172 Erickson, D. J., J. T. Merrill, and R. A. Duce (1986), Seasonal estimates of global atmospheric
2173 sea-salt distributions, *J. Geophys. Res.*, *91*, 1067–1072.

2174 Facchini, M. C., M. Rinaldi, S. Decesari, C. Carbone, E. Finessi, M. Mircea, S. Fuzzi, D.
2175 Ceburnis, R. Flannigan, E. D. Nilsson, G. de Leeuw, M. Martino, J. Woeltjen, and C. D.
2176 O’Dowd (2008), Primary submicron marine aerosol dominated by insoluble organic colloids
2177 and aggregates, *Geophys. Res. Lett.*, *35*, L17814, doi: 10.1029/2008GL034210.

2178 Freilich, M.H., and B. A. Vanhoff (2006), The accuracy of preliminary WindSat vector wind
2179 measurements: Comparisons with NDBC buoys and QuikSCAT, *IEEE Trans. Geosci. Remote*
2180 *Sensing*, *44*, 622–637.

2181 Frouin, R., M. Schwindling, and P.-Y. Deschamps (1996), Spectral reflectance of sea foam in the
2182 visible and near-infrared: In situ measurements and remote sensing implications, *J. Geophys.*
2183 *Res.*, *101*(C6), 14,361–14,371.

2184 Fuentes E., H. Coe, H., D. Green, D., G. De Leeuw and G. McFiggans (2010), Laboratory-
2185 generated primary marine aerosol via bubble-bursting and atomization, *Atmos. Meas. Tech.*, *3*,
2186 141–162.

2187 Gaiser, P. W, K. M. St Germain, E. M. Twarog, G. A. Poe, W. Purdy, D. Richardson, W.
2188 Grossman, W. L. Jones, D. Spencer, G. Golba, J. Cleveland, L. Choy, R. M. Bevilacqua, and
2189 P. S. Chang (2004), The WindSat spaceborne polarimetric microwave radiometer: Sensor
2190 description and early orbit performance, *IEEE Trans. Geosci. Remote Sensing*, *42*, 2347–
2191 2361.

2192 Geever, M., C. D. O’Dowd, S. van Ekeren, R. Flanagan, E. D. Nilsson, G. de Leeuw, and Ü.
2193 Rannik (2005), Submicron sea spray fluxes, *Geophys. Res. Lett.*, *32*, L15810, doi:
2194 10.1029/2005GL023081.

2195 Gong, S. L. (2003), A parameterization of sea-salt aerosol source function for sub- and super-
2196 micron particles, *Global Biogeochem. Cycles*, *17*(4), 1097, doi: 10.1029/2003GB002079.

2197 Gong, S. L., L. A. Barrie, and J.-P. Blanchet (1997), Modeling sea-salt aerosols in the
2198 atmosphere. 1. Model development, *J. Geophys. Res.*, *102*(D3), 3805–3818.

2199 Gong, S. L., L. A. Barrie., and M. Lazare (2002), Canadian Aerosol Module (CAM): A size-
2200 segregated simulation of atmospheric aerosol processes for climate and air quality models. 2.
2201 Global sea-salt aerosol and its budgets, *J. Geophys. Res.*, *107*(D24), 4779, doi:
2202 10.1029/2001JD002004.

2203 Gong, S. L., L. A. Barrie, J.-P. Blanchet, K. von Salzen., U. Lohmann, G. Lesins, L. Spacek, L.
2204 M. Zhang, E. Girard, H. Lin, R. Leaitch, H. Leighton, P. Chylek, and P. Huang (2003),
2205 Canadian Aerosol Module: A size-segregated simulation of atmospheric aerosol processes for
2206 climate and air quality models. 1. Module development, *J. Geophys. Res.*, *108*(D1), 4007, doi:
2207 10.1029/2001JD002002, 2003.

2208 Grini, A., G. Myhre, J. K. Sundet, and I. S. A. Isaksen (2002), Modeling the annual cycle of sea
2209 salt in the global 3D model Oslo CTM2: Concentrations, fluxes, and radiative impact, *J.*
2210 *Climate*, *15*, 1717–1730.

2211 Guan, C., W. Hu, J. Sun, and R. Li (2007), The whitecap coverage model from breaking
2212 dissipation parametrizations of wind waves, *J. Geophys. Res.*, *112*, C05031, doi:
2213 10.1029/2006JC003714.

2214 Hill, M. K., B. J. Brooks, S. J. Norris, M. H. Smith, I. M. Brooks, G. de Leeuw, and J. J. N.
2215 Lingard (2008), A Compact Lightweight Aerosol Spectrometer Probe (CLASP), *J. Atmos.*
2216 *Oceanic Technol.*, *25*, 1996–2006, doi: 10.1175/2008JTECHA1051.1.

2217 Hoffman, E. J., and R. A. Duce (1976), Factors influencing the organic carbon content of marine
2218 aerosols: A laboratory study, *J. Geophys. Res.*, *81*, 3667–3670.

2219 Hoppel, W. A., G. M. Frick, and J. W. Fitzgerald (2002), Surface source function for sea-salt
2220 aerosol and aerosol dry deposition to the ocean surface, *J. Geophys. Res.*, *107*(D19), 4382,
2221 doi: 10.1029/2001JD002014.

2222 IPCC (2007), *Climate Change 2007: The Physical Science Basis. Contribution of Working*
2223 *Group I to the Fourth Assessment Report of the Intergovernmental Panel on Climate Change*,
2224 edited by S. Solomon, D. Qin, M. Manning, Z. Chen, M. Marquis, K. B. Averyt, M. Tignor,
2225 and H. L. Miller, 996 pp., Cambridge University Press, New York.

2226 Jessup, A. T., C. J. Zappa, M. R. Loewen, and V. Hesany (1997), Infrared remote sensing of
2227 breaking waves, *Nature*, 385, 52–55, doi: 10.1038/385052a0.

2228 Kaimal, J. C., and J. J. Finnigan (1994), *Atmospheric Boundary Layer Flows: Their Structure*
2229 *and Measurement*, 289 pp., Oxford University Press, New York.

2230 Keene, W. C., H. Maring, J. R. Maben, D. J. Kieber, A. A. P. Pszenny, E. E. Dahl, M. A.
2231 Izaguirre, A. J. Davis, M. S. Long, X. Zhou, L. Smoydzin, and R. Sander (2007), Chemical
2232 and physical characteristics of nascent aerosols produced by bursting bubbles at a model air-
2233 sea interface, *J. Geophys. Res.*, 112, D21202, doi: 10.1029/2007JD008464.

2234 Koch, D., G. A. Schmidt, and C. V. Field (2006), Sulfur, sea salt and radionuclide aerosols in
2235 GISS ModelE, *J. Geophys. Res.*, 111, D06206, doi: 10.1029/2004JD005550.

2236 Koepke, P. (1986), Remote sensing signature of whitecaps, in *Oceanic Whitecaps and Their Role*
2237 *in Air–Sea Exchange Processes*, edited by E. C. Monahan and G. M. Niocaill, pp. 251–260,
2238 D. Reidel, Dordrecht.

2239 Kokhanovsky, A. A. (2004), Spectral reflectance of whitecaps, *J. Geophys. Res.*, 109, C05021,
2240 doi: 10.1029/2003JC002177.

2241 Kroeker, K.L. (2009), Photography’s bright future, *Communications of the ACM*, 52(2), 11-13,
2242 doi:10.1145/1461928.1661933.

2243 Lafon, C., J. Piazzola, P. Forget, O. le Calve, and S. Despiau (2004), Analysis of the variations
2244 of the whitecap fraction as measured in a coastal zone, *Boundary Layer Meteorol.*, 111, 339–
2245 360.

2246 Lafon, C., J. Piazzola, P. Forget, and S. Despiau (2007), Whitecap coverage in coastal
2247 environment for steady and unsteady wave field conditions, *J. Marine Systems*, 66, 38–46.

2248 Langmann, B., S. Varghese, E. Marmer, E. Vignati, J. Wilson, P. Stier, and C. O’Dowd (2008a),
2249 Aerosol distribution over Europe: A model evaluation study with detailed aerosol
2250 microphysics, *Atmos. Chem. Phys.*, 8, 1591–1607.

- 2251 Langmann, B., C. Scannell, and C. D. O'Dowd (2008b), New Directions: Organic matter
2252 contribution to marine aerosols and cloud condensation nuclei, *Atmos. Environ.*, *42*, 7821–
2253 7822.
- 2254 Latham, J. (1990), Control of global warming?, *Nature*, *347*, 339-340.
- 2255 Leck, C., and E. K. Bigg (1999), Aerosol production over remote marine areas—A new route,
2256 *Geophys. Res. Lett.*, *23*, 3577–3581.
- 2257 Leck, C., and E. K. Bigg (2005a), Biogenic particles in the surface microlayer and overlaying
2258 atmosphere in the central Arctic Ocean during summer, *Tellus*, *57B*, 305–316, doi:
2259 10.1111/j.1600-0889.2005.00148.x.
- 2260 Leck, C., and E. K. Bigg (2005b), Source and evolution of the marine aerosol—A new
2261 perspective, *Geophys. Res. Lett.*, *32*, L19803, doi: 10.1029/2005GL023651.
- 2262 Leck, C., and E. K. Bigg (2008), Comparison of sources and nature of the tropical aerosol with
2263 the summer high Arctic aerosol, *Tellus*, *60B*, 118–126, doi: 10.1111/j.1600-
2264 0889.2007.00315.x.
- 2265 Lewis, E. R. (2008), An examination of Köhler theory resulting in an accurate expression for the
2266 equilibrium radius ratio of a hygroscopic aerosol particle valid up to and including relative
2267 humidity 100%, *J. Geophys. Res.*, *113*, D03205, doi: 10.1029/2007JD008590.
- 2268 Lewis, E. R., and S. E. Schwartz (2004), *Sea Salt Aerosol Production: Mechanisms, Methods,*
2269 *Measurements and Models—A Critical Review*, 413 pp., American Geophysical Union,
2270 Washington, D.C.
- 2271 Liu, X., and J. E. Penner (2002), Effect of Mt. Pinatubo H₂SO₄/H₂O aerosol on ice nucleation in
2272 the upper troposphere using a global chemistry and transport model (IMPACT), *J. Geophys.*
2273 *Res.*, *107*(D12), doi: 10.1029/2001JD000455.
- 2274 Marmorino, G. O., and G. B. Smith (2005), Bright and dark ocean whitecaps observed in the
2275 infrared, *Geophys. Res. Lett.*, *32*, L11604, doi: 10.1029/2005GL023176.
- 2276 Mårtensson, E. M., E. D. Nilsson, G. de Leeuw, L. H. Cohen, and H. C. Hansson (2003),
2277 Laboratory simulations of the primary marine aerosol production, *J. Geophys. Res.*, *108*(D9),
2278 4297, doi: 10.1029/2002JD002263.

2279 Massel, S. R. (2007), *Ocean Waves Breaking and Marine Aerosol Fluxes*, 323 pp., Springer,
2280 New York.

2281 Middlebrook, A. M., D. M. Murphy, and D. S. Thomson (1998), Observation of organic material
2282 in individual particles at Cape Grim during the First Aerosol Characterization Experiment
2283 (ACE 1), *J. Geophys. Res.*, *103*, 16,475–16,483.

2284 Monahan, E. C., and I. G. Ó Muircheartaigh (1980), Optimal power-law description of oceanic
2285 whitecap coverage dependence on wind speed, *J. Phys. Oceanogr.*, *10*, 2094–2099.

2286 Monahan, E. C., C. W. Fairall, K. L. Davidson, and P. Jones-Boyle (1983), Observed inter-
2287 relations between 10 m winds, ocean whitecaps and marine aerosols, *Q. J. R. Meteorol. Soc.*,
2288 *109*, 379–392.

2289 Monahan, E. C., D. E. Spiel, K. L. Davidson (1986), A model of marine aerosol generation via
2290 whitecaps and wave disruption, pp. 167–174, in *Oceanic Whitecaps and Their Role in Air-Sea*
2291 *Exchange Processes*, edited by E. C. Monahan and G. MacNiocaill, D. Reidel, Dordrecht.

2292 Myhre, G., T. K. Berntsen, J. M. Haywood, J. K. Sundet, B. N. Holben, M. Johnsrud, and F.
2293 Stordal (2003), Modeling the solar radiative impact of aerosols from biomass burning during
2294 the Southern African Regional Science Initiative (SAFARI-2000) experiment, *J. Geophys.*
2295 *Res.*, *108*(D13), 8501, doi: 10.1029/2002JD002313.

2296 Nilsson, E. D., and Ü. Rannik (2001), Turbulent aerosol fluxes over the Arctic Ocean. 1. Dry
2297 deposition over sea and pack ice, *J. Geophys. Res.*, *106*(D23), 32,125–32,137.

2298 Nilsson, E. D., Ü Rannik, E. Swietlicki, C. Leck, P. P. Aalto, J. Zhou, and M. Norman (2001),
2299 Turbulent aerosol fluxes over the Arctic Ocean. 2. Wind-driven sources from the sea, *J.*
2300 *Geophys. Res.*, *106*(D23), 32,139–32,154.

2301 Nordberg, W., J. Conaway, D. B. Ross, and T. Wilheit (1971), Measurements of microwave
2302 emission from a foam-covered, wind-driven sea, *J. Atm. Sci.*, **28**, 429-435.

2303 Norris, S. J., I. M. Brooks, G. de Leeuw, M. H. Smith, M. M. Moerman, and J. J. N. Lingard
2304 (2008), Eddy covariance measurements of sea spray particles over the Atlantic Ocean, *Atmos.*
2305 *Chem. Phys.*, *8*, 555–563.

2306 Novakov, T., C. E. Corrigan, J. E. Penner, C. C. Chuang, O. Rosario, and O. L. Mayol Bracero
2307 (1997), Organic aerosols in the Caribbean trade winds: A natural source? *J. Geophys. Res.*,
2308 *102*, 21,307–21,313.

2309 O’Dowd, C.D., and G. de Leeuw (2007), Marine Aerosol Production: a review of the current
2310 knowledge. *Phil. Trans. R. Soc. A365*, 1753–1774, doi:10.1098/rsta.2007.2043.

2311 O’Dowd, C. D., M. H. Smith, I. E. Consterdine, and J. A. Lowe (1997), Marine aerosol, sea salt,
2312 and the marine sulphur cycle: A short review, *Atmos. Environ.*, *31*, 73–80.

2313 O’Dowd, C. D., M. C. Facchini, F. Cavalli, D. Ceburnis, M. Mircea, S. Decesari, S. Fuzzi, Y. J.
2314 Yoon, J.-P. Putaud (2004), Biogenically driven organic contribution to marine aerosol,
2315 *Nature*, *431*, 676–680, doi: 10.1038/nature02959.

2316 O’Dowd, C. D., B. Langmann, S. Varghese, C. Scannell, D. Ceburnis, and M. C. Facchini
2317 (2008), A combined organic-inorganic sea-spray source function, *Geophys. Res. Letts.*, *35*,
2318 L01801, doi: 10.1029/2007GL030331.

2319 O’Reilly, J. E., S. Maritorena, B. G. Mitchell, D. A. Siegel, K. L. Carder, S. A. Garver, M.
2320 Kahru, and C. McClain (1998), Ocean color chlorophyll algorithms for SeaWiFS, *J. Geophys.*
2321 *Res.*, *103*(C11), 24,937–24,953, doi:10.1029/98JC02160.

2322 Oppo, C., S. Bellandi, N. Degli Innocenti, A. M. Stortini, G. Loglio, E. Schiavuta, and R. Cini
2323 (1999), Surfactant components of marine organic matter as agents for biogeochemical
2324 fractionation and pollutant transport via marine aerosols, *Marine Chem.*, *63*, 235–253.

2325 Padmanabhan, S., S. C. Reising, W. E. Asher, L. A. Rose, and P. W. Gaiser (2006), Effects of
2326 foam on ocean surface microwave emission inferred from radiometric observations of
2327 reproducible breaking waves, *IEEE Trans. Geosci. Remote Sensing*, *44*, 569–583.

2328 Petelski, T. (2003), Marine aerosol fluxes over open sea calculated from vertical concentration
2329 gradients, *J. Aerosol Sci.*, *34*, 359–371.

2330 Petelski, T. (2005). Coarse aerosol concentration over the North Polar waters of the Atlantic.
2331 *Aerosol Science and Technology*, *39*, 695-700.

2332 Petelski, T., and J. Piskozub (2006), Vertical coarse aerosol fluxes in the atmospheric surface
2333 layer over the North Polar waters of the Atlantic, *J. Geophys. Res.*, *111*, C06039, doi:
2334 10.1029/2005JC003295.

2335 Petelski, T., and J. Piskozub (2007), Reply to comment by Edgar L Andreas on “Vertical coarse
2336 aerosol fluxes in the atmospheric surface layer over the North Polar Waters of the Atlantic,”
2337 *J. Geophys. Res.*, *112* (C11), doi:10.1029/2007JC004399.

2338 Pitari, G., E. Mancini, V. Rizi, and D. T. Shindell (2002), Impact of future climate and emissions
2339 changes on stratospheric aerosols and ozone, *J. Atmos. Sci.*, *59*, 414–440.

2340 Prospero, J.M. (2002), The Chemical and Physical Properties of Marine Aerosols: An
2341 Introduction, in *Chemistry of Marine Water and Sediments*, edited by A. Gianguzza, E.
2342 Pellizzetti and S. Sammarano, pp. 35-82, Springer-Verlag Berlin, Heidelberg.

2343 Putaud, J.-P., R. Van Dingenen, M. Mangoni, A. Virkkula, F. Raes, H. Maring, J. M. Prospero,
2344 E. Swietlicki, O. H. Berg, R. Hillamo, and T. Mäkela (2000), Chemical mass closure and
2345 assessment of the origin of the submicron aerosol in the marine boundary layer and the free
2346 troposphere at Tenerife during ACE-2, *Tellus*, *52B*, 141–168.

2347 Reddy, M. S., O. Boucher, Y. Balkanski, and M. Schulz (2005), Aerosol optical depths and
2348 direct radiative perturbations by species and source type, *Geophys. Res. Lett.*, *32*, L12803,
2349 doi: 10.1029/2004GL021743.

2350 Resch, F., and G. Afeti (1992), Submicron film drop production by bubbles in seawater, *J.*
2351 *Geophys. Res.*, *97*, 3679–3683.

2352 Reul, N., and B. Chapron (2003), A model of sea-foam thickness distribution for passive
2353 microwave remote sensing applications, *J. Geophys. Res.*, *108*(C10), 3321, doi:
2354 10.1029/2003JC001887.

2355 Rose, L. A., W. E. Asher, S. C. Reising, P. W. Gaiser, K. M. St. Germain, D. J. Dowgiallo, K. A.
2356 Horgan, G. Farquharson, and E. J. Knapp (2002), Radiometric measurements of the
2357 microwave emissivity of foam, *IEEE Trans. Geosci. Remote Sensing*, *40*, 2619–2625.

2358 Satheesh S.K., and Moorthy K.K.: 2005. Radiative effects of natural aerosols: A review. *Atm.*
2359 *Env.* **39**: 2089-2110.

2360 Schulz, M., G. de Leeuw, and Y. Balkanski (2004), Sea-salt aerosol source functions and
2361 emissions, in *Emission of Atmospheric Trace Compounds*, pp. 333–359, edited by C. Granier,
2362 P. Artaxo, and C. E. Reeves, Kluwer, Dordrecht.

2363 Sellegri, K., C. D. O'Dowd, Y. J. Yoon, S. G. Jennings, and G. de Leeuw (2006), Surfactants
2364 and submicron sea spray generation, *J. Geophys. Res.*, *111*, D22215, doi:
2365 10.1029/2005JD006658.

2366 Slinn, S. A., and W. G. N. Slinn (1980), Predictions for particle deposition on natural waters,
2367 *Atmos. Environ.*, *14*, 1013–1016.

2368 Smith, M. H., and N. M. Harrison (1998), The sea spray generation function, *J. Aerosol. Sci.*, *29*
2369 (Suppl. 1), S189–S190.

2370 Smith, M. H., P. M. Park, and I. E. Consterdine (1993), Marine aerosol concentrations and
2371 estimated fluxes over the sea, *Q. J. R. Meteorol. Soc.*, *119*, 809–824.

2372 Soloviev, A., M. Donelan, H. Graber, B. Haus, and P. Schlüssel (2007), An approach to
2373 estimation of near-surface turbulence and CO₂ transfer velocity from remote sensing data, *J.*
2374 *Marine Systems*, *66*, 182–194.

2375 Spiel, D. E. (1995), On the birth of jet drops from bubbles bursting on water surfaces, *J.*
2376 *Geophys. Res.*, *100*, 4995–5006.

2377 Stier, P., J. Feichter, S. Kinne, S. Kloster, E. Vignati, J. Wilson, L. Ganzeveld, I. Tegen, M.
2378 Werner, Y. Balkanski, M. Schulz, and O. Boucher (2005), The aerosol-climate model
2379 ECHAM5-HAM, *Atmos. Chem. Phys.*, *5*, 1125–1156.

2380 Sugihara, Y., H. Tsumori, T. Ohga, H. Yoshioka, and S Serizawa (2007), Variation of whitecap
2381 coverage with wave-field conditions, *J. Marine Systems*, *66*, 47–60.

2382 Takemura, T., H. Okamoto, Y. Maruyama, A. Numaguti, A. Higurashi, and T. Nakajima (2000),
2383 Global three-dimensional simulation of aerosol optical thickness distribution of various
2384 origins, *J. Geophys. Res.*, *105*, 17,853–17,873.

2385 Takemura, T., T. Nakajima, O. Dubovik, B. N. Holben, and S. Kinne, (2002), Single-scattering
2386 albedo and radiative forcing of various aerosol species with a global three-dimensional model,
2387 *J. Climate*, *15*, 333–352.

2388 Textor, C., M. Schulz, S. Guibert, S. Kinne, Y. Balkanski, S. Bauer, T. Berntsen, T. Berglen, O.
2389 Boucher, M. Chin, F. Dentener, T. Diehl, R. Easter, H. Feichter, D. Fillmore, S. Ghan, P.
2390 Ginoux, S. Gong, A. Grini, J. Hendricks, L. Horowitz, P. Huang, I. Isaksen, T. Iversen, S.
2391 Kloster, D. Koch, A. Kirkevåg, J. E. Kristjansson, M. Krol, A. Lauer, J. F. Lamarque, X. Liu,
2392 V. Montanaro, G. Myhre, J. Penner, G. Pitari, S. Reddy, Ø. Seland, P. Stier, T. Takemura, and
2393 X. Tie (2006), Analysis and quantification of the diversities of aerosol life cycles within
2394 AeroCom, *Atmos. Chem. Phys.*, 6, 1777–1813.

2395 Thorpe, S. A. (1992), Bubble clouds and the dynamics of the upper ocean, *Q. J. R. Meteorol.*
2396 *Soc.*, 118, 1–22.

2397 Tyree, C. A., V. M. Hellion, O. A. Alexandrova, and J. O. Allen (2007), Foam droplets
2398 generated from natural and artificial seawaters, *J. Geophys. Res.*, 112, D12204, doi:
2399 10.1029/2006JD007729.

2400 Vignati, E., M. C. Facchini, M. Rinaldi, C. Scannell, D. Ceburnis, J. Sciare, M. Kanakidou, S.
2401 Myriokefalitakis, F. Dentener, and C. D. O’Dowd (2010), Global scale emission and
2402 distribution of sea spray aerosol: Sea-salt and organic enrichment, *Atmos. Environ.*, 44, 670–
2403 677.

2404 Wang, Q., E. C. Monahan, W. E. Asher, and P. M. Smith (1995), Correlations of whitecap
2405 coverage and gas transfer velocity with microwave brightness temperature for plunging and
2406 spilling breaking waves, in *Air-water gas transfer*, B. Jähne and E.C. Monahan, Eds., AEON
2407 Verlag & Studio, Hanau, 217-225.

2408 Whitlock, C. H., D. S. Bartlett, and E. A. Gurganus (1982), Sea foam reflectance and influence
2409 on optimum wavelength for remote sensing of ocean aerosols, *Geophys. Res. Lett.*, 9, 719–
2410 722.

2411 Woodcock, A. H. (1948), Note concerning human respiratory irritation associated with high
2412 concentrations of plankton and mass mortality of marine organism, *J. Marine Res.*, 7, 56–62.

2413 Woolf, D. K. (2005), Parametrization of gas transfer velocities and sea-state-dependent wave
2414 breaking, *Tellus 57B*, 87–94.

2415 Yoon, Y. J., D. Ceburnis, F. Cavalli, O. Jourdan, J.-P. Putaud, M. C. Facchini, S. Descari, S.
2416 Fuzzi, K. Sellegri, S. G. Jennings, and C. D. O'Dowd (2007), Seasonal characteristics of the
2417 physicochemical properties of North Atlantic marine atmospheric aerosols, *J. Geophys. Res.*,
2418 *112*, D04206, doi: 10.1029/2005JD007044.

2419 Zakey, A. S., F. Giorgi, and X. Bi (2008), Modeling of sea salt in a regional climate model:
2420 Fluxes and radiative forcing, *J. Geophys. Res.*, *113*, D14221, doi:10.1029/2007JD009209

2421 Zhao, D., and Y. Toba (2001), Dependence of whitecap coverage on wind and wind-wave
2422 properties, *J. Oceanogr.*, *57* 603–616.
2423

2424 **Figure Captions**

2425 Figure 1. Annual-average dry SSA mass production flux as computed by several chemical
2426 transport and general circulation models participating in the AeroCom aerosol model
2427 intercomparison [Textor *et al.*, 2006]. A global mean production flux of $10 \text{ g m}^{-2} \text{ yr}^{-1}$ over the
2428 world ocean corresponds to a total global production rate of approximately 3500 Tg yr^{-1} . For
2429 identification of the models, production methods employed, and references see Table 1. Number
2430 given in each panel denotes global annual SSA production in $10^{12} \text{ kg yr}^{-1}$.

2431
2432 Figure 2. Whitecap fraction W as a function of wind speed at 10 m above the sea surface U_{10} ,
2433 from five new data sets (color symbols) and from previous studies that used film photography
2434 (gray symbols) as summarized in Table 20 of Lewis and Schwartz [2004] and in Table 2 (data
2435 sets 1-5, 7-17, 21, 26) of Anguelova and Webster [2006]. Points on abscissa denote values less
2436 than or equal to 1×10^{-6} . The formulation of Monahan and O’Muircheartaigh [1980], Eq. 9, is
2437 also shown.

2438
2439 Figure 3. Whitecap fraction W as a function of wind speed at 10 m above the sea surface U_{10} ,
2440 arithmetically averaged in intervals of 1 m s^{-1} , obtained with the algorithm of Anguelova and
2441 Webster [2006] (blue) using annually-averaged (1998) observations of brightness temperature T_B
2442 from Special Sensor Microwave Imager (SSM/I) in clear sky (no clouds) locations all over the
2443 globe. The corresponding U_{10} values are also from SSM/I. Error bars on W values represent one
2444 standard deviation of the data points falling in each U_{10} bin; the apparent asymmetry of the error
2445 bars is a consequence of plotting on the logarithmic ordinate scale. Also shown (gray) are bin-
2446 average values of W from previous photographic determinations shown in Figure 2 and the
2447 formulation of Monahan and OMuircheartaigh [1980], Eq. 9.

2448
2449 Figure 4. Size distributions of SSA production flux normalized to maximum value in
2450 representation $dF/d\log r_{80}$ as a function of r_{80} from laboratory experiments [Mårtensson *et al.*,
2451 2003, Figure 4c; Sellegri *et al.*, 2006, Figures 2 and 4; Keene *et al.*, 2007, Figure 3 for 5 L min^{-1} ;
2452 Tyree *et al.*, 2007, Table 1, artificial seawater, salinity 33; and Fuentes *et al.*, 2010, Figure 6] and

2453 field measurements [*Clarke et al.*, 2006, formulation presented in text; *Norris et al.*, 2008,
2454 Figure 6 at U_{10} 5, 10, and 12 m s⁻¹]. Uncertainties in the original data are not shown.

2455
2456 Figure 5. Dependence of total SSA number production flux per white area in laboratory
2457 experiments of *Mårtensson et al.* [2003], using artificial seawater (salinity 33) at two different
2458 temperatures, *Keene et al.* [2007], using natural (low-productivity) seawater, *Tyree et al.* [2007],
2459 using artificial seawater (salinity 33), on bubble volume flux (volume of air in bubbles rising to
2460 the water surface per unit area and time).

2461
2462 Figure 6. (a) Mass fraction of sea salt, water-soluble organic matter (WSOM), and water-
2463 insoluble organic matter (WIOM) as a function of particle radius sampled at approximately 70%
2464 RH, (a) for seawater bubble-bursting chamber experiments with fresh seawater, conducted in a
2465 shipboard laboratory in a plankton bloom over the N.E. Atlantic (May-June 2006), (b) for clean
2466 marine air at Mace Head, Ireland, May-June 2006, and (c) for clean marine air 200-300 km
2467 offshore west-northwest of Mace Head in a plankton bloom coincident in time with
2468 aforementioned samples. Adapted from *Facchini et al.* [2008].

2469
2470 Figure 7. Average mass concentration of total particulate matter (black line, right axis) and mass
2471 fraction (colors, left axis) of sea salt, NH₄, nss-SO₄, NO₃, water-soluble organic matter
2472 (WSOM), water-insoluble organic matter (WIOM), and black carbon (BC) in several size ranges
2473 for North Atlantic marine aerosol sampled at Mace Head, Ireland, in clean marine air during
2474 periods of (a) low biological activity, November (2002) January (2003) and February (2003)
2475 November 2002; and (b) high biological activity, March-October, (2002). Radius corresponds to
2476 relative humidity approximately 70%. For low biological activity mass concentrations of aerosol
2477 constituents other than sea salt were below detection limits for the size range 0.03-0.06 μm.
2478 Oceanic chlorophyll-a concentrations over the North Atlantic for periods of (c) low and (d) high
2479 biological activity are five year averages (1998-2002) over the same months as for the
2480 composition measurements, based on satellite measurements of ocean color (courtesy of

2481 SeaWiFS Project, NASA/Goddard Space Flight Center and ORBIMAGE). Adapted from
2482 O’Dowd et al. [2004].

2483
2484 Figure 8. Vertical profiles of mass concentration of sea salt, water-soluble inorganic matter
2485 (WIOM), non-sea-salt sulfate, and water-soluble organic matter (WSOM) at Mace Head, Ireland,
2486 normalized to the sum of the concentrations of the species at the three heights, for particle radius
2487 (at ambient relative humidity) less than $0.5 \mu\text{m}$ sampled in clean marine air. All values are
2488 averages of nine individual 7-day samples analyzed from April-October, 2005 except WIOM,
2489 which is shown for an average of three samples where a positive WIOM flux was observed and
2490 which represented periods when the organic-enriched waters were within the flux footprint as
2491 discussed in text. Uncertainty bars represent the standard deviation from the normalized
2492 concentration average. Adapted from *Ceburnis et al.* [2008].

2493
2494 Figure 9. Parameterizations of size-dependent SSA production flux discussed in text and
2495 presented in the Appendix, evaluated for wind speed $U_{10} = 8 \text{ m s}^{-1}$ (or $U_{22} = 8 \text{ m s}^{-1}$ for *Geever et*
2496 *al.*; 2005). Also shown are central values (curves) and associated uncertainty ranges (bands)
2497 from review of *Lewis and Schwartz* [2004], which denote subjective estimates by those
2498 investigators based on the statistical wet deposition method (green), the steady-state deposition
2499 method (blue), and taking into account all available methods (black); no estimate was provided
2500 for $r_{80} < 0.1 \mu\text{m}$. Lower axis denotes radius at 80% relative humidity, r_{80} , except for formulations
2501 of *Nilsson et al.* [2001], *Mårtensson et al.* [2003], and *Clarke et al.* [2006] which are in terms of
2502 dry particle diameter, d_p , approximately equal to r_{80} , and those of *Geever et al.* [2005], *Petelski*
2503 *and Piskozub* [2006] (dry deposition method), and *Norris et al.* [2008] which are in terms of
2504 ambient radius, r_{amb} . Formulation of *Petelski and Piskozub* [2006] by the dry deposition method
2505 is based on expression in Appendix. Formulations of *Tyree et al.* [2007] are for artificial
2506 seawater of salinity 33 at the two specified bubble volume fluxes. Formulations of *Nilsson et al.*
2507 [2001] and *Geever et al.* [2005] of particle number production flux without size resolution are
2508 plotted arbitrarily as if the flux is independent of r_{amb} over the size ranges indicated to yield the
2509 measured number flux as an integral over that range.

2510

2511 Figure 10. Mass fraction of water-insoluble organic matter WIOM in sea-spray aerosol with
2512 $0.1 \mu\text{m} \leq r_{\text{amb}} \leq 0.5 \mu\text{m}$ measured at Mace Head, Ireland under clean marine conditions as a
2513 function of spatial-average oceanic surface-water chlorophyll-a concentration over an upwind
2514 grid of $1000 \text{ km} \times 1000 \text{ km}$ as determined from MODIS satellite measurements of ocean color,
2515 revised from *O'Dowd et al.* [2008] and provided by C. O'Dowd, 2010. Original fit presented by
2516 *O'Dowd et al.* [2008] and fits to revised data presented by *Langmann et al.* [2008b, corrected by
2517 *Vignati et al.*, 2010] and *Vignati et al.* [2010] are also shown.

2518

2519 Figure 11. Global distribution of mass flux of sea salt (upper panel) and water-insoluble organic
2520 matter WIOM (lower panel) in sea spray with $0.1 \mu\text{m} < r_{80} < 1 \mu\text{m}$ averaged over a one-year
2521 period in 2002–2003 using the TM5 chemical transport model [*Vignati, et al.*, 2010; *E. Vignati,*
2522 private communication, 2010].

2523 **Tables.**

2524 Table 1. Information on sea-salt production methods for model calculations of sea-salt
2525 production in Figure 1. Adapted from *Textor et al.* [2006].

2526

2527 Table 2. Methods used to determine SSA production flux.

2528

2529 Table 3. Location and time of observations and accompanying meteorological and oceanographic
2530 factors (U_{10} , X , T_w , ΔT)¹ for new measurements of whitecap fraction shown in Figure 2.

2531

2532 Table 4. Experimental investigations of sea-spray production by laboratory bubble plumes.

2533

2534 Table 1. Information on sea-salt production methods for model calculations of sea-salt production in Figure 1. Adapted from *Textor et al.* [2006].

2535

Model	Sea-salt module	Winds	SSA production method	Reference for SSA production method	Global dry SSA mass production /(10^{12} kg yr ⁻¹)	Maximum $r_{80}/\mu\text{m}$ of emitted particles
ARQM	<i>Gong et al.</i> [2003]	model derived	interactive	<i>Gong et al.</i> [2003]	118	41
GISS	<i>Koch et al.</i> [2006]	model derived	interactive	<i>Monahan et al.</i> [1986]	2.2	8.6
GOCART	<i>Chin et al.</i> [2002]	GEOS-DAS ^a	interactive	<i>Monahan et al.</i> [1986]; <i>Gong et al.</i> [2003]	9.9	10
KYU (Sprintars)	<i>Takemura et al.</i> [2002]	model derived	interactive	<i>Erickson et al.</i> [1986]; <i>Takemura et al.</i> [2000]	3.9	10
LOA	<i>Reddy & Boucher</i> [2004]; <i>Reddy et al.</i> [2005a, b]	model derived	interactive	<i>Monahan et al.</i> [1986]	3.5	20
LSCE	<i>Schulz et al.</i> [2004]	ECMWF ^b	interactive	<i>Schulz et al.</i> [2004] fit to <i>Monahan et al.</i> [1986]; <i>Smith & Harrison</i> [1998]	21.9	15 ^c
MPI_HAM	<i>Stier et al.</i> [2005]	model derived	interactive	<i>Schulz et al.</i> [2004] fit to <i>Monahan et al.</i> [1986]; <i>Smith & Harrison</i> [1998]	5.1	8 ^c
PNNL	<i>Easter et al.</i> [2004]	model derived	interactive	<i>Gong et al.</i> [2002]	7.4	15 ^c
UIO-CTM	<i>Myhre et al.</i> [2003]	ECMWF ^b	interactive	<i>Grini et al.</i> [2002]	9.5	50
ULAQ	<i>Pitari et al.</i> [2002]	ECMWF ^b	precalculated monthly	<i>Gong et al.</i> [1997]	3.5	20.5
UMI	<i>Liu & Penner</i> [2002]	ECMWF ^b	precalculated monthly	<i>Gong et al.</i> [1997]	3.8	10
Aerocom source ^d	<i>Dentener et al.</i> [2006]	ECMWF ^b	precalculated daily	<i>Gong et al.</i> [2003]	7.9	10

2536

2537 ^a GEOS-DAS: Goddard Earth Observing System Model, Data Assimilation System

2538 ^b ECMWF: European Centre for Medium-Range Weather Forecasts

2539 ^c Estimated radius below which 95% of sea-salt mass is emitted, using respective geometric mean diameter and lognormal width

2540 ^d The "Aerocom source" refers to a source function employed in joint Aerocom B experiments that compared the consequences of differences in representation of processes

2541 comprising the life cycles of aerosol species in the atmosphere by removing diversity in the different models caused by differing emissions [Dentener et al., 2006].

2542 Table 2. Methods used to determine SSA production flux.

2543

Method	Flux^a	$r_{80}/\mu\text{m}$ range^b	Comments
Steady-state dry deposition	Eff	3-25	Easy to apply
Concentration buildup	Eff	< ~10	Has been applied only once; holds promise
Statistical wet deposition	Eff	< ~1	Simple, provides constraint on production flux
Micrometeorological	Eff	< ~10	Several such methods
Whitecap	Int	< ~10	Several approaches; typically measures production flux from laboratory-generated whitecaps
Bubble	Int	< ~100	Requires knowledge of several quantities
Along-wind flux	Int	> ~50	Laboratory measurements; often incorrectly applied
Direct observation	Int	> ~500	Has been applied only in laboratory
Vertical impaction	Int	> ~250	Has been applied once in oceanic conditions

2544 ^a “Int” and “Eff” refer to interfacial and effective SSA production fluxes, respectively.

2545 ^b Approximate range of $r_{80}/\mu\text{m}$ to which the method can or has typically been applied.

2546

2547

2548 Table 3. Location and time of observations and accompanying meteorological and oceanographic factors (U_{10} , X , T_w , ΔT)¹ for new measurements of whitecap fraction shown in
 2549 Figure 2.

2550

Ref.	Platform	Location	Time period	U_{10} range (m s ⁻¹)	X (km)	T_w (°C)	ΔT (°C)	Additional parameters ²	Data points	Images per data point	Averaging period (min)	Medium	Image rate (sec ⁻¹)	Geom. mean of ratio ³ to <i>MO'M80</i>
<i>Lafon et al.</i> , 2004	ship	Gulf of Lyon, Mediterranean	Mar-Apr, 1998	6-17	8-90	13	-2.65 to +6.25	u^* , f_p , H_s	45	10-25	5 to 12.5	Film	0.033	0.64
<i>Lafon et al.</i> , 2007	tower	Toulon-Hyères Bay, Mediterranean	Oct-Nov, 2001	10-18	<30	14	NA	u^* , f_p , H_s	29	24	12	Film	0.033	0.52
<i>Sugihara et al.</i> , 2007	tower	Tanabe Bay, Wakayama, Japan	Nov-Dec, 2003; Feb-Mar, 2004	4.4-16.4	Coastal	NA	-11 to 0	u^* , T_p , c_p , H_s	91	600	10	Digital video	1	0.35
<i>Callaghan et al.</i> , 2008a	tower	Martha's Vineyard, Massachusetts, USA	Nov, 2002	3-12	3-20	NA	NA	ϕ_w , f_p , c_p / u^* , \vec{u}_c	73	400-1200	20	Digital photo	1	0.24
<i>Callaghan et al.</i> , 2008b	ship	Northeast Atlantic	Jun-Jul, 2006	4.5-23	200, 500, >500	13-14	-3.86 to -0.13	T_a , T_w for 44 data points	107	100-782	30	Digital video	0.5	0.46

2551

2552

2553 ¹ Meteorological and oceanographic factors:

2554 U_{10} : Wind speed at 10 m above the sea surface

2555 X : Fetch (the length of water over which wind has blown)

2556 T_w : Water temperature

2557 $\Delta T = T_a - T_w$: Difference between air temperature T_a and water temperature

2558 ² Additional parameters (directly measured or calculated):

2559 u^* : Wind friction velocity

2560 H_s : Significant wave height

2561 f_p : Frequency peak of wave spectrum

2562 T_p : Peak wave period

2563 c_p : Phase speed of dominant waves

2564 c_p / u^* : Wave age

2565 ϕ_w : Wind direction

2566 $\overset{\mathbf{r}}{u}_c$: Ocean current velocity (magnitude and direction)

2567 ³ Geometric mean of the ratios of measured values of W to those calculated using the formulation
2568 of *Monahan and O’Muircheartaigh* [1980], Eq. 9 in the text.

2569

2570

2571

2572 Table 4. Experimental investigations of sea-spray production by laboratory bubble plumes.

2573

Study	Medium	Organic added	Bubble production method(s)	Bubble rise distance/cm	White area/cm ²	Temp/°C	Salinity
<i>Mårtensson et al., 2003</i>	artificial seawater	none	diffuser ¹	4	3	-2, 5, 15, 25	0, 9.2, 33
<i>Sellegrì et al., 2006</i>	artificial seawater	sodium dodecyl sulfate	weir, diffusers ²	2	not stated	4, 23	not stated, presumably near 35
<i>Tyree et al., 2007</i>	seawater, artificial seawater, mixtures	oleic acid	diffusers ³	32-40	180	20-25	1, 10, 20, 33, 70
<i>Keene et al., 2007</i>	seawater	none	diffuser ²	~115	~150-300	~27	not stated, presumably near 35
<i>Facchini et al., 2008</i>	seawater	none	water jet	not stated	400	not stated, presumably ~13	not stated, presumably near 35
<i>Fuentes et al., 2010</i>	artificial seawater, seawater	<i>Thalassiosira rotula</i> exudate	water jets, diffusers ⁴	4-10	200	18-20	35

2574 ¹ pore size (presumably diameter) 20-40 µm

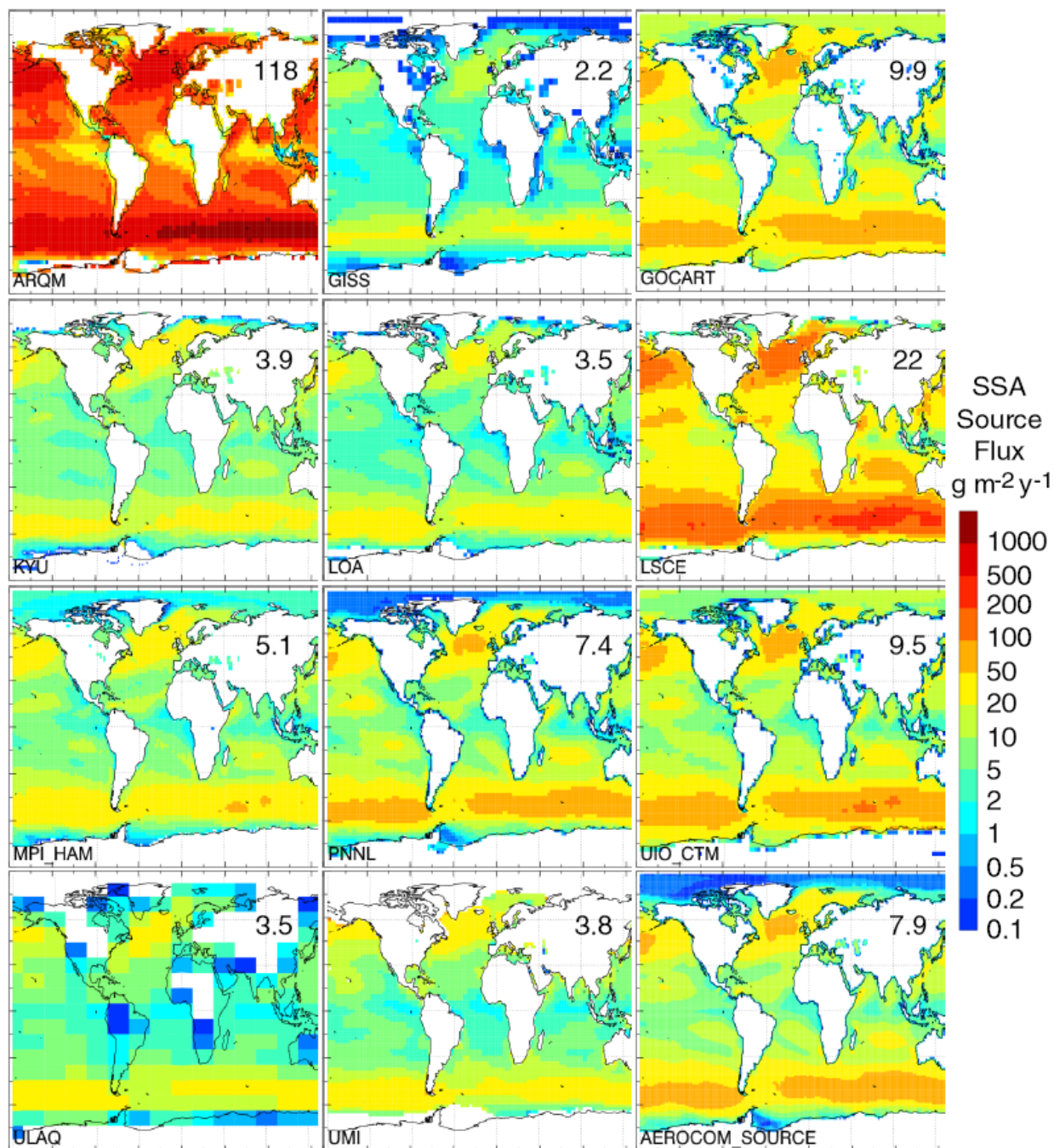
2575 ² pore size(s) not specified

2576 ³ pore sizes (presumably diameters) of 80 µm and 140 µm

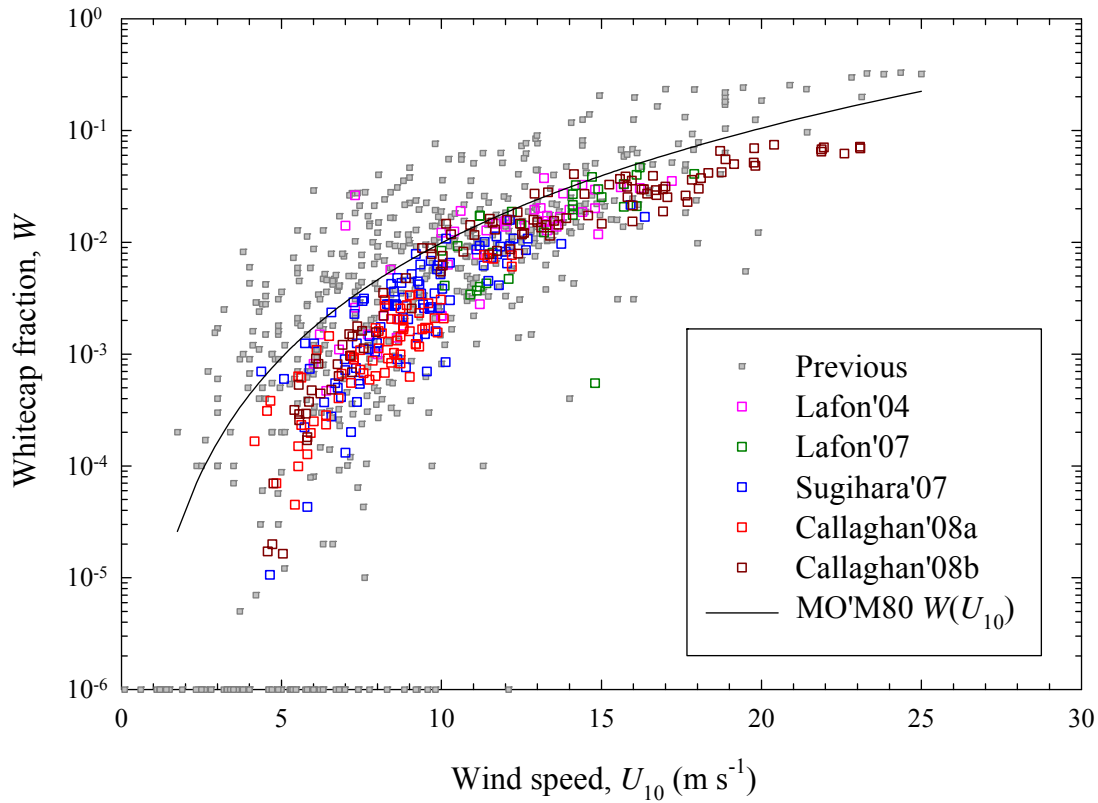
2577 ⁴ one a sintered glass filter with mean pore size (presumably diameter) 30 µm, the other an

2578 aquarium diffuser with unspecified pore size

2579

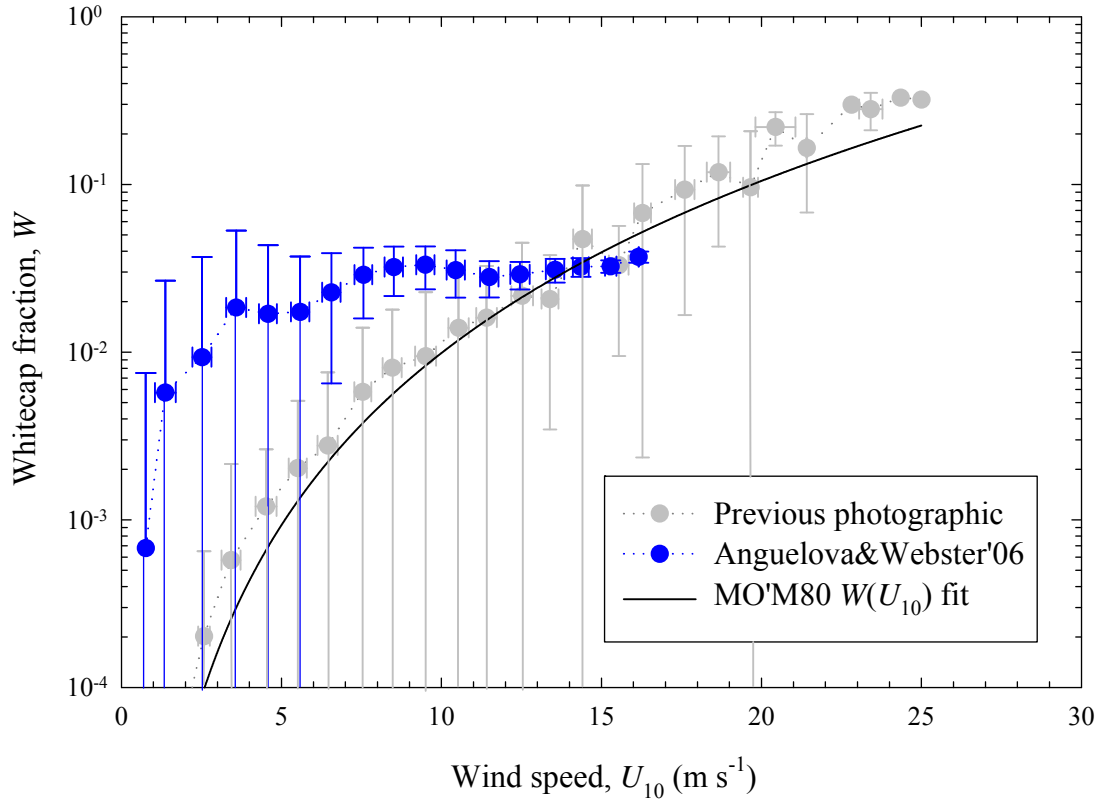


2581
 2582 Figure 1. Annual-average dry SSA mass production flux as computed by several chemical
 2583 transport and general circulation models participating in the AeroCom aerosol model
 2584 intercomparison [Textor *et al.*, 2006]. A global mean production flux of $10 \text{ g m}^{-2} \text{ yr}^{-1}$ over the
 2585 world ocean corresponds to a total global production rate of approximately 3500 Tg yr^{-1} . For
 2586 identification of the models, production methods employed, and references see Table 1. Number
 2587 given in each panel denotes global annual SSA production in $10^{12} \text{ kg yr}^{-1}$.



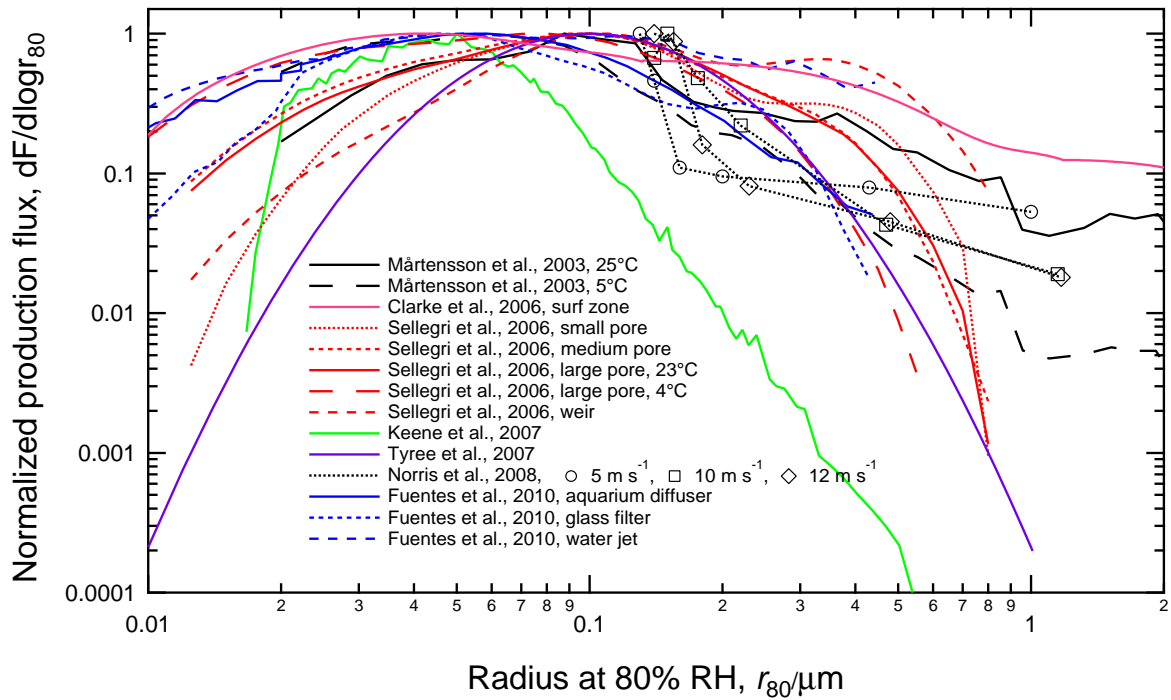
2588

2589 Figure 2. Whitecap fraction W as a function of wind speed at 10 m above the sea surface U_{10} ,
 2590 from five new data sets (color symbols) and from previous studies that used film photography
 2591 (gray symbols) as summarized in Table 20 of *Lewis and Schwartz* [2004] and in Table 2 (data
 2592 sets 1-5, 7-17, 21, 26) of *Anguelova and Webster* [2006]. Points on abscissa denote values less
 2593 than or equal to 1×10^{-6} . The formulation of *Monahan and O'Muircheartaigh* [1980], Eq. 9, is
 2594 also shown.



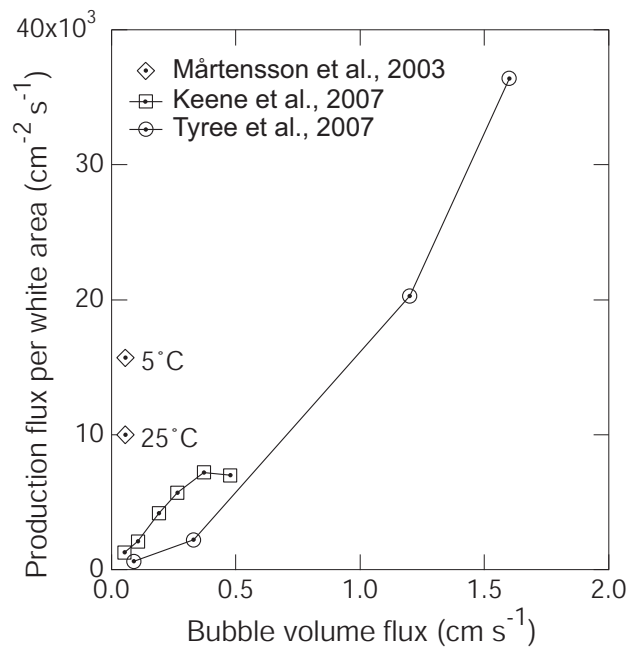
2595

2596 Figure 3. Whitecap fraction W as a function of wind speed at 10 m above the sea surface U_{10} ,
 2597 arithmetically averaged in intervals of 1 m s^{-1} , obtained with the algorithm of *Anguelova and*
 2598 *Webster* [2006] (blue) using annually-averaged (1998) observations of brightness temperature T_B
 2599 from Special Sensor Microwave Imager (SSM/I) in clear sky (no clouds) locations all over the
 2600 globe. The corresponding U_{10} values are also from SSM/I. Error bars on W values represent one
 2601 standard deviation of the data points falling in each U_{10} bin; the apparent asymmetry of the error
 2602 bars is a consequence of plotting on the logarithmic ordinate scale. Also shown (gray) are bin-
 2603 average values of W from previous photographic determinations shown in Figure 2 and the
 2604 formulation of *Monahan and OMuircheartaigh* [1980], Eq. 9.



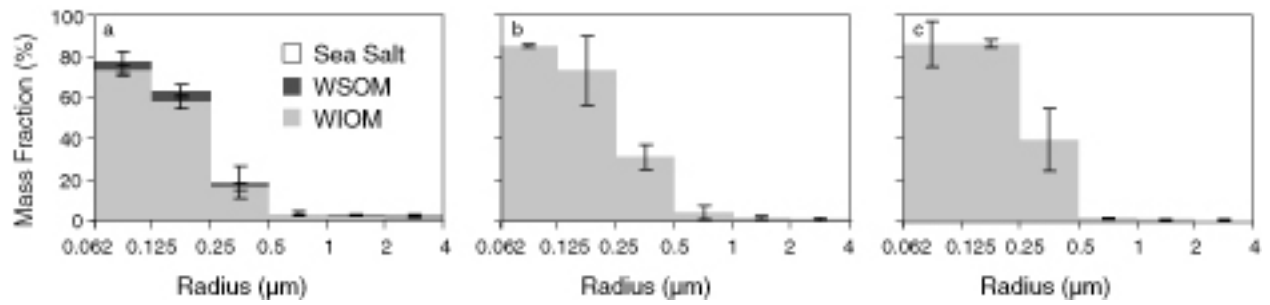
2605

2606 Figure 4. Size distributions of SSA production flux normalized to maximum value in
 2607 representation $dF/d\log r_{80}$ as a function of r_{80} from laboratory experiments [Mårtensson *et al.*,
 2608 2003, Figure 4c; Sellegri *et al.*, 2006, Figures 2 and 4; Keene *et al.*, 2007, Figure 3 for 5 L min^{-1} ;
 2609 Tyree *et al.*, 2007, Table 1, artificial seawater, salinity 33; and Fuentes *et al.*, 2010, Figure 6] and
 2610 field measurements [Clarke *et al.*, 2006, formulation presented in text; Norris *et al.*, 2008,
 2611 Figure 6 at U_{10} 5, 10, and 12 m s^{-1}]. Uncertainties in the original data are not shown.



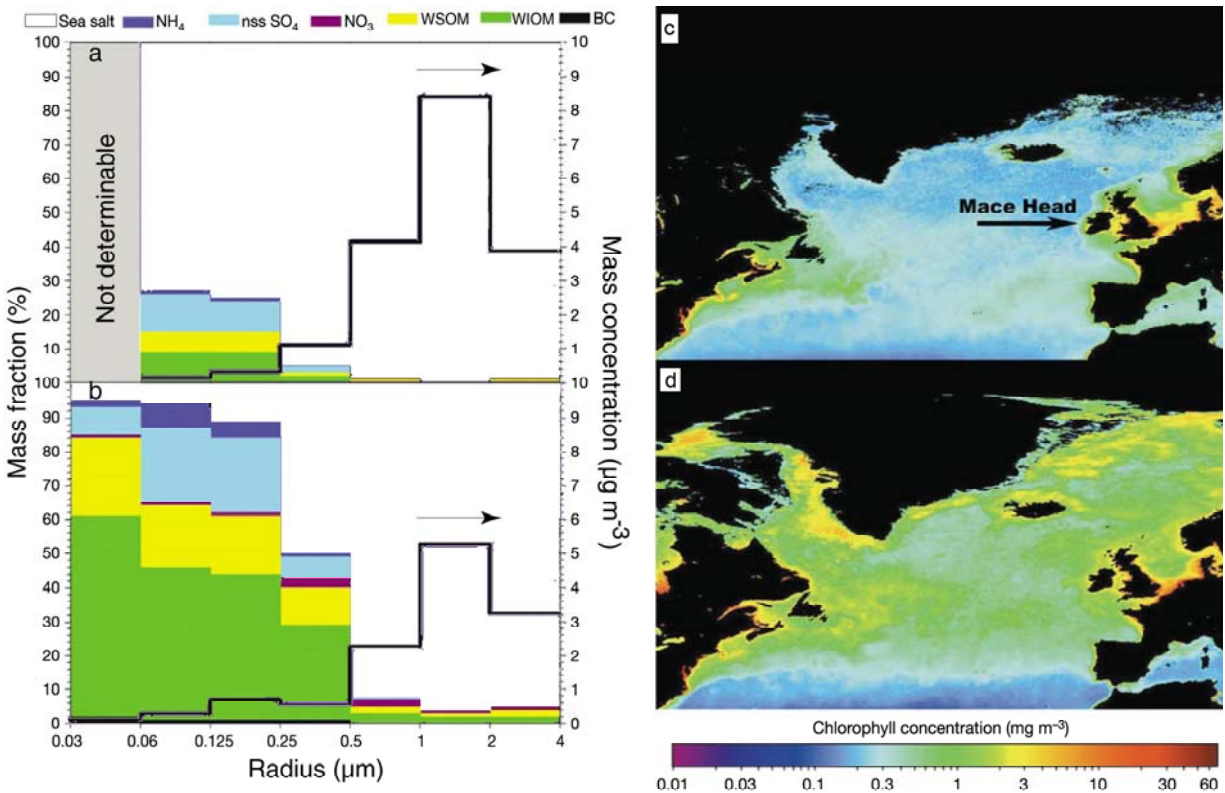
2612

2613 Figure 5. Dependence of total SSA number production flux per white area in laboratory
 2614 experiments of *Mårtensson et al.* [2003], using artificial seawater (salinity 33) at two different
 2615 temperatures, *Keene et al.* [2007], using natural (low-productivity) seawater, *Tyree et al.* [2007],
 2616 using artificial seawater (salinity 33), on bubble volume flux (volume of air in bubbles rising to
 2617 the water surface per unit area and time).



2618

2619 Figure 6. (a) Mass fraction of sea salt, water-soluble organic matter (WSOM), and water-
 2620 insoluble organic matter (WIOM) as a function of particle radius sampled at approximately 70%
 2621 RH, (a) for seawater bubble-bursting chamber experiments with fresh seawater, conducted in a
 2622 shipboard laboratory in a plankton bloom over the N.E. Atlantic (May-June 2006), (b) for clean
 2623 marine air at Mace Head, Ireland, May-June 2006, and (c) for clean marine air 200-300 km
 2624 offshore west-northwest of Mace Head in a plankton bloom coincident in time with
 2625 aforementioned samples. Adapted from *Facchini et al.* [2008].



2626

2627 Figure 7. Average mass concentration of total particulate matter (black line, right axis) and mass

2628 fraction (colors, left axis) of sea salt, NH₄, nss-SO₄, NO₃, water-soluble organic matter

2629 (WSOM), water-insoluble organic matter (WIOM), and black carbon (BC) in several size ranges

2630 for North Atlantic marine aerosol sampled at Mace Head, Ireland, in clean marine air during

2631 periods of (a) low biological activity, November (2002) January (2003) and February (2003); and

2632 (b) high biological activity, March-October, (2002). Radius corresponds to relative humidity

2633 approximately 70%. For low biological activity mass concentrations of aerosol constituents other

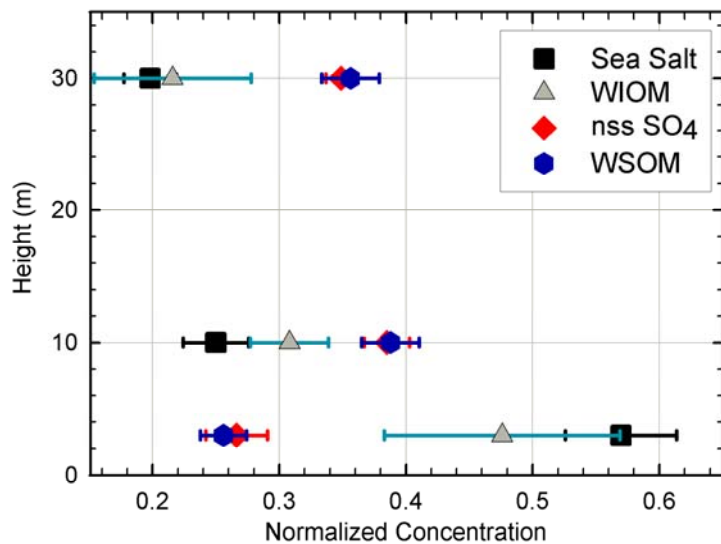
2634 than sea salt were below detection limits for the size range 0.03-0.06 μm . Oceanic chlorophyll-a

2635 concentrations over the North Atlantic for periods of (c) low and (d) high biological activity are

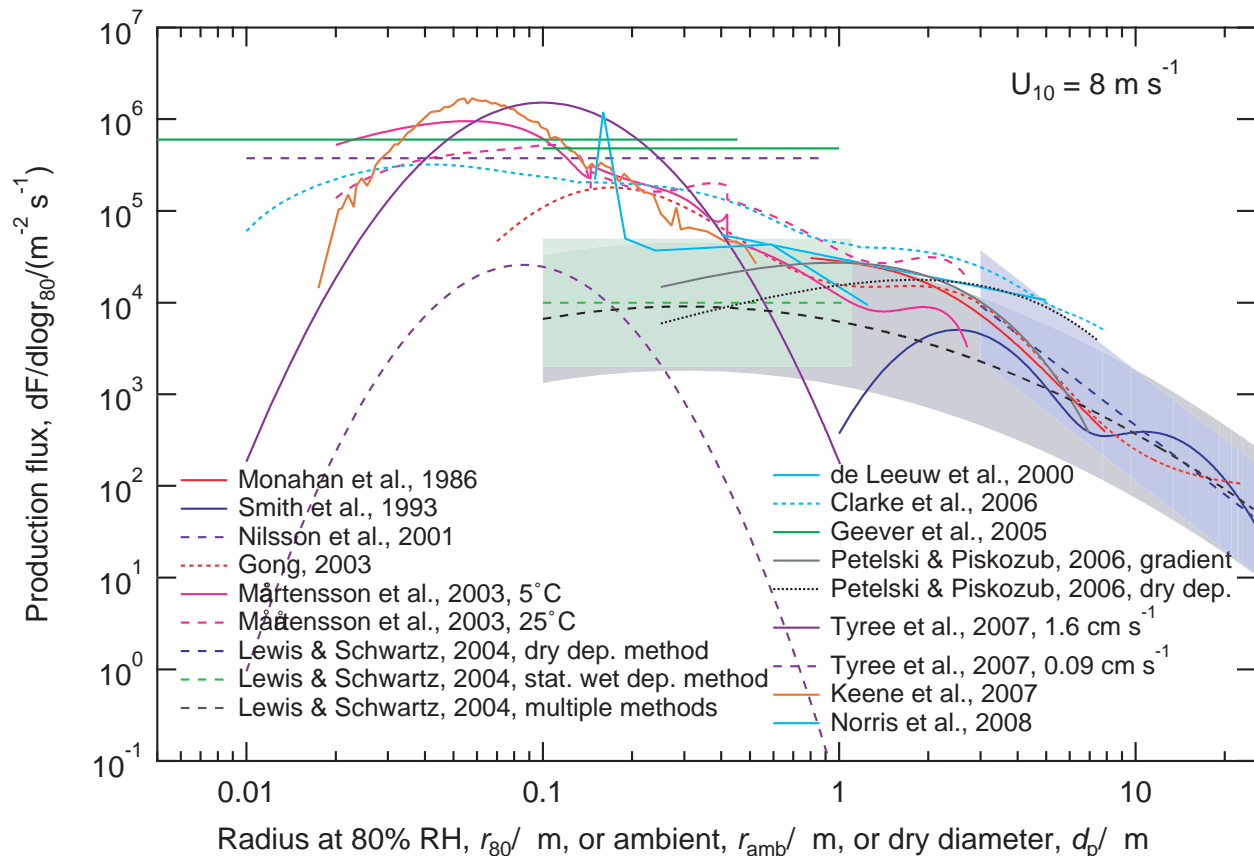
2636 five year averages (1998-2002) over the same months as for the composition measurements,

2637 based on satellite measurements of ocean color (courtesy of SeaWiFS Project, NASA/Goddard

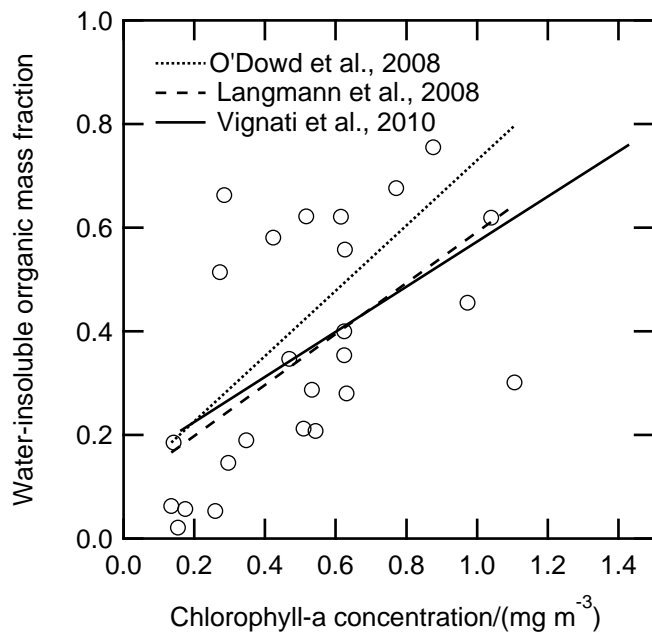
2638 Space Flight Center and ORBIMAGE). Adapted from O'Dowd et al. [2004].



2639
 2640 Figure 8. Vertical profiles of mass concentration of sea salt, water-soluble inorganic matter
 2641 (WIOM), non-sea-salt sulfate, and water-soluble organic matter (WSOM) at Mace Head, Ireland,
 2642 normalized to the sum of the concentrations of the species at the three heights, for particle radius
 2643 (at ambient relative humidity) less than 0.5 μm sampled in clean marine air. All values are
 2644 averages of nine individual 7-day samples analyzed from April-October, 2005 except WIOM,
 2645 which is shown for an average of three samples where a positive WIOM flux was observed and
 2646 which represented periods when the organic-enriched waters were within the flux footprint as
 2647 discussed in text. Uncertainty bars represent the standard deviation from the normalized
 2648 concentration average. Adapted from *Ceburnis et al.* [2008].

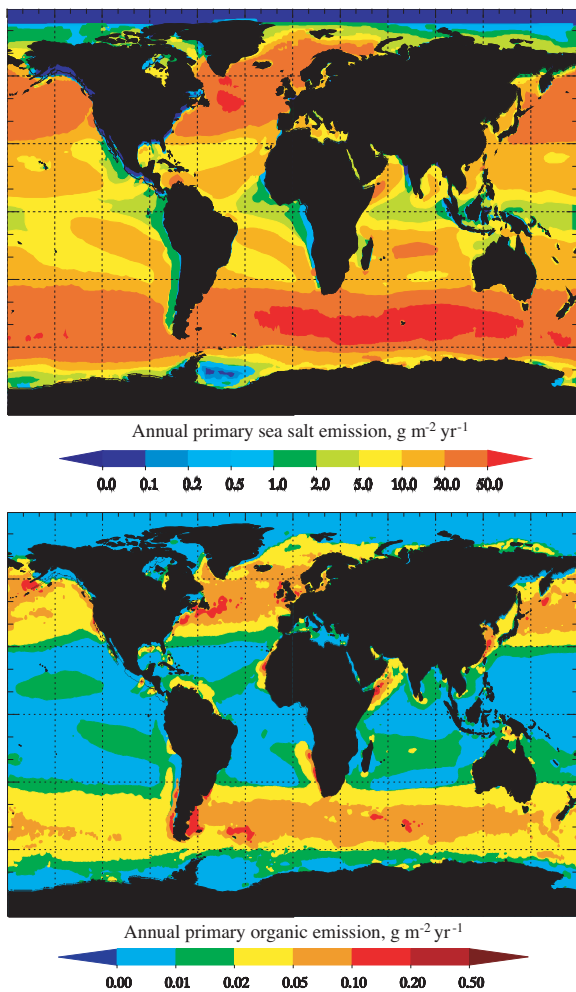


2649
 2650 Figure 9. Parameterizations of size-dependent SSA production flux discussed in text and
 2651 presented in the Appendix, evaluated for wind speed $U_{10} = 8 \text{ m s}^{-1}$ (or $U_{22} = 8 \text{ m s}^{-1}$ for *Geever et*
 2652 *al.*; 2005). Also shown are central values (curves) and associated uncertainty ranges (bands)
 2653 from review of *Lewis and Schwartz* [2004], which denote subjective estimates by those
 2654 investigators based on the statistical wet deposition method (green), the steady-state deposition
 2655 method (blue), and taking into account all available methods (black); no estimate was provided
 2656 for $r_{80} < 0.1 \mu\text{m}$. Lower axis denotes radius at 80% relative humidity, r_{80} , except for formulations
 2657 of *Nilsson et al.* [2001], *Mårtensson et al.* [2003], and *Clarke et al.* [2006] which are in terms of
 2658 dry particle diameter, d_p , approximately equal to r_{80} , and those of *Geever et al.* [2005], *Petelski*
 2659 *and Piskozub* [2006] (dry deposition method), and *Norris et al.* [2008] which are in terms of
 2660 ambient radius, r_{amb} . Formulation of *Petelski and Piskozub* [2006] by the dry deposition method
 2661 is based on expression in Appendix. Formulations of *Tyree et al.* [2007] are for artificial
 2662 seawater of salinity 33 at the two specified bubble volume fluxes. Formulations of *Nilsson et al.*
 2663 [2001] and *Geever et al.* [2005] of particle number production flux without size resolution are
 2664 plotted arbitrarily as if the flux is independent of r_{amb} over the size ranges indicated to yield the
 2665 measured number flux as an integral over that range.



2666

2667 Figure 10. Mass fraction of water-insoluble organic matter WIOM in sea-spray aerosol with
 2668 $0.1 \mu\text{m} \leq r_{\text{amb}} \leq 0.5 \mu\text{m}$ measured at Mace Head, Ireland under clean marine conditions as a
 2669 function of spatial-average oceanic surface-water chlorophyll-a concentration over an upwind
 2670 grid of $1000 \text{ km} \times 1000 \text{ km}$ as determined from MODIS satellite measurements of ocean color,
 2671 revised from *O'Dowd et al.* [2008] and provided by C. O'Dowd, 2010. Original fit presented by
 2672 *O'Dowd et al.* [2008] and fits to revised data presented by *Langmann et al.* [2008b, corrected by
 2673 *Vignati et al.*, 2010] and *Vignati et al.* [2010] are also shown.



2674
 2675 Figure 11. Global distribution of mass flux of sea salt (upper panel) and water-insoluble organic
 2676 matter WIOM (lower panel) in sea spray with $0.1 \mu\text{m} < r_{80} < 1 \mu\text{m}$ averaged over a one-year
 2677 period in 2002–2003 using the TM5 chemical transport model [Vignati, *et al.*, 2010; E. Vignati,
 2678 private communication, 2010].
 2679